ANALYSIS AND SIMULATION OF THE TARGET-ATTACKER AND THE TARGET-ATTACKER-DEFENDER PROBLEMS

By

Mostafa Ali Rushdi

A Thesis Submitted to the
Faculty of Engineering at Cairo University
in Partial Fulfillment of the
Requirements for the Degree of
MASTER OF SCIENCE
in
Aerospace Engineering

AEROSPACE ENGINEERING DEPARTMENT
FACULTY OF ENGINEERING, CAIRO UNIVERSITY
GIZA, EGYPT
2017

ANALYSIS AND SIMULATION OF THE TARGET-ATTACKER AND THE TARGET-ATTACKER-DEFENDER PROBLEMS

By

Mostafa Ali Rushdi

A Thesis Submitted to the
Faculty of Engineering at Cairo University
in Partial Fulfillment of the
Requirements for the Degree of
MASTER OF SCIENCE
in
Aerospace Engineering

Under the Supervision of

Prof. Ayman H. Kassem	Prof. Gamal El-Bayoumi
....	....
Professor	Professor
Aerospace Engineering Department	Aerospace Engineering Department
Faculty of Engineering, Cairo University	Faculty of Engineering, Cairo University

AEROSPACE ENGINEERING DEPARTMENT
FACULTY OF ENGINEERING, CAIRO UNIVERSITY
GIZA, EGYPT
2017

ANALYSIS AND SIMULATION OF THE TARGET-ATTACKER AND THE TARGET-ATTACKER-DEFENDER PROBLEMS

By

Mostafa Ali Rushdi

A Thesis Submitted to the
Faculty of Engineering at Cairo University
in Partial Fulfillment of the
Requirements for the Degree of
MASTER OF SCIENCE
in
Aerospace Engineering

Approved by the Examining Committee:

Prof. Ayman H. Kassem, Thesis Main Advisor

Prof. Third E. Name, Member

Prof. Second S. Name, Internal Examiner

Prof. First S. Name, External Examiner

AEROSPACE ENGINEERING DEPARTMENT
FACULTY OF ENGINEERING, CAIRO UNIVERSITY
GIZA, EGYPT
2017

Engineer's Name:	Mostafa Ali Rushdi	
Date of Birth:	26/10/1991	
Nationality:	Egyptian	
E-mail:	morushdi@gmail.com	
Phone:	0111-4000-606	
Address:	Postal Address	
Registration Date:	10/10/2014	
Awarding Date:	14/7/2015	
Degree:	Master of Science	
Department:	Aerospace Engineering	

Supervisors:

Prof. Ayman H. Kassem
Prof. Gamal El-Bayoumi

Examiners:

Prof. First S. Name	(External examiner)
Prof. Second S. Name	(Internal examiner)
Prof. Ayman H. Kassem	(Thesis main advisor)
Prof. Third E. Name	(Member)

Title of Thesis:

Analysis and Simulation of the Target-Attacker and the Target-Attacker-Defender Problems

Key Words:

Pursuit-Evasion, Analysis and Simulation, Apollonius circle, Voronoi diagram, Optimal strategy.

Summary:
This thesis studies the Taget-Attacker problem and the Taret-Attacker-Defender problem, and introduces a unified analytical overview with numerical simulations.

Table of Contents

List of Tables

List of Figures

Abstract

This thesis deals with two scenarios of active target defense. The first scenario is a two-agent pursuit-evasion problem that involves a Target (aircraft) in opposition to an Attacker (missile). The Target tries to evade (avoid being captured) the Attacker. This first problem will be referred to herein as the TA problem as it concerns the Target (T) and Attacker(A). The second scenario is a three-agent pursuit-evasion problem that involves three agents, the Target, the Attacker and the Defender. The Attacker missile pursues a Target aircraft that is being helped by a Defender missile which tries to intercept the Attacker before it reaches the Target. This second problem will be referred to herein as the TAD problem as it concerns the Target (T), the Attacker(A), and the Defender (D). We first consider the TA problem, in which we search for a path that the Target can move on to escape from the Attacker. All the evasion techniques depend on the time of the turn that the Target makes when it detects the Attacker (Missile) and the objective is to maximize the Missile acceleration till the Missile power bleed. We choose the escaping trajectory as a polynomial with unknown coefficients, then decide the values of these coefficients so as to make the Missile exert a maximum acceleration to bleed its power as fast as possible before it reaches the Target. We explain the meaning of proportional navigation, and subsequently simulate two- dimensional proportional-navigation equations using MATLAB and Simulink. After dealing with the TA problem, the thesis shifts to the TAD problem. In this latter problem, a differential game arises in which a team is formed by the Target and the Defender which cooperate to maximize the separation between the Target and the point where the Defender intercepts the Attacker, while the Attacker tries to minimize this separation. This thesis offers a unified analytic treatment of the aforementioned problem based on the construction of two Apollonius circles. The treatment includes all possibilities of the ratio between the speeds of the Attacker and Defender. A criticality condition is derived from which two important entities are obtained, namely: (a) the critical Target speed normalized *w.r.t.* the Attacker speed, and (b) the Voronoi diagram bordering the safe or escape region for the Target Optimal strategies. This Voronoi diagram is shown to obey a complex sixth-degree polynomial when the Defender differs in speed from the Attacker. This polynomial reduces to a real fourth-degree polynomial when the Defender and Attacker are similar, i.e., are of equal speeds. Beside unifying previously published results in a common setting, this thesis simplifies all computations by using intuitionistic plane-geometric arguments rather than the more tedious analytic-geometric manipulations. Moreover, the thesis extends existing results by adding some novel results, thereby giving a complete picture of all cases of interest. The analysis in this thesis is supplemented by extensive computations using MATLAB to solve the complex high-order polynomial equations and to plot the Voronoi diagrams under a variety of pertinent parameters. The numerical results and plots obtained allow useful and insightful interpretation and are in exact agreement with numerical solution of the corresponding two-point boundary value problem.

Part I

INTRODUCTION AND LITERATURE REVIEW

Chapter 1: Introduction and Literature Review

This thesis deals with two scenarios of active target defense involving:

1. Two-agent pursuit-evasion: a Target (aircraft) in opposition to an Attacker (missile). The Target tries to evade (avoid being captured) the Attacker. This problem will be referred to herein as the TA problem as it concerns the Target (T) and Attacker (A).

2. Three-agent pursuit-evasion where each agent has a specific role. A two-agent team consists of a Target (aircraft) and a Defender (missile) cooperating in opposition to an Attacker (missile). The Target tries to evade the Attacker and avoid being captured by him. The Defender cooperates with and assists the Target by trying to intercept(capture and destroy) the Attacker before the latter captures the Target. This problem will be referred to herein as the TAD problem as it concerns a triad consisting of the Target (T), Attacker (A), and Defender (D).

The following two sections pertain to a brief introduction and literature survey of the TA and TAD problem.

1.1 The TA problem

Solutions to the TA problem are called homing missile guidance laws, and the most popular among them is a control law called proportional navigation [1, 2, 3], which is analogous to classical proportional control. The underlying basic concept is that if the direct Target-Attacker line-of-sight time rate is diminished, i.e., if the direct TA Line-of-Sight ceases to change its direction then (for a non-maneuvering, constant velocity Target) the Attacker is on a collision course. If the Target is considered smart or maneuvering, then variations to the proportional navigation are needed so as to minimize the miss distance. These variations have been given optimal-control interpretations through linear quadratic Gaussian (LQG) formulations, and a variety of other techniques [4, 5, 6, 7, 8, 9, 10, 11, 12, 13, 14, 15, 16, 17, 18, 19, 20, 21, 22, 23, 24, 25, 26, 27, 28, 29, 30, 31].

The literature has investigated manifold variations of the TA problem (including the TAD problem, producing a large amount of results, and a huge number of publications (see, *e. g.*, [9, 10, 31, 32, 33, 34]. The study of pursuit evasion games can be traced back to the von Neumanns hide-and-seek games [35], where a hider chooses one cell of a two-dimensional grid in which to hide himself and a seeker chooses a subset of cells of the grid (usually one row and one column) in which to seek the hider. If the seeker selects the cell chosen by the hider, then the hider is captured and the seeker wins the game. Otherwise, the hider wins the game. Starting from this seminal work, adversarial pursuit evasion settings have been modeled by a variety of mathematical techniques. Notable among these are the optimal-control formulation and the differential-game one [7, 36, 37].

The fundamental conceptual difference between missile guidance laws based on optimal control theory and those based on differential game theory is in the assumptions made by the guidance laws on the future trajectory and maneuvering capabilities of the Target. Optimal control theory assumes that the future maneuver strategy of the Target is completely defined, either in open-loop or closed-loop form [7]. The feedback nature of missile guidance laws allows the missile to make corrections for inaccurate predictions of the maneuvers of the Target. The optimal-control formulation is appropriate only when future maneuver time history, or strategy, of the Target is known or can be justifiably assumed or accurately predicted. One possible perspective is to design strategies that maximize performance of the Attacker against a worst-case Target [32]. In such a setting, the Target is usually considered to be of infinite speed, complete awareness of the location and intent of the Attacker, and full knowledge of the conflict environment. Such a method guarantees the success of the pursuit, defined, for example, by capture of the Target in a finite time. However, this powerful-adversary model may yield solutions that are too conservative in practical applications. A better alternative is to use probabilistic formulations addressing average-case behaviours [32].

The most suitable (and presumably most successful) mathematical framework for analyzing conflicts controlled by two independent agents is in the realm of dynamic or differential games. Thus, the scenario of intercepting a maneuverable Target has to be formulated as a zero-sum pursuitevasion game [36]. The roles of the game players are clearly defined, the interceptor (Attacker) is the pursuer and the Target is the evader. The natural cost function of such a zero-sum game is the miss distance (the distance of the closest approach, or in other words the smallest norm of the separation vector), to be minimized by the pursuer and maximized by the evader. The game solution provides simultaneously the missiles guidance law (the optimal pursuer strategy), the worst Target maneuver (the optimal evader strategy), and the resulting guaranteed miss distance (the value of the game). As a consequence, the game solution provides a guidance law that is robust with respect to the Target maneuver structure.

Many prominent extensions of the TA problem are currently problems of hot research. In addition to the celebrated TAD problem (to be fully introduced in section 1.2), we give a glimpse of problems of contemporary interest in the following (far-from-conclusive) list

- Three-dimensional pursuit-evasion [1, 5, 21, 37],
- Fuzzy guidance laws [23, 25],
- Non-conventional or modern approaches for interception [6, 20],
- Lyapunov-based non-linear guidance [16].
- Incorporation of probabilistic uncertainty in the location, behavior, and/or sensor observations of the Target.

1.2 The TAD problem

The TAD problem constitutes a dynamic differential game [38, 39, 40, 41, 42, 43, 44, 45, 46] and is of interest in aerospace, control, and robotics engineering. We will consider herein recent formulations and treatments of this problem [47, 48, 49, 50, 51, 52], though there exist other formulations and treatments of it that span almost half a century [53, 54, 55, 19, 56, 57, 58, 59, 60, 61]. Table 1.1 shows several variants of this generic problem in a variety of settings, contexts or disciplines. The TAD problem is a generalization of the classical problem of a single pursuer and a single evader [62, 63, 64, 65, 66]. In fact, the TAD is essentially

Area	Agent 1	Agent 2	Agent 3	References
Aerospace	Target	Attacker(missile)	Defender(missiles)	[47, 48, 49, 50, 51]
Biology	Prey	Predator	Protector	[56, 61]
Society	Lady	Bandits	Bodyguards	[55]
Criminology	Robber	Policemen/Cops	Gangsters	[78]

Table 1.1: A variety of settings or contexts for the same generic problem

a duplication of this classical problem, since in the TAD problem, the Attacker plays the double role of being a pursuer for the Target, and at the same time an evader for the Defender [19]. The TAD problem is also a special case of a more general pursuit-evasion problem in which there are multiple Attackers and multiple Defenders [67, 68, 69, 70, 71]. Many common threads are shared by all these problems, such as the solution of differential games [38, 39, 40, 41, 42, 43, 44, 45, 46] and the construction of Apollonius circles [72, 73, 74, 75] and Voroni diagrams [76, 77, 78, 79, 80, 81, 82, 81].

1.3 Thesis Contribution

As stated earlier, this thesis has contributions to both TA and TAD problems.

In the TA problem, we search for a path that the Target can move on to escape from the Attacker. All the evasion techniques depend on the time of the turn that the Target makes when it detects the Attacker (Missile) and the objective is to maximize the Missile acceleration till the Missile power bleed. We choose the escaping trajectory as a polynomial with unknown coefficients, then decide the values of these coefficients so as to make the Missile exert a maximum acceleration to bleed its power as fast as possible before it reaches the Target. We explain the meaning of proportional navigation, and subsequently simulate two- dimensional proportional-navigation equations using MATLAB and Simulink.

This thesis also offers a unified analytic treatment of the TAD problem based on the construction of two Apollonius circles. The treatment includes all possibilities of the ratio between the speeds of the Attacker and Defender.Note that the case of a slow Defender appears here for the first time, while the treatment of the cases of fast Defender or similar Defender is extended and augmented with novel results and new insights. A criticality condition is derived from which the two following important entities are obtained

- the critical Target speed normalized w.r.t. the Attacker's speed so as to be a dimensionless quantity,
- the Voronoi diagram bordering the safe or escape region for the Target.

Optimal strategies are also studied, and are shown to obey a complex sixth-degree polynomial when the Defender differs in speed from the Attacker. This polynomial reduces to a real fourth-degree polynomial when the Defender and Attacker are similar in speed. Beside unifying previously published results in a common setting, this thesis simplifies all computations by using intuitionistic plane-geometric arguments rather than the more tedious analytic-geometric manipulations. Moreover, the thesis extends existing results by adding some novel results, thereby giving a complete picture of all cases of interest. The analysis in this thesis is supplemented by extensive computations using MATLAB to solve the complex high-order polynomial equations and to plot the Voronoi diagrams under a variety of pertinent parameters. The numerical results and plots obtained allow useful and insightful interpretations and are in exact agreement with numerical solution of the corresponding two-point boundary value problem.

1.4 Thesis Outline

This thesis consists of four parts. Part I comprises the current chapter of the introduction and literature survey. Part II pertains to the TA problem and consists of chapters 2-5. Chapter 2 is an introduction of the TA problem, while chapter 3 is devoted to a brief discussion of guidance laws. Chapter 4 constitutes a prominent cornerstone of the thesis as it reports extensive simulation results for the TA problem obtained via Matlab and simulink. Chapter 5 discusses a game-theoretic formulation of the TA problem. It is followed by Part III of the thesis on the TAD problem, which consists of chapters 6-10. Chapter 6 introduces the TAD problem, lists the assumptions, notation and nomenclature used therein, discusses the general concepts and properties of an Apollonius circle [72, 73, 74, 75], and then specializes these to the cases of the AD Apollonius circle and the TA Apollonius circle. Chapter 7 derives a criticality condition which constitutes a quadratic equation that is later solved for the critical dimensionless ratio between the Target speed and Attacker speed. The same criticality condition is then rephrased in Chapter 8 as a relation between the initial coordinates x_T and y_T of the Target. This relation leads to the Voronoi diagram bordering the *safe* or *escape* region R_e of the Target. This Voronoi diagram is published for the first time when the Defender is fast or slow. It includes as a special case the much simpler diagram for a similar Defender that has already appeared in [49]. Chapter 9 develops optimal strategies for the three constituents of the differential game. Chapter 10 explores the simulation of the optimal heading angle. The thesis is concluded with its last part (Part IV) which is a single (chapter 11) that summarizes the thesis contributions and points out possible directions for further work.

Part II

TARGET-ATTACKER PROBLEM

Chapter 2: Introduction for TA problem

2.1 Problem Statement

In this Part, we consider a two-agent pursuit-evasion problem that involves a Target (aircraft) in opposition to an Attacker (missile). The Target tries to evade the Attacker and avoid being captured by him. We will try to find a simple technique for target evasion, so we should have a look at evasion techniques. The missile is on the ground, its position is (0,0). The plane is flaying is the air, its position is (10000,40000).

2.2 Evasion techniques

Each missile type has its own fundamental weaknesses and though some of these weaknesses or limitations may be kept secret by the missiles manufacturer, many of them can be easily inferred by the manufacturer's opponents through observation. Propulsion is one of the most prominent limitations of any missile. Most contemporary missiles employ rocket propulsion which enjoys the two advantages of a high thrust/weight ratio and a small size. The typical thrust profile of such a propellant rocket is that of an initial high impulse burn to accelerate up to cruise speed, which is followed by a slower sustainer burn. Once the propellant is burned out, the rocket will continue due to inertia until drag takes its toll. The maneuvering ability of such a missile depends critically on its speed and therefore the amount of wing and body lift it can generate. Immediately after launch the missile has poor maneuverability due to its low speed, but this improves as its cruise speed is reached. Maneuverability will peak at the instant when the sustainer is about to burn out as the weapon has its lowest mass and a high energy state while still possessing powerplant thrust. After sustainer burnout, the missile will bleed off its energy which reduces its ability to follow through maneuvers. Ideally, a missile airframe will employ a combination of wing and body lift to provide maximum turn rate with minimum energy bleed throughout all phases of its flight while maximizing range.

The aircraft must exploit every known weakness of the missile's system to defeat the missile. Missiles are a visible threat which act on a timescale that allows some tangible response. An aircraft maximizes its chances of survival by maintaining a high energy state, and by possessing a system of early and accurate warning. Figure 2.1 displays tree-like taxonomy of the techniques that can be used by an aircraft to avoid being hit by an attacking missile. The figure shows that there are two main classes of such techniques. The first class is that of kinematics-based tactics (maneuvers) and is, in fact, the genuine class of evasion techniques studied in aeronautical engineering and is the class of interest in this thesis. The second class of evasion techniques are not based on kinematics but are of proven practical utility. The advent of Fourth Generation Air-Air Missiles (AAMs) and 'double digit' Surface-Air missiles (SAMs) has somewhat decreased what could be achieved by using maneuver techniques. Nevertheless, these techniques remain effective against many conventional and legacy weapons, provided the aircraft has the required performance capabilities. Kinematics-based techniques are still of paramount importance form both the theoretical and practical points of view.

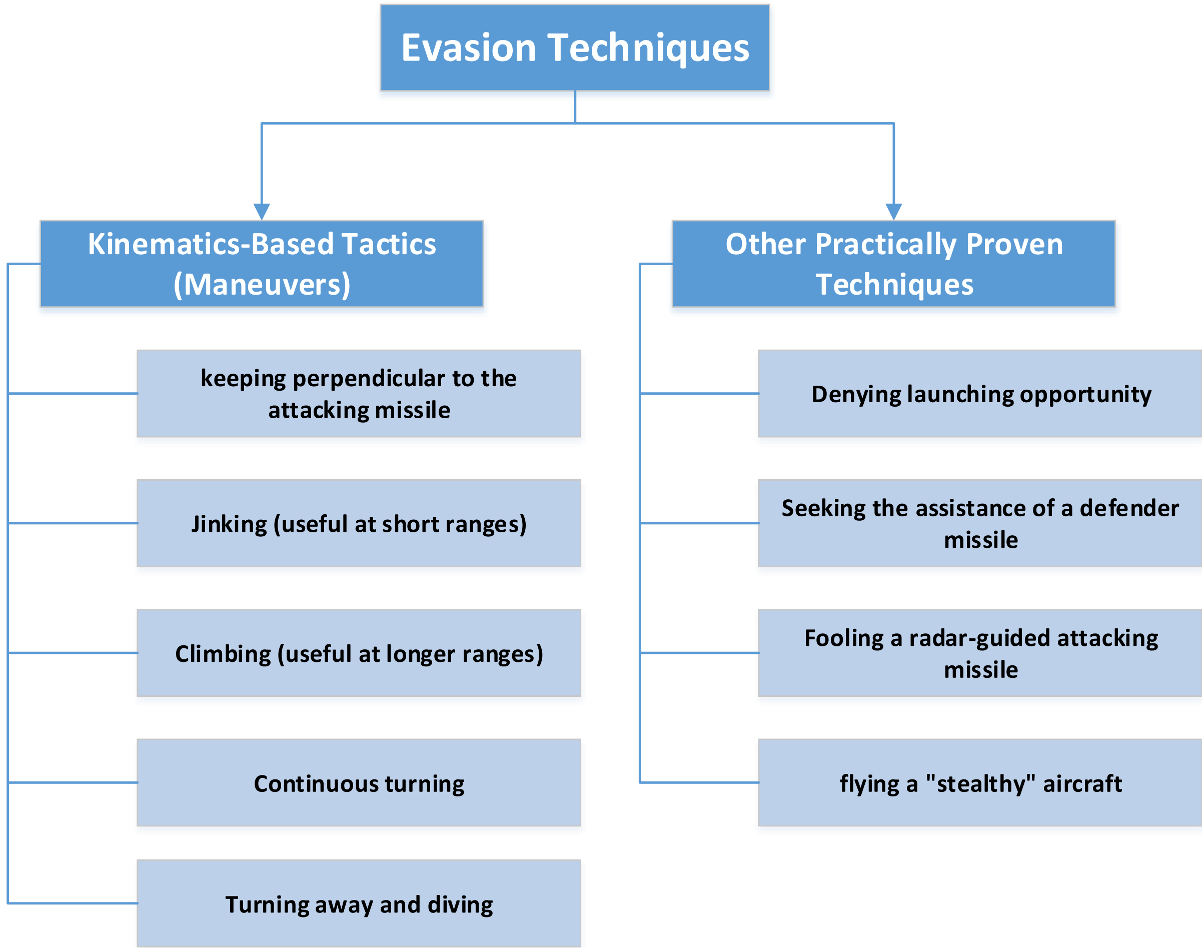

Figure 2.1: Taxonomy of evasion techniques

Before explaining the taxonomy given in Figure 2.1, we list a few useful observations, namely

- The missile is typically faster than the aircraft (otherwise, the aircraft can evade the missile by simply running away from it without having to maneuver).
- The missile cannot turn tighter than the aircraft, so it takes a longer path.
- The control mechanism of the missile is much simpler and is of less capability than that of the aircraft. In order to pull as tight turn as the aircraft, it must exercise an acceleration that is far beyond its capability.
- The missile always attempts to trace the target and not to lead it. Thus, if the target changes heading, it will be necessary for the Missile to change heading similarly, but this is too difficult for it to achieve.
- The main problem for an aircraft when evading a missile is how to compensate for the missile's speed superiority. This makes timing a somewhat critical issue for the aircraft.

The most important kinematics-based evasion techniques are :

1. **keeping perpendicular to the attacking missile:**
Perpendicularity evading is the maneuver technique used when the missile is fired head-on at a beyond visual range (BVR). The target turns hard to either left or right so as to fly at roughly a 90 degrees angle to the attacking missile. This perpendicular orientation or beam aspect (3 o'clock position or 9 o'clock position) should allow visual acquisition and tracking of the incoming missile, particularly if it is originally fired from 6 o'clock position. Perpendicularity evading forces the missile to bleed off its energy and to possibly lead the target. Once the target aircraft makes a hard turn to reverse its direction, the missile with its far larger turn circle will be unable to compensate. The aircraft might have to constantly maneuver to keep perfectly perpendicular to the missile to keep it from locking on to it. Figure 2.2 illustrates the perpendicularity evading maneuver technique.

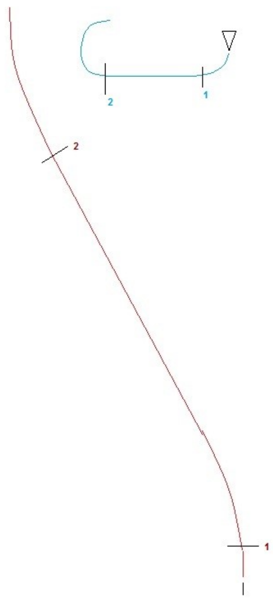

Figure 2.2: Illustration of the perpendicularity evading maneuver technique

2. **Jinking (useful at short ranges):**
The word "jinking" means literally "to suddenly change direction" and essentially belongs to the specialized jargon of aeronautical engineering. In the jinking maneuver, the aircraft must be positioned so that it is at an acute angle (30-60 degrees are optimum) relative to the missiles flight path. Once the missile gets closer, the aircraft will make a hard turn in the opposite direction. As there is a time lag between the aircraft changing its direction and the missile following it (for several reasons, most important of which is the missiles inertia), this will cause the missile to head in the wrong direction until it manages to correct, and also to bleed off its limited energy. Usually the missile will fly past the aircraft and miss. Figure 2.3 illustrates the jinking evading maneuver technique.

Figure 2.3: Illustration of the jinking maneuver technique

3. **Climbing (useful at longer ranges):**
   Since at a long range the missile will have burned out its engine, it will rely on inertia to keep flying, and climbing will mean that it will bleed off energy rapidly. Once the missile reaches a close range (maybe around 1,500 meters), the aircraft should dive for the ground, then pull up. This will allow the aircraft to gain kinematic energy and use it to evade the missile. Figure 2.4 illustrates the climbing evading maneuver technique.

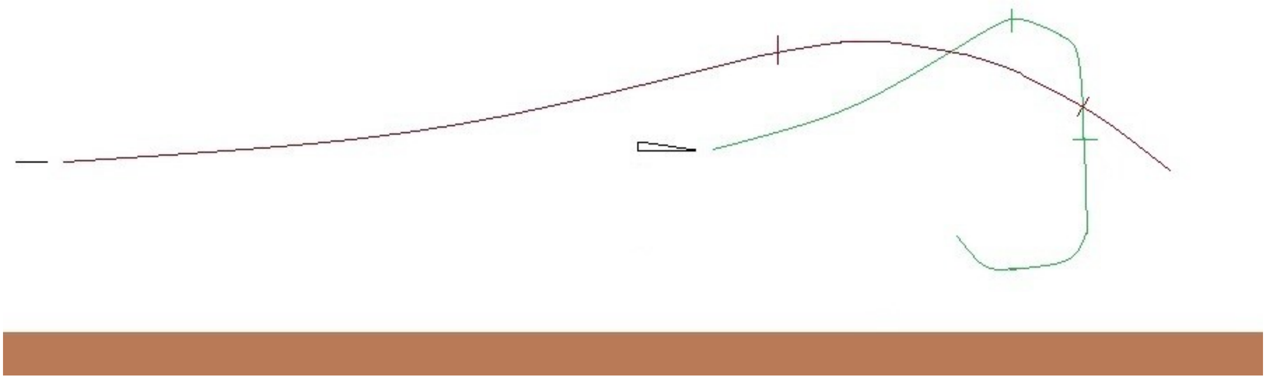

Figure 2.4: Illustration of the climbing maneuver technique

4. **Continuous turning:**
   The aircraft places the missile at a 3 oclock or a 9 oclock position. It then maintains a sufficient turn to keep the missile turning all the time. This tactic forces the missile to execute a continuous turn, bleeding its energy the entire time, making it easier for the aircraft to outturn the missile once it comes close. Figure 2.5 illustrates the continuous turning maneuver technique.

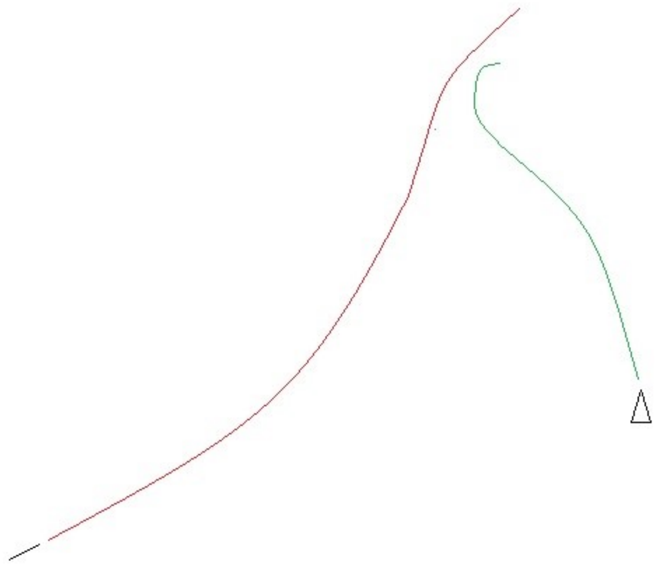

Figure 2.5: Illustration of the continuous turning maneuver technique

5. **Turning away and diving :**
   The aircraft turns away from the attacking missile and dives for the ground, gaining speed and putting as much distance as possible between itself and the missile. This tactic is not useful on its own at shorter ranges, and the pilot must evade the missile physically by pulling the aircraft into the turn and forcing the missile to overshoot once the missile comes sufficiently close. This ”Going to ground” tactic also confuses the missile’s guidance via ”back scatter” from objects on the ground

To make this thesis self-contained, we now add a brief description of other practical evasion techniques that are not of kinematic origin, and are therefore outside the main scope of this thesis:

1. **Denying launching opportunity:**
   The famous proverb ”*prevention is better than cure*” indicates that it is better to stop something undesirable from happening than it is to deal with it after it has already happened. Therefore, the best tactic for the aircraft when dealing with Surface-Air missile (SAM) sites is to prevent the launching of a missile by remaining safely outside of the known envelope or launching cone of the missile. This tactic is called the maneuver of denying the missile-launching site an opportunity to shoot. In fact, flying over SAM-infested hostile territory is asking to get hit, and should be avoided by all means. Of course, the tactic of denying launching opportunity is not an evasion one per se, albeit it is a very prudent one, indeed. In line with this tactic is the fact that the first mission objective in any offensive air operation is to destroy every hostile radar and SAM installation.

2. **Seeking the assistance of a defender missile:**
   The aircraft (or some of its air or surface allies) might launch a defender missile to

intercept and stop the attacking missile, hopefully before this attacker reaches it. This kind of active evasion changes our current TA problem to the more sophisticated TAD problem, to be discussed in the second part of this thesis.

3. **Fooling a radar-guided attacking missile:**
   Physically avoiding the enemy missile is not the only option for a targeted aircraft. If the missile is radar-guided, it can be misguided, decoyed, fooled, or deceived by the aircraft via electronic signal jamming or by dispensing or deploying a bundle of flares and chaff (tiny metal pieces) followed by changing course. The missile is caused to lose lock on the target and have either a miss or a premature detonation (When missiles lose the lock they either self-destruct or continue flying in a straight course). The aircraft might receive assistance from nearby friendly planes for jamming enemy radar on a broad range of frequencies (typically hostile ones).

4. **Flying a ”stealthy” aircraft:**
   Modern stealthy aircrafts have extremely small radar cross-sections, are impossibly quiet, are hard to see in the day or night, and have a heat signature not that much warmer than the ground they fly over. No one can target what radars, heat sensors, and human eyes and ears cannot detect. Drones are particularly effective with stealth, as the lack of need to support a pilot can grant them a cross-section smaller than a bird on radar. A very hot area of research in electromagnetics nowadays is to develop meta-materials that are essentially invisible over a broad band of frequencies.

Now we want to search for a path that the Target can move on it to escape from the Attacker. All the evasion techniques depend on the time of the turn that the Target makes when it detects the Attacker (Missile) and the objective is to maximize the Missile acceleration till the Missile power bleed. We will choose the escaping trajectory as a polynomial with unknown coefficients, then try to find these coefficients which make the Missile exert a maximum acceleration to bleed its power as fast as we can before it reaches the Target.

2.3 Assumptions, Notation, and Nomenclature

Assumptions

1. Both the Attacker and Target travel at constant speeds.

2. The Attacker’s speed is larger than that of the Target. Otherwise, the Target will be unconditionally or trivially capable of escaping.

3. Gravitational and drag effects are neglected for simplicity.

4. The maximum g-force a typical person can handle is 5G

5. The maximum g-force a pilot fighter (with safety equipments) could resist is 10G.

6. The maximum g-force for a sprint missile is 100G.

7. The range for Tactical missile defense, which has short ranges is 18 $\rightarrow$ 20 Kilometer, approximately 59000 $\rightarrow$ 66000 feet.

Notation

- n_c : Acceleration command (for the Missile) in m/s^2.
- N' : Effective navigation ratio, a unit-less designer-chosen gain (usually in the range of $3 \rightarrow 5$).
- V_c : Missile-Target closing velocity.
- λ : line-of-sight angle.
- $\dot{\lambda}$: line of sight rate.
- R_{TM} : length of the line of sight.
- L : Missile lead angle.
- HE : Heading error.
- $\dot{\beta}$: angular velocity of the Target.
- V_{T1}, V_{T2} : Target velocity components in the Earth fixed coordinate system.
- V_{M1}, V_{M2} : Missile velocity components in the Earth fixed coordinate system.

Nomenclature

Inertial coordinate system: fixed to the surface of a flat-Earth model (the 1 axis is down-range and the 2 axis can either be altitude or cross-range).

Missile lead angle: theoretically correct angle for the missile to be on a collision triangle with the Target.

Heading error (HE) : angle representing the initial deviation of the Missile from the collision triangle.

line of sight: The imaginary line connecting the Missile and Target.

length of the line of sight (R_{TM}): Instantaneous separation between Missile and Target.

Miss distance : The point of closest approach of the Missile and Target.

Closing velocity (V_c): the negative rate of change of the distance from the Missile to the Target $Vc = -\dot{R_{TM}} = -\frac{d}{dt}R_{TM}$.

Chapter 3: Guidance Laws

In this chapter, we will illustrate some types of guidance laws. We will be in the side of the Attacker, trying to hit the target. There is three main types of guidance laws:

3.1 Proportional Navigation

In this section, we will illustrate some fundamentals of missile guidance, focusing on the proportional navigation technique, which is one of the simplest guidance laws.

What is proportional navigation?

The proportional navigation guidance law issues acceleration commands, perpendicular to the instantaneous missile-target line-of-sight, which are proportional to the line-of-sight rate and closing velocity. Mathematically, the guidance law can be stated as

$$n_c = N' V_c \dot{\lambda} \tag{3.1}$$

where n_c is the acceleration command (for the missile) in (m/s^2), N' is the the effective navigation ratio, a unit-less designer-chosen gain (usually in the range of $3 \rightarrow 5$), V_c is the missile-target closing velocity in (m/s) and $\dot{\lambda} = \frac{d\lambda}{dt}$ is the rate of the line-of-sight angle and is in (rad/s). Note that (3.1) is dimensionally homogeneous, since n_c has the dimension

$$\begin{aligned}[n_c] &= [N'][V_c][\dot{\lambda}] \\ &= (1)(LT^-1)(T^-1) \\ &= LT^-2\end{aligned} \tag{3.2}$$

which is the appropriate dimension of linear acceleration.

3.1.1 Simulation of proportional navigation equations in 2-D

In this subsection we will introduce the equations of proportional navigation and the sequence to get a simulation for the path of the Target and the Attacker and how the missile acceleration will be affected during this simulation.

The simulation inputs are the initial location of the Missile (R_{M1}, R_{M2}) and the initial location of the Target (R_{T1}, R_{T2}), Target speed V_T, Missile speed V_M, and effective navigation ratio N'.

There are two types of **error sources** that cause the Attacker to miss the Target; they are the heading error (HE) and the acceleration of the Target (n_T) called the Target maneuver.

proportional navigation differential equations

The components of Target velocity

$$V_{T1} = -V_T \cos(\beta) \tag{3.3}$$

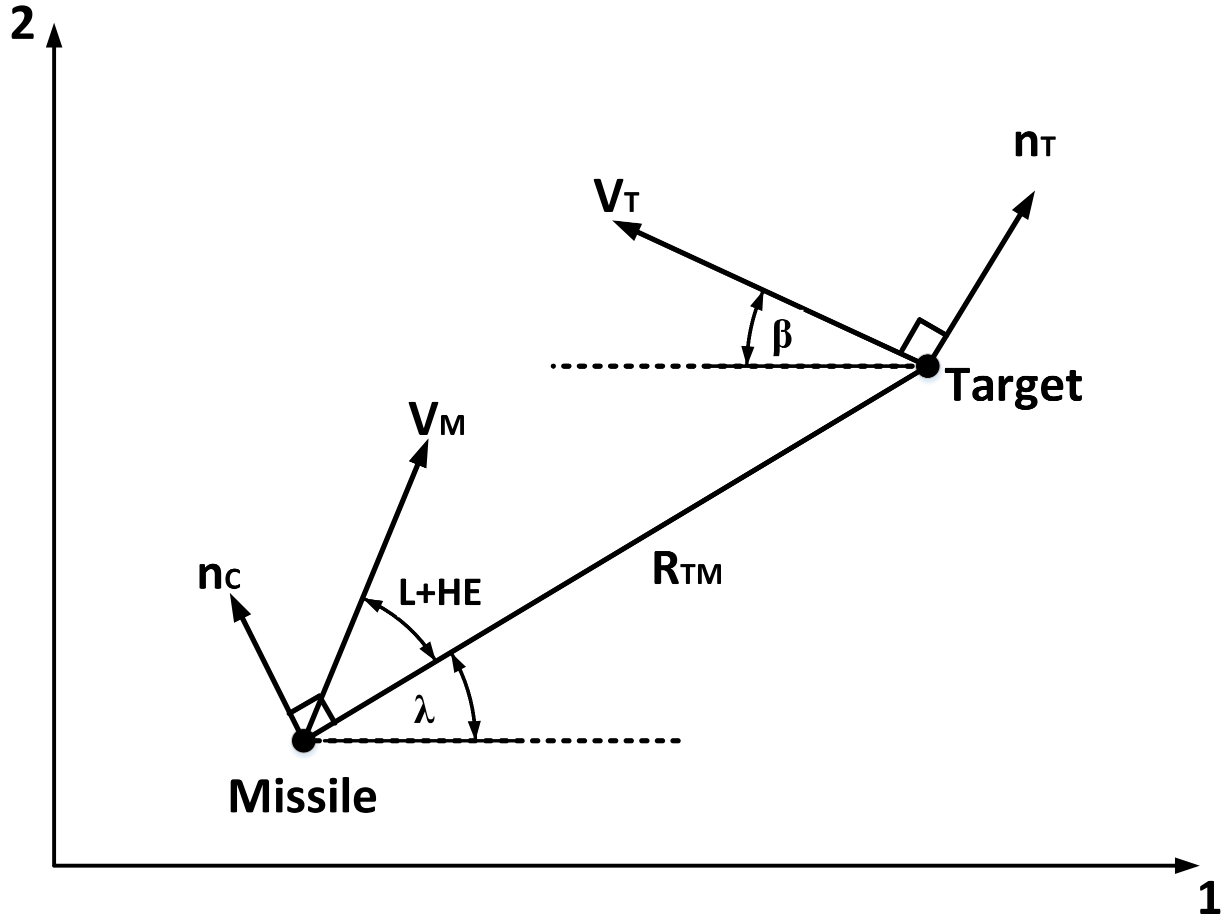

Figure 3.1: Two dimensional Missile-Target engagement geometry.

$$V_{T2} = V_T \sin(\beta) \tag{3.4}$$

Relative missile-target separation

$$R_{TM1} = RT1 - R_{M1} \tag{3.5}$$

$$R_{TM2} = RT2 - R_{M2} \tag{3.6}$$

from the previous 2 equations we get

$$R_{TM} = \sqrt{R_{TM1}^2 + R_{TM2}^2} \tag{3.7}$$

line of sight angle

$$\lambda = \tan^{-1}(\frac{R_{TM2}}{R_{TM1}}) \tag{3.8}$$

missile lead angle

$$L = \sin^{-1}(\frac{V_T \sin(\beta + \lambda)}{V_M}) \tag{3.9}$$

the angle between the downrange axis and V_M vector is $\theta = \lambda + L$

Missile velocity components

$$V_{M1} = V_M \cos(\theta + HE) \tag{3.10}$$

$$V_{M2} = V_M \sin(\theta + HE) \tag{3.11}$$

Relative velocity components

$$V_{TM1} = V_{T1} - V_{M1} \tag{3.12}$$

$$V_{TM2} = V_{T2} - V_{M12} \tag{3.13}$$

closing velocity it is the negative rate of change of the distance from the missile to the target $Vc = -\dot{R_{TM}}$, so we have to differentiate eq(3.7)

$$\dot{R_{TM}} = \frac{1}{2}(R_{TM1}^2 + R_{TM2}^2)^{\frac{-1}{2}}[2R_{TM1}\dot{R_{TM1}} + 2R_{TM2}\dot{R_{TM2}}]$$

we see that so we get

$$V_c = -\dot{R_{TM}} = -\frac{R_{TM1}V_{TM1} + R_{TM2}V_{TM2}}{R_{TM}} \tag{3.14}$$

line of sight rate we have to differentiate eq(3.8) using the rule $\tan^{-1} x = \frac{dx}{1+x^2}$

$$\begin{aligned}\dot{\lambda} &= [\frac{1}{1 + (\frac{R_{TM2}}{R_{TM1}})^2}](\frac{\dot{R_{TM2}}}{R_{TM1}}) \\ &= \frac{R_{TM1}^2}{R_{TM1}^2 + R_{TM2}^2}[\frac{R_{TM1}\dot{R_{TM2}} - R_{TM2}\dot{R_{TM1}}}{R_{TM1}^2}] \\ &= \frac{R_{TM1}V_{TM2} - R_{TM2}V_{TM1}}{R_{TM1}^2}\end{aligned} \tag{3.15}$$

magnitude of the missile guidance command

$$n_c = N' V_c \dot{\lambda} \tag{3.16}$$

missile acceleration components

$$a_{M1} = -n_c \sin\lambda \tag{3.17}$$

$$a_{M2} = -n_c \cos\lambda \tag{3.18}$$

angular velocity of the target

$$\dot{\beta} = \frac{n_T}{V_T} \tag{3.19}$$

we will solve all the equations in this section using second-order Runge-Kutta numerical integration procedure. If we have a first order differential equation of the form

$$\dot{x} = f(x,t)$$

where t is time, we seek to find a recursive relationship for x as a function of time. With the second-order RungeKutta numerical technique, the value of x at the next integration interval h is given by

$$x_{k+1} = x_k + \frac{hf(x,t)}{2} + \frac{hf(x,t+h)}{2}$$

3.2 Augmented Proportional Navigation

3.3 Optimal Guidance

Chapter 4: Optimization for escaping maneuver

In this chapter, we will be in the Target side, trying to find an optimized escaping maneuver from the Attacker. We will use two optimization techniques, *Monte Carlo* and *Genetic algorithm*.

4.1 Models & Simulations

In this section we will simulate equations in sec. 3.1.1 for proportional navigation using MATLAB and Simulink. The following figure is a flowchart illustrating the steps of calculations using the equations in sec. 3.1.1 till we plot the trajectories.

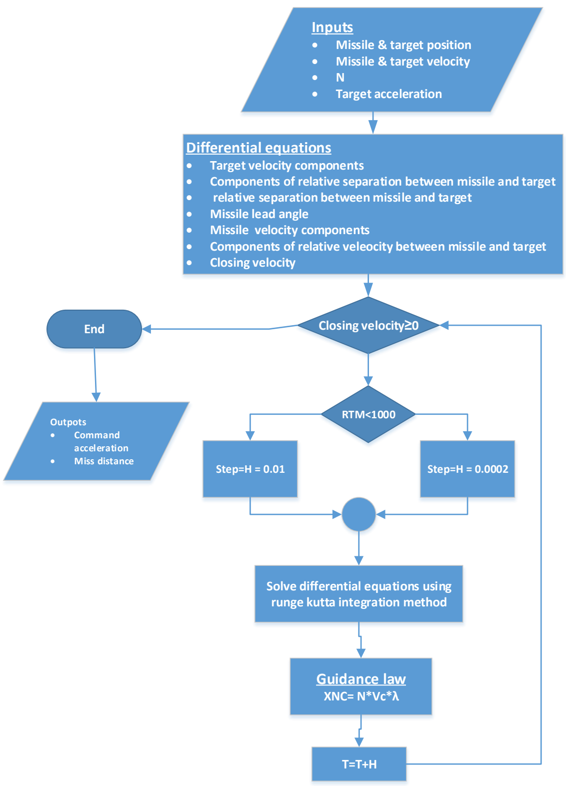

Figure 4.1: Flowchart illustrating the steps of calculations using the equations in sec. 2.3 till we plot the trajectories.

4.1.1 Simulation for some target maneuver cases [using MATLAB]

In this subsection we will use MATLAB to simulate equations in sec. 3.1.1 for proportional navigation. We will solve the differential equations using second-order Runge-Kutta numerical integration technique, then we will draw the trajectories of the pursuit and evader for 4 cases for the Target maneuver error source, and we will deduce the effect of the effective navigation ratio N' and the other type of the error source; Heading error.

4.1.1.1 Zero Target maneuver

In this case the evader (Target - plane) does not do any effort to scape, it just moves in a straight line, as we see in Fig. 4.2. So the pursuer (Attacker - Missile) does not have to bleed much energy to reach the Target.

In the case of **zero Heading error** the effective navigation ratio has no effect on the simulation engagement at all. The missile's acceleration will be zero as in Fig. 4.3.

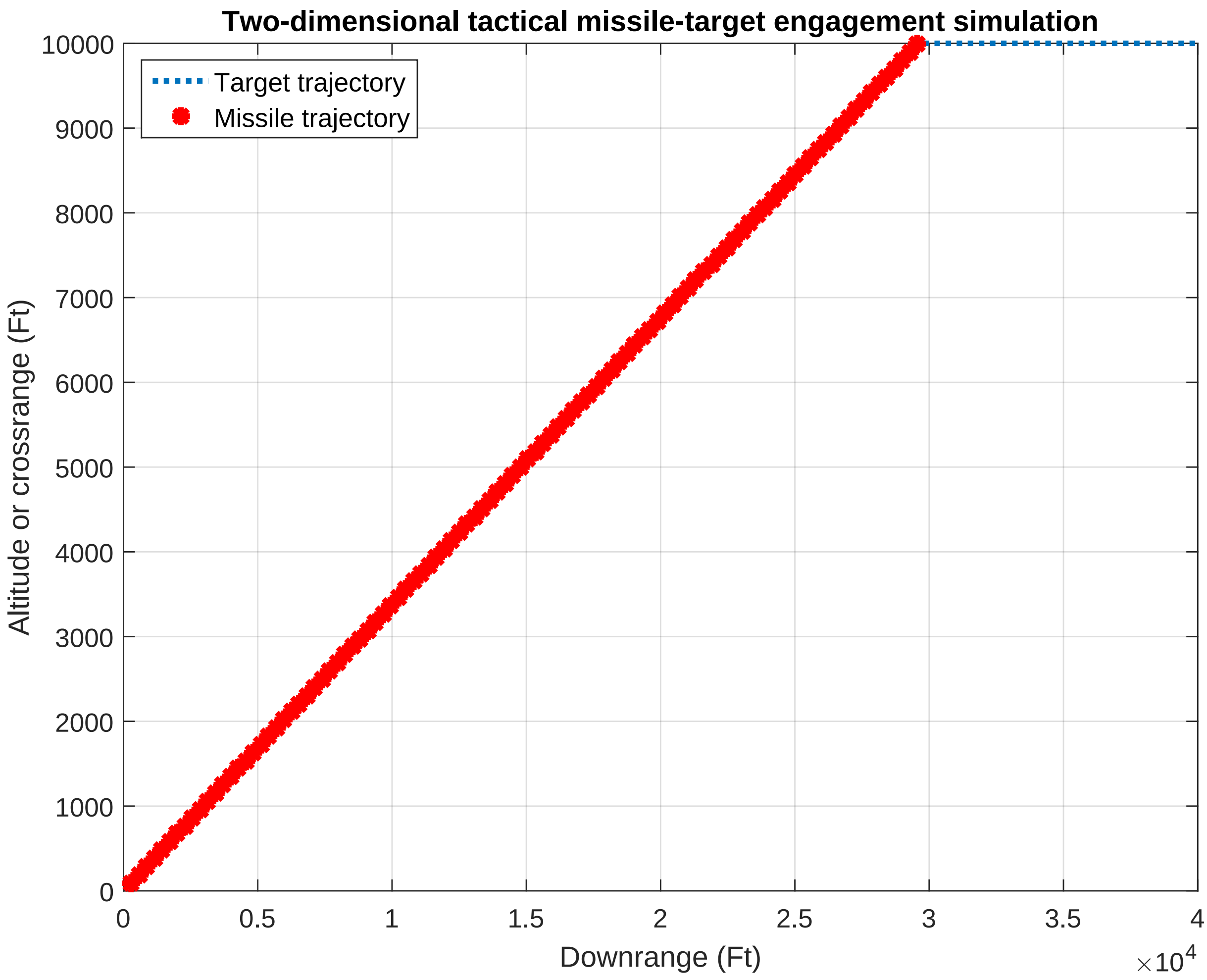

Figure 4.2: Trajectory of the target and attacker in case of zero target maneuver with zero heading error and $N' = 4$.

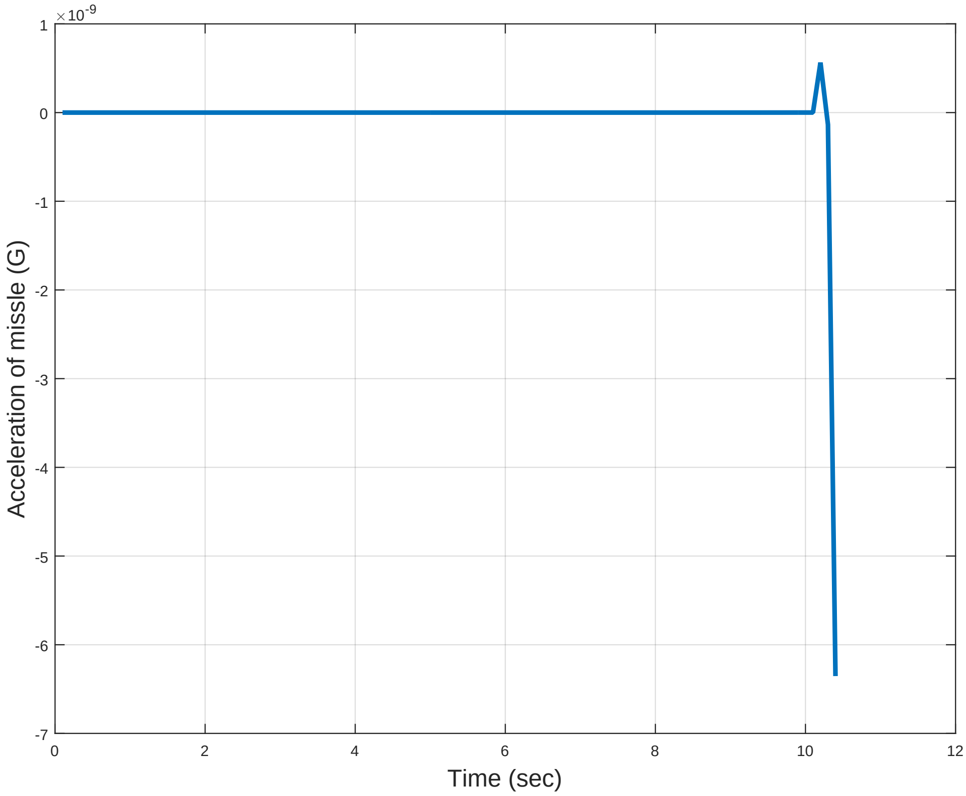

Figure 4.3: Missile acceleration in case of zero target maneuver with zero heading error and $N' = 4$.

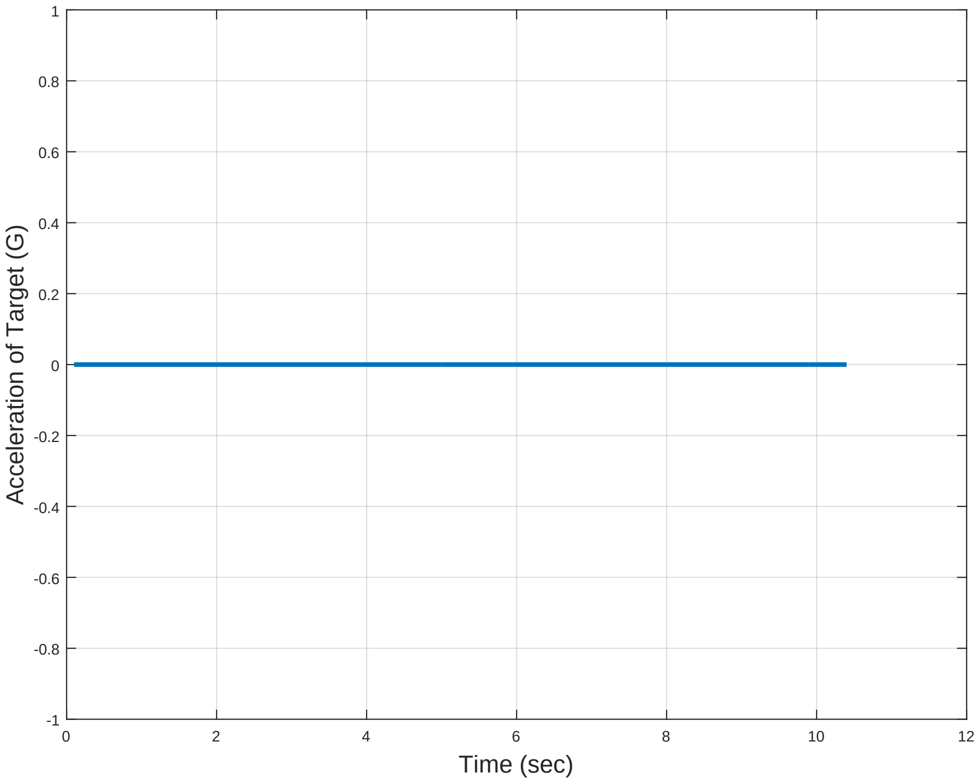

Figure 4.4: Target acceleration in case of zero target maneuver with zero heading error and $N' = 4$.

In the case of **Heading error = -20** increasing the effective navigation ratio causes heading error to be removed rapidly as we see from Fig. 4.5, Fig. 4.7 and Fig. 4.9. The effective navigation ratio has an effect on the acceleration of the missile; the way that the missile will bleed energy as we see from Fig. 4.6 , Fig. 4.8 and Fig. 4.10. The total acceleration (area under the curve) is increasing inversely proportional with the effective navigation ratio N' .

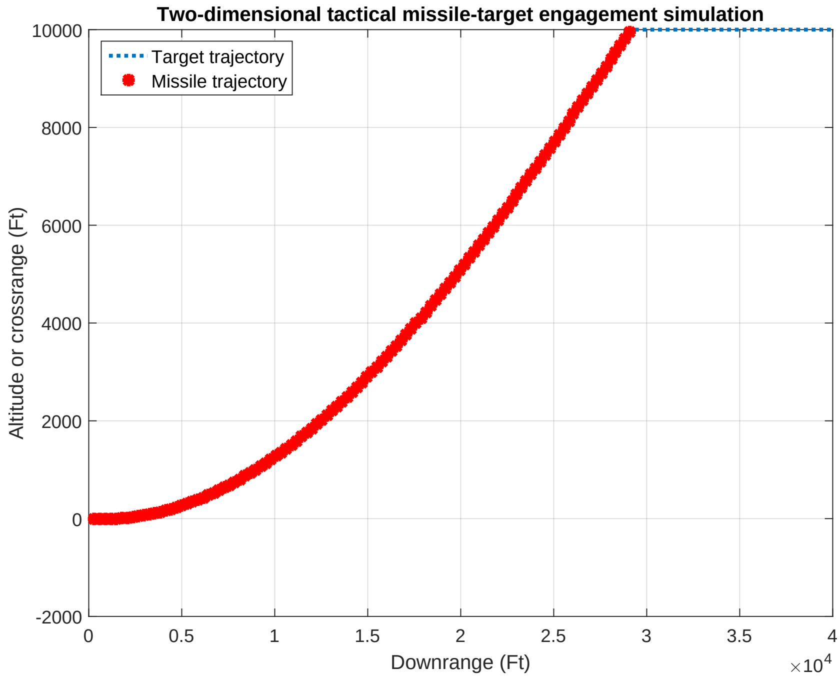

Figure 4.5: Trajectory of the target and attacker in case of zero target maneuver with heading error=-20 and $N' = 3$.

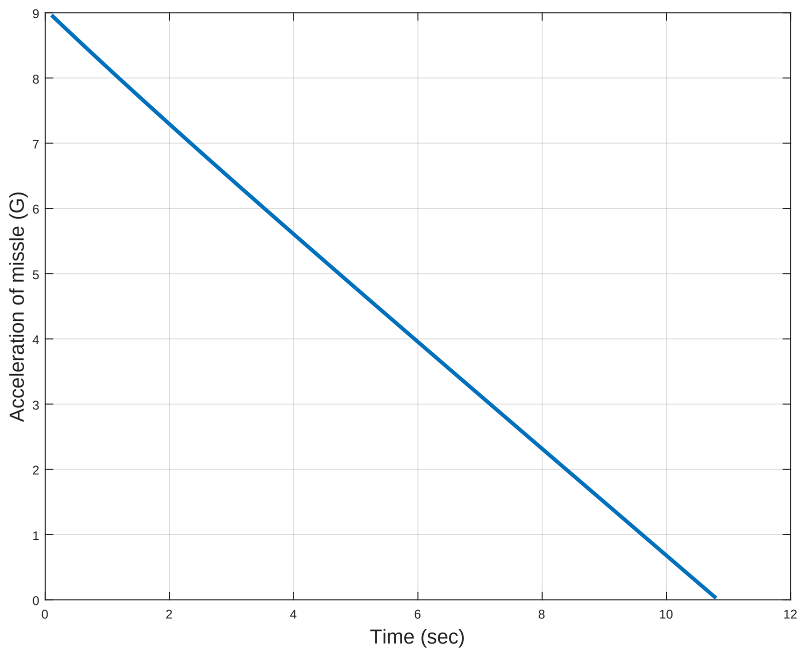

Figure 4.6: Missile acceleration in case of zero target maneuver with heading error=-20 and $N' = 3$.

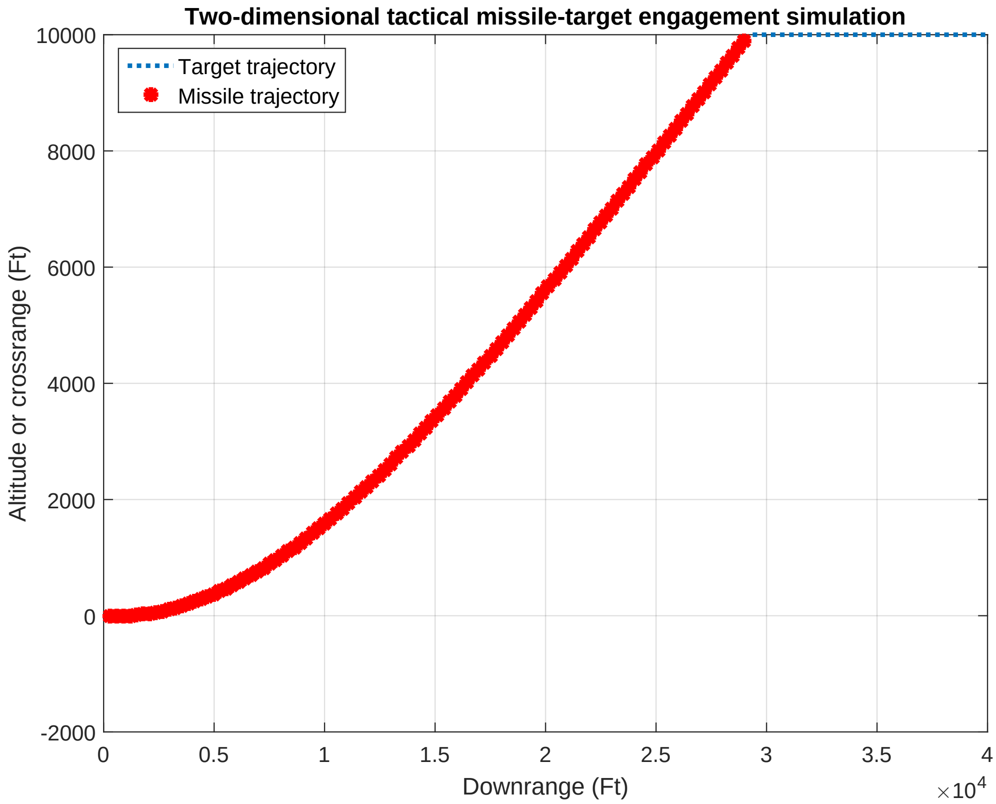

Figure 4.7: Trajectory of the target and attacker in case of zero target maneuver with heading error=-20 and $N' = 4$.

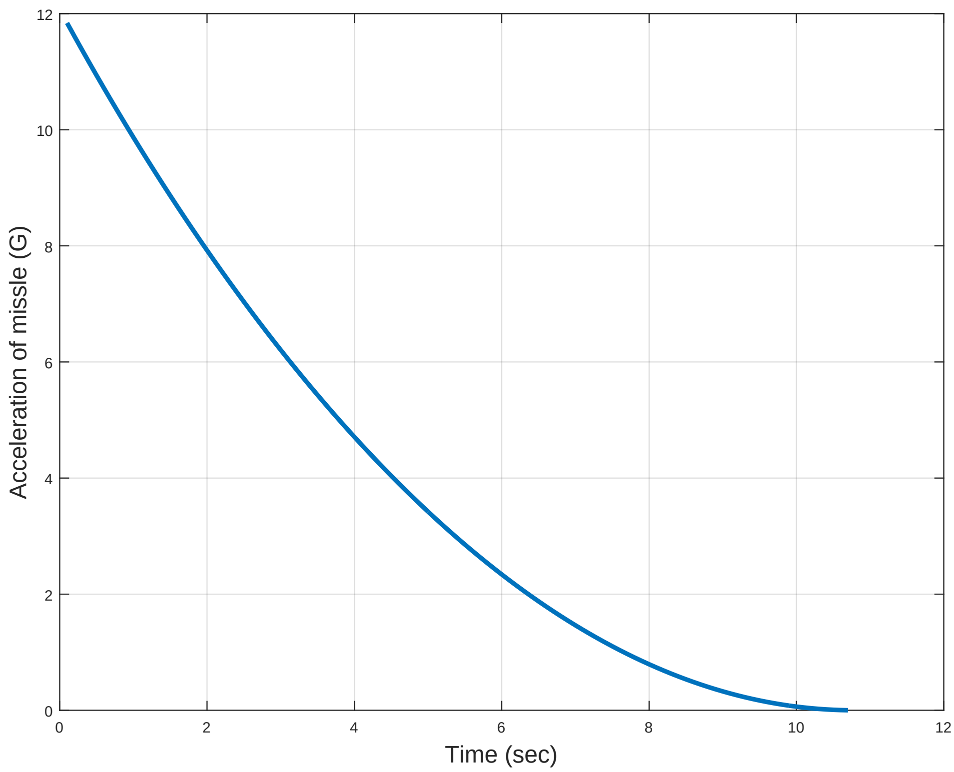

Figure 4.8: Missile acceleration in case of zero target maneuver with heading error=-20 and $N' = 4$.

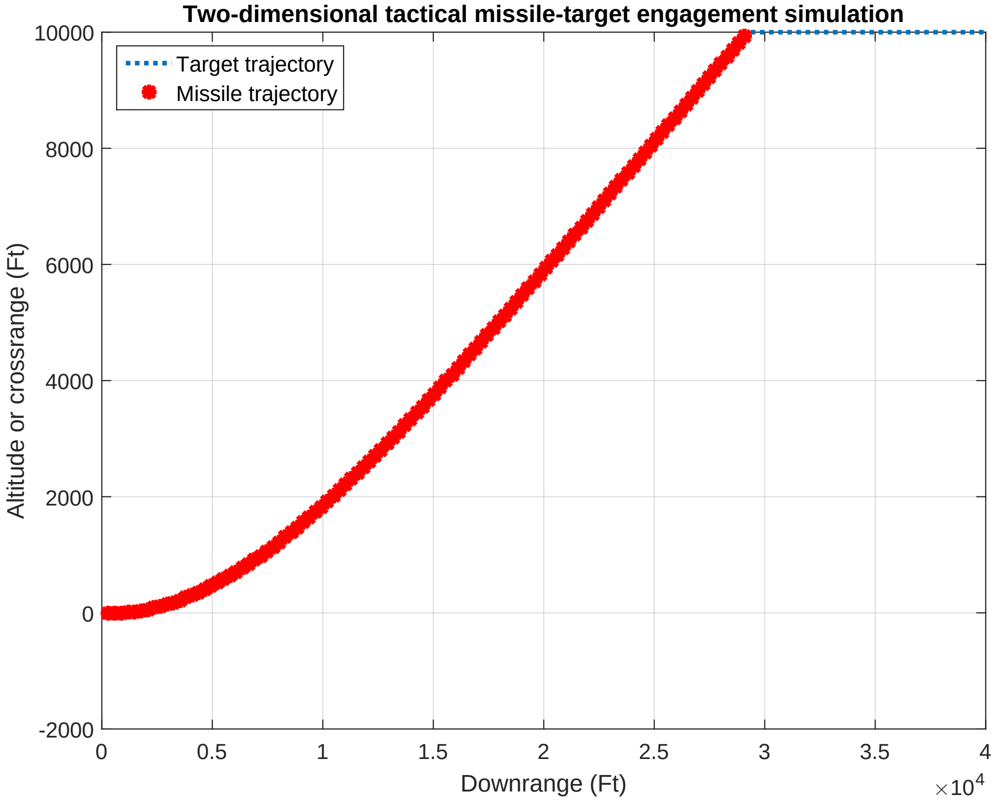

Figure 4.9: Trajectory of the target and attacker in case of zero target maneuver with heading error=-20 and $N' = 5$.

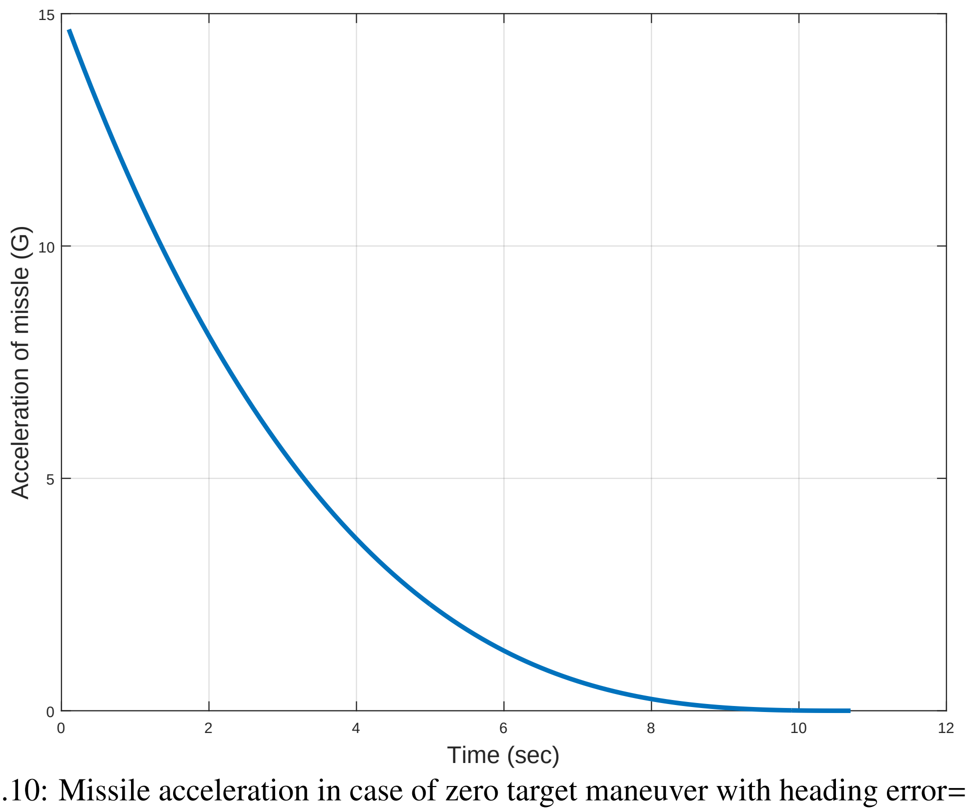

Figure 4.10: Missile acceleration in case of zero target maneuver with heading error=-20 and $N' = 5$.

4.1.1.2 Constant Target maneuver

In this case the target does some effort to escape from the attacker, in the form of constant acceleration (in our example target acceleration = $5G$). We see from Fig. 4.12 and Fig. 4.15 that a higher effective navigation ratio yields less acceleration to hit maneuvering target, and causes the missile to lead the target slightly more than a lower effective navigation ratio does, as we see from Fig. 4.11 and Fig. 4.14.

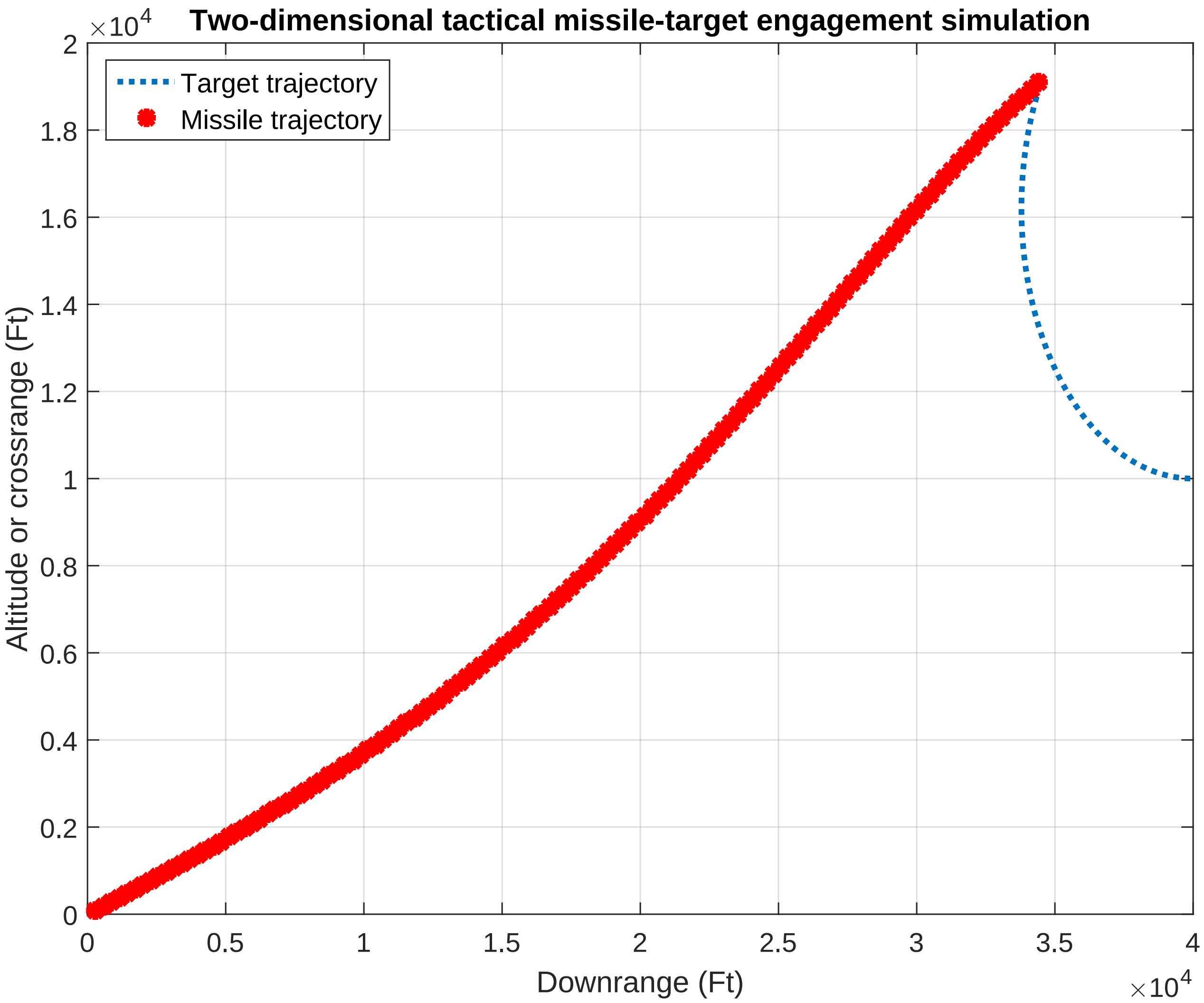

Figure 4.11: Trajectory of the target and attacker in case of constant target maneuver=5G with heading error=0 and $N' = 3$.

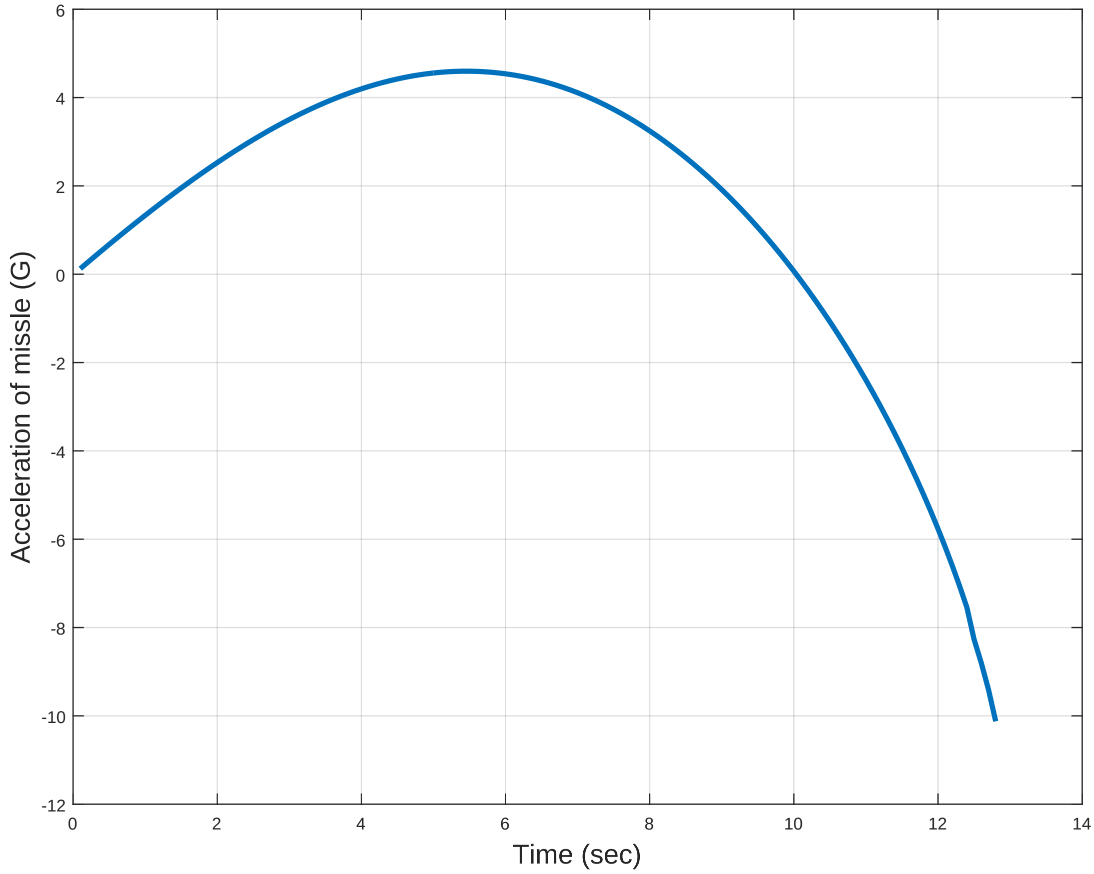

Figure 4.12: Missile acceleration in case of constant target maneuver=5G with heading error=0 and $N' = 3$.

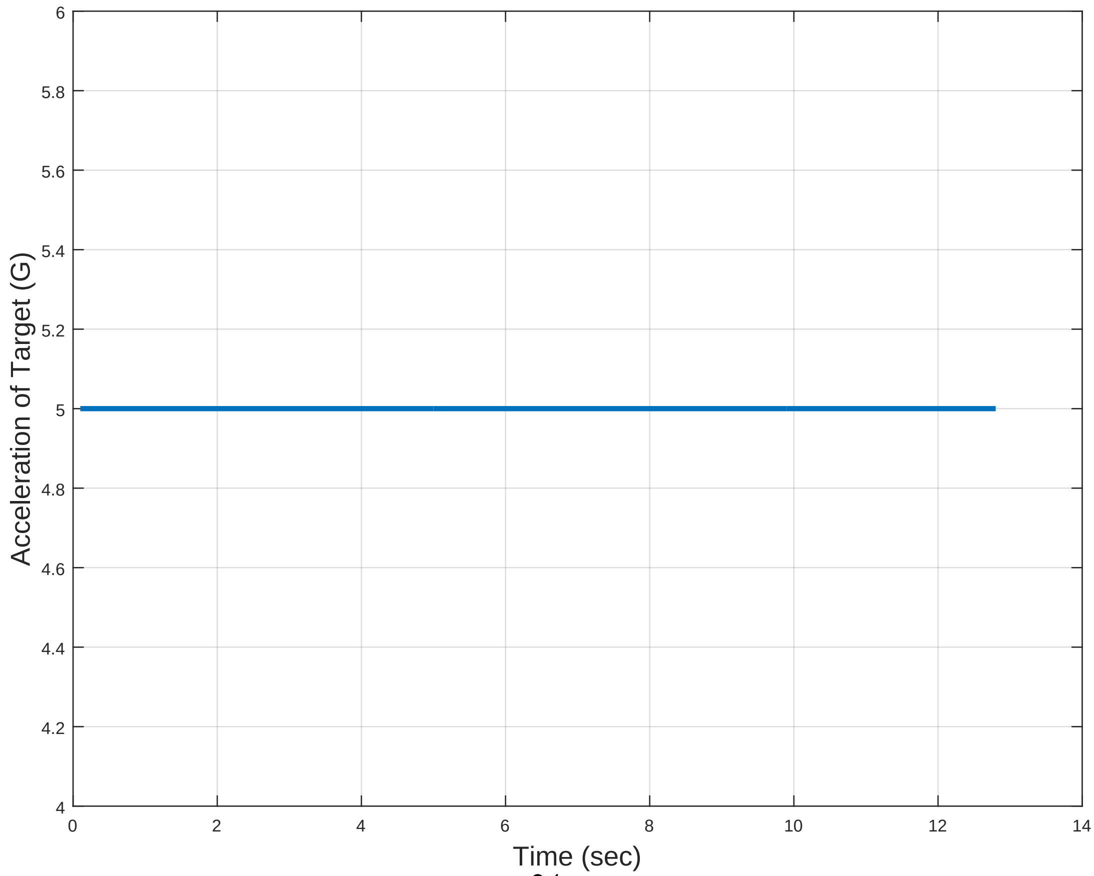

Figure 4.13: Target acceleration in case of zero target maneuver with zero heading error and $N' = 3$.

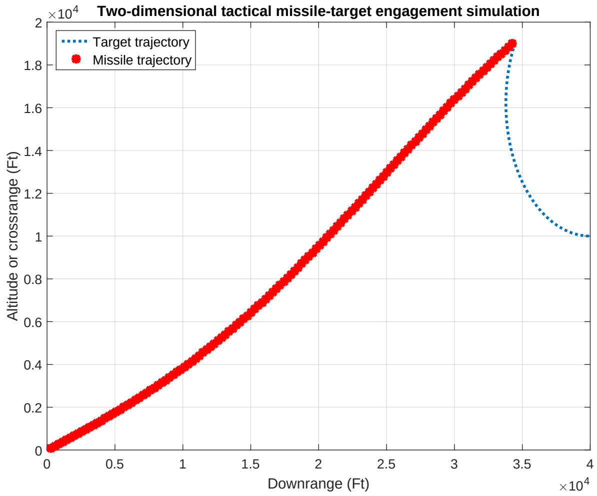

Figure 4.14: Trajectory of the target and attacker in case of constant target maneuver=5G with heading error=0 and $N' = 5$.

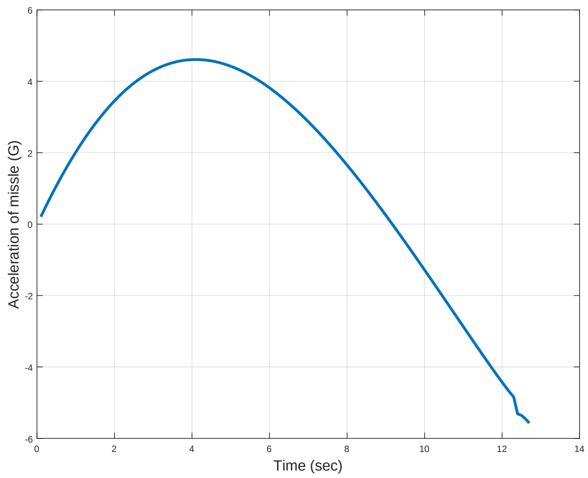

Figure 4.15: Missile acceleration in case of constant target maneuver=5G with heading error=0 and $N' = 5$.

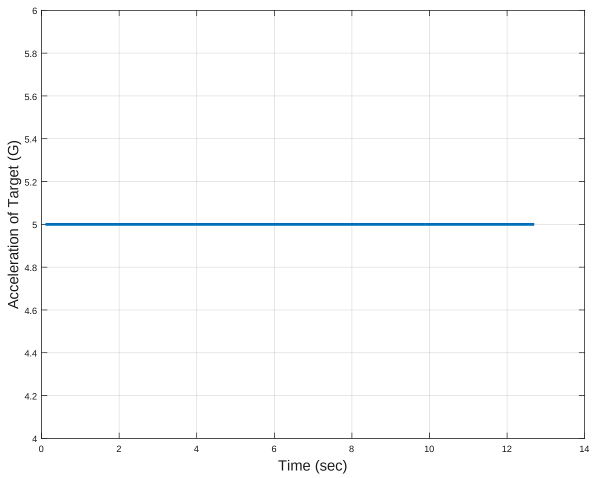

Figure 4.16: Target acceleration in case of zero target maneuver with zero heading error and $N' = 5$.

4.1.1.3 Polynomial Target maneuver

Now we will make the Target maneuver as a polynomial in the form

$$f(t) = c_0 + c_1 T + c_2 T^2 + c_3 T^3 + ... + c_N T^N \tag{4.1}$$

where T is time , c are unknown coefficients of the polynomial and N is the polynomial degree. In our simulation we choose N reasonably $3 \rightarrow 5$ and the coefficients are randomly generated then we solve the proportional navigation equations to get values for two important parameters, namely the miss distance and the command acceleration for the Missile. Then, we calculate the cost function depends on these two parameters, as our target is to maximize miss distance to make the target safe, and maximize command acceleration for the missile, so it bleeds energy before it catches the target. We will do this process many times till the number of runs we need. The next figures shows the trajectories of the Target and Missile for N=3,4 and corresponding missile and target accelerations for each case. In the first case (N=3), as we see from Fig. 4.19 the target have to exert $50G$ to escape from the attacker, these amount of G'es is very high and the pilot could not withstand all this amount. Also, form Fig. 4.18 the attacker have to exert 120 G, this will not happen and the missile's energy will bleed at 100 G after 5 sec. Here the simulation did not till us a complete vision about what will happen. We have to take in consideration the amount of G's that the pilot could resist, so we will use genetic algorithm technique to generate the polynomial because it is easy to control the maximum target acceleration in this method. The second case (N=4), is hypothetical case because the pilot will die in less than 1 sec. If the technology improved and the scientists invent a pilot suit that could resist these huge amount of G'es, then we can take this solution in consideration.

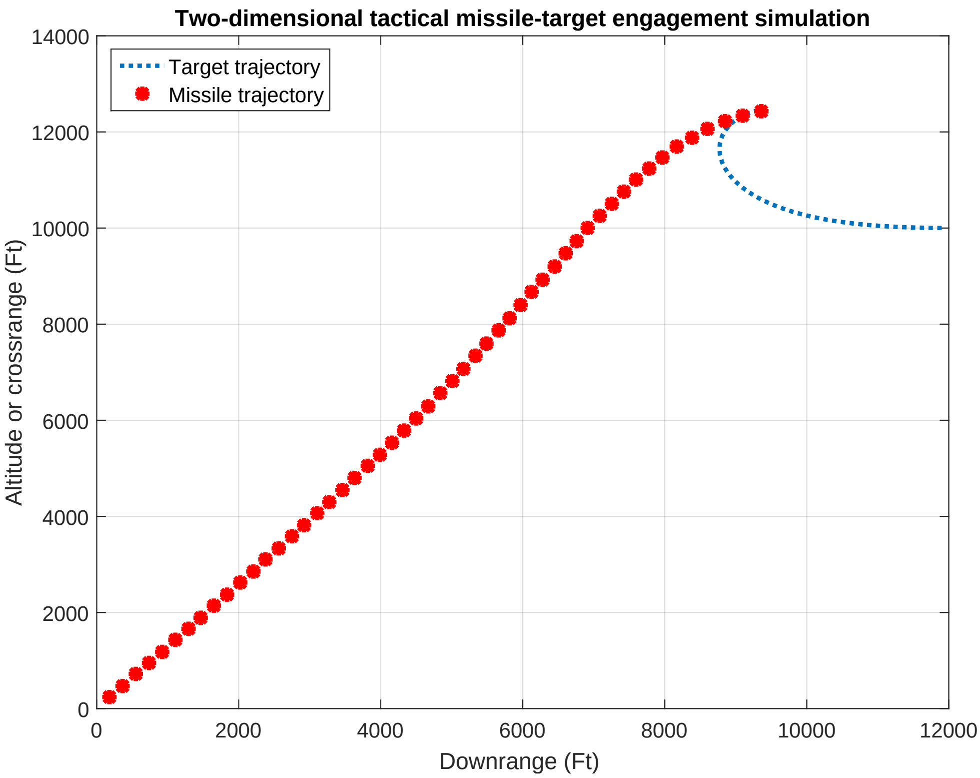

Figure 4.17: Trajectory of the target and attacker in case of polynomial of degree N=3 target maneuver with zero heading error and $N' = 3$.

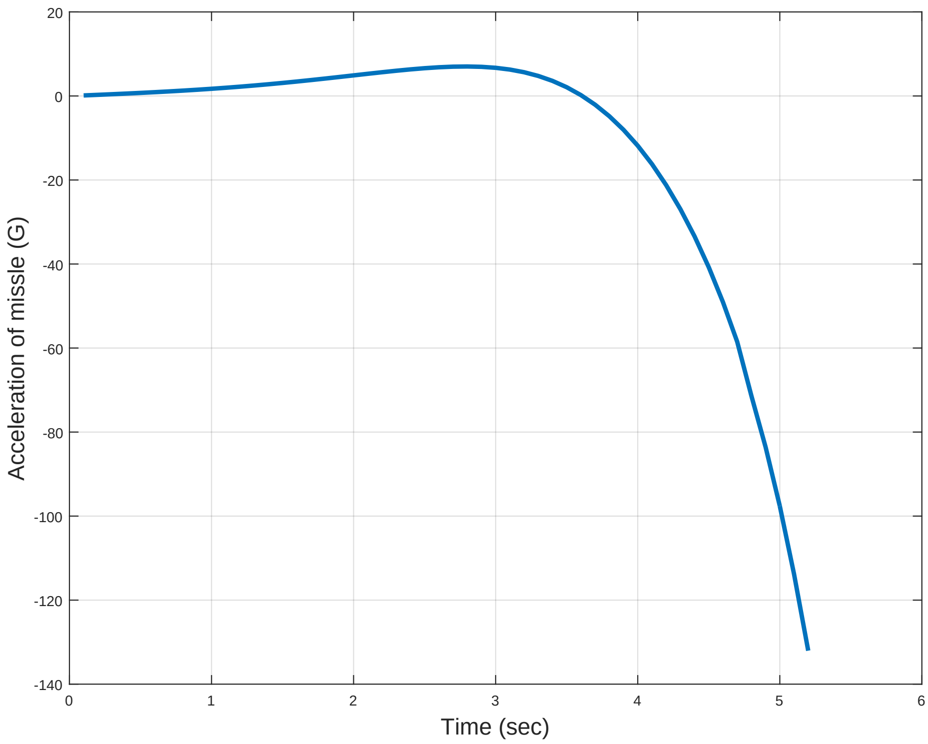

Figure 4.18: Missile acceleration in case of polynomial of degree N=3 target maneuver with zero heading error and $N' = 3$.

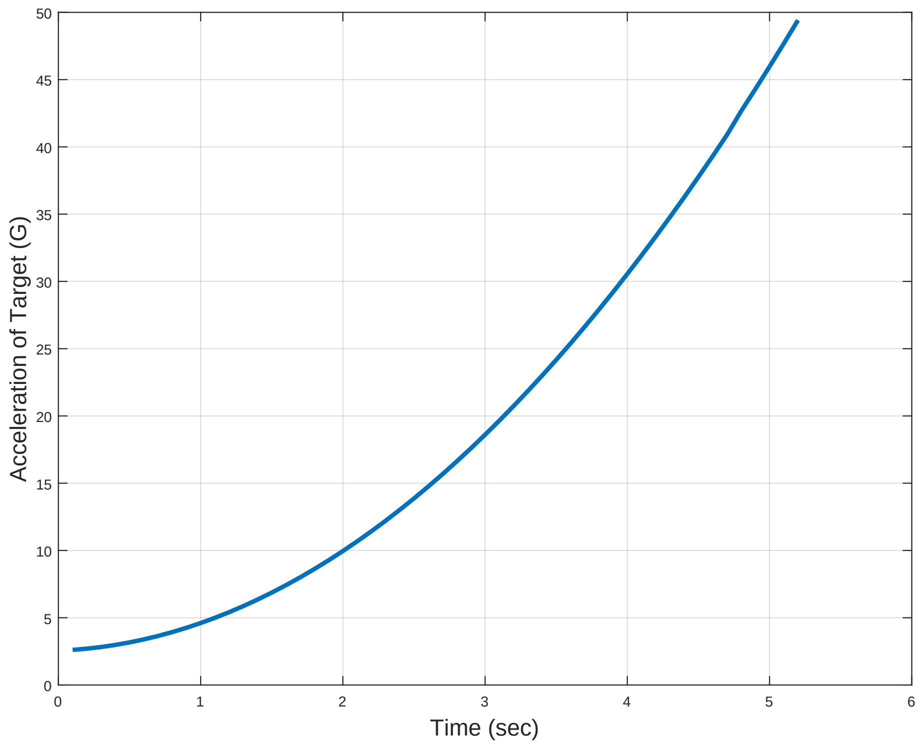

Figure 4.19: Target acceleration in case of polynomial of degree N=3 target maneuver with zero heading error and $N' = 3$.

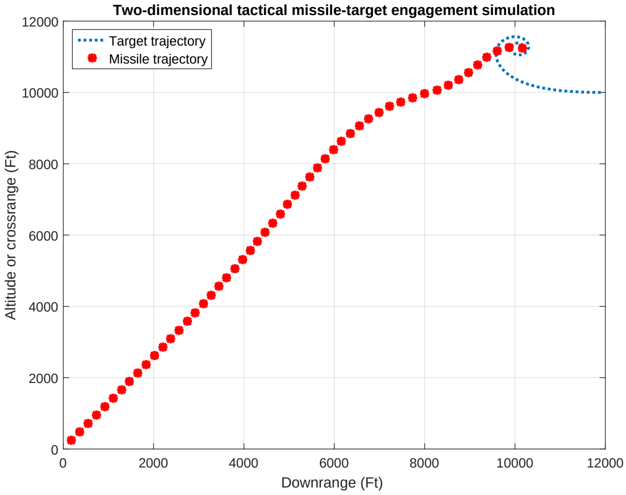

Figure 4.20: Trajectory of the target and attacker in case of polynomial of degree N=4 target maneuver with zero heading error and $N' = 3$.

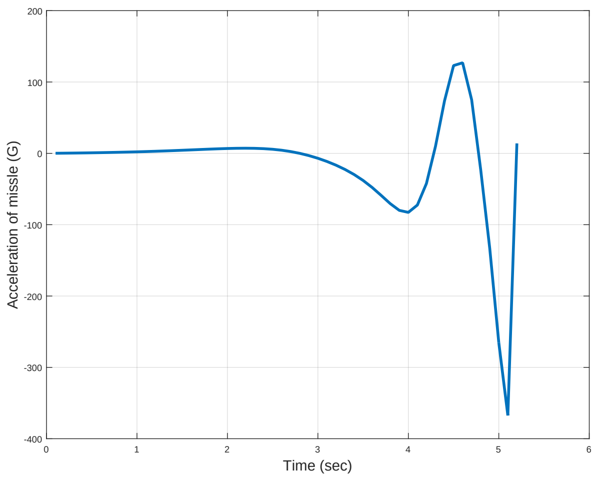

Figure 4.21: Missile acceleration in case of polynomial of degree N=4 target maneuver with zero heading error and $N' = 3$.

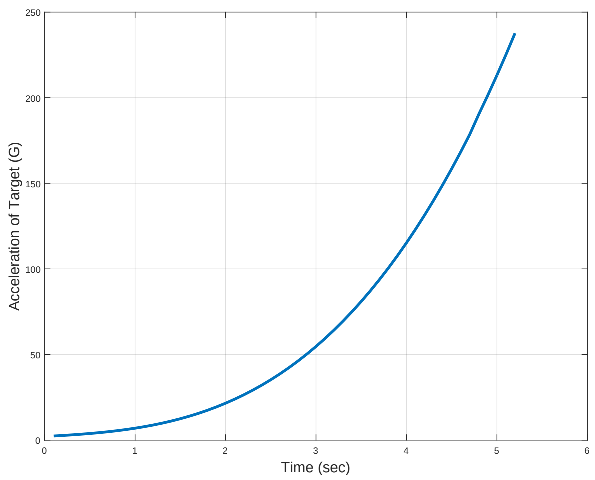

Figure 4.22: Target acceleration in case of polynomial of degree N=4 target maneuver with zero heading error and $N' = 3$.

4.1.1.4 Trapezoidal Target maneuver

Now we will make the Target maneuver as a trapezoidal function (as a general case of tooth and square maneuvers) illustrated in Fig. 4.23

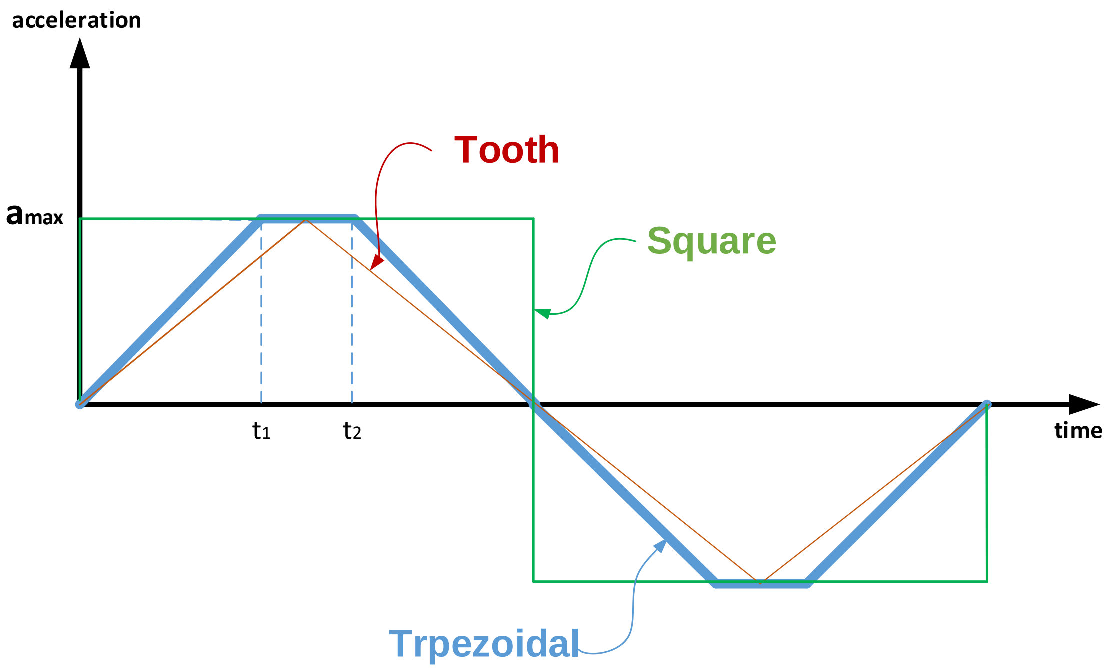

Figure 4.23: Trapezoidal Target maneuver.

In the simulation we choose the value for maximum acceleration. The time of beginning the ramp (which is 0), and the time at the end of the descent, t_1 and t_2 are variables.

We have two cases: **First case:** the maneuver is *symmetric* so we have two extreme cases.

- when t_1 is equal to zero (there is no ascend ramp) so t_2 is at the middle of the maneuver; this leads to *square* target maneuver.

- when t_1 equals t_2 at the quarter of the maneuver; this leads to *tooth* target maneuver.

Varying t_1 and t_2, starting from the square case till the tooth case, until we find the optimum solution based on or cost function which depends on the values of the miss distance and Missile acceleration.

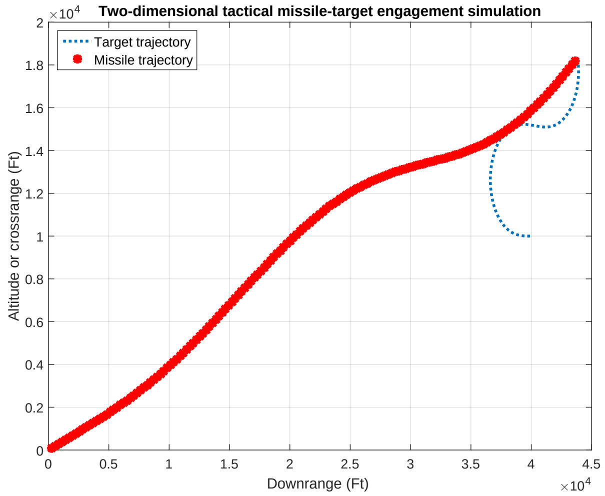

Figure 4.24: Trajectory of the target and attacker in case of symmetric trapezoidal target maneuver with zero heading error and $N' = 5$.

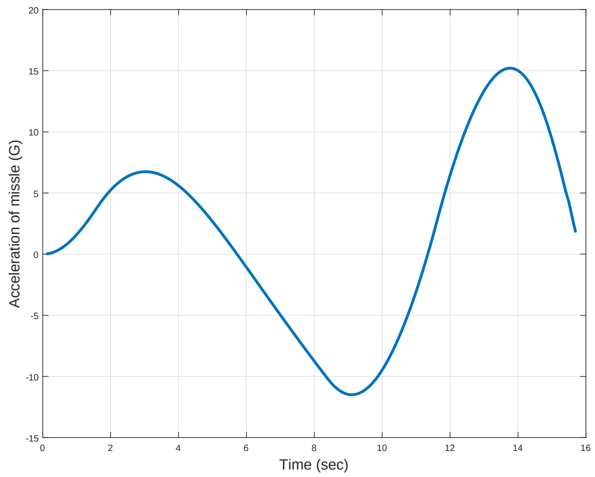

Figure 4.25: Missile acceleration in case of symmetric trapezoidal target maneuver with zero heading error and $N' = 5$.

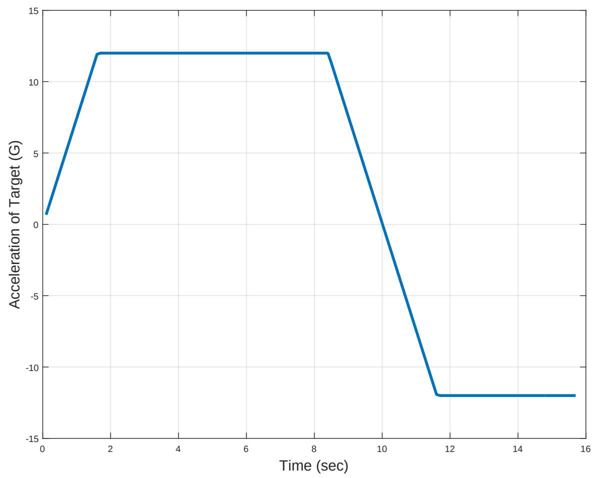

Figure 4.26: Target acceleration in case of symmetric trapezoidal N=4 target maneuver with zero heading error and $N' = 5$.

Second case: the maneuver is *not symmetric* so we put a first value for t_1 (starting with zero) and varying t_2 till we scan all the domain, then change t_1 slightly and scan all the domain again with t_2 till we find the optimum solution.

What about if the optimum solution for the target maneuver did not have Identical halves? and all the slops are not related to each other. We will try to figure that using genetic algorithm in the next section.

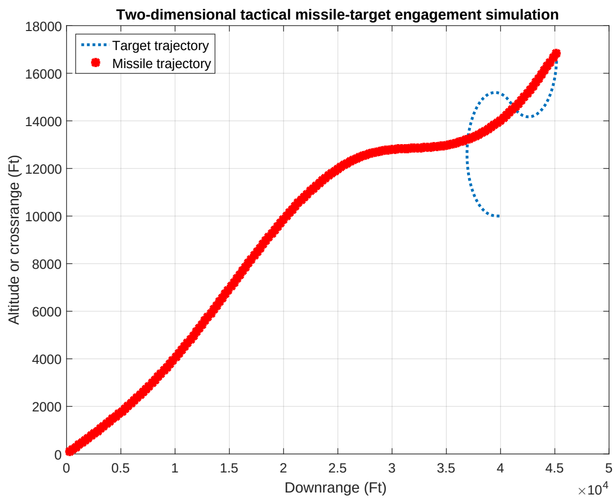

Figure 4.27: Trajectory of the target and attacker in case of trapezoidal target maneuver with zero heading error and $N' = 5$.

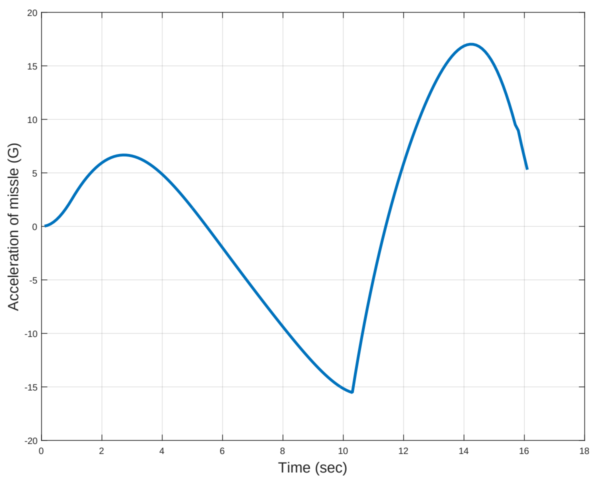

Figure 4.28: Missile acceleration in case of trapezoidal target maneuver with zero heading error and $N' = 5$.

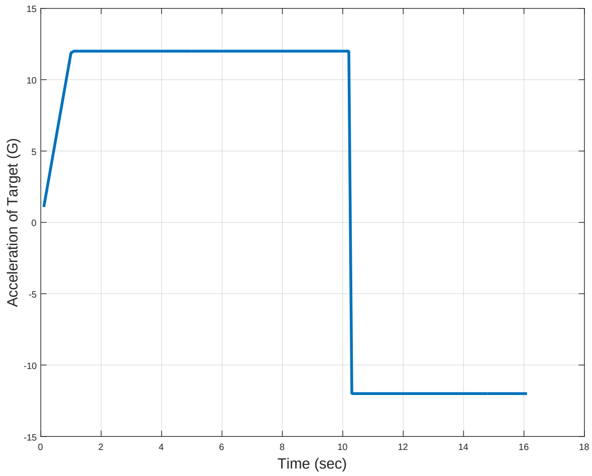

Figure 4.29: Target acceleration in case of trapezoidal N=4 target maneuver with zero heading error and $N' = 5$.

4.2 Guidance Toolbox

All the previous results could be generated from a simple GUI (graphic user interface), (Fig.4.30). The inputs for this GUI is the locations and velocities for the Target (plane) and the Attacker (missile). Then the user have to choose the guidance law, which is the way that the Attacker tracking the Target, and there is 3 options :

- Proportional Navigation (PN)
- Augmented Proportional Navigation
- Optimal Guidance

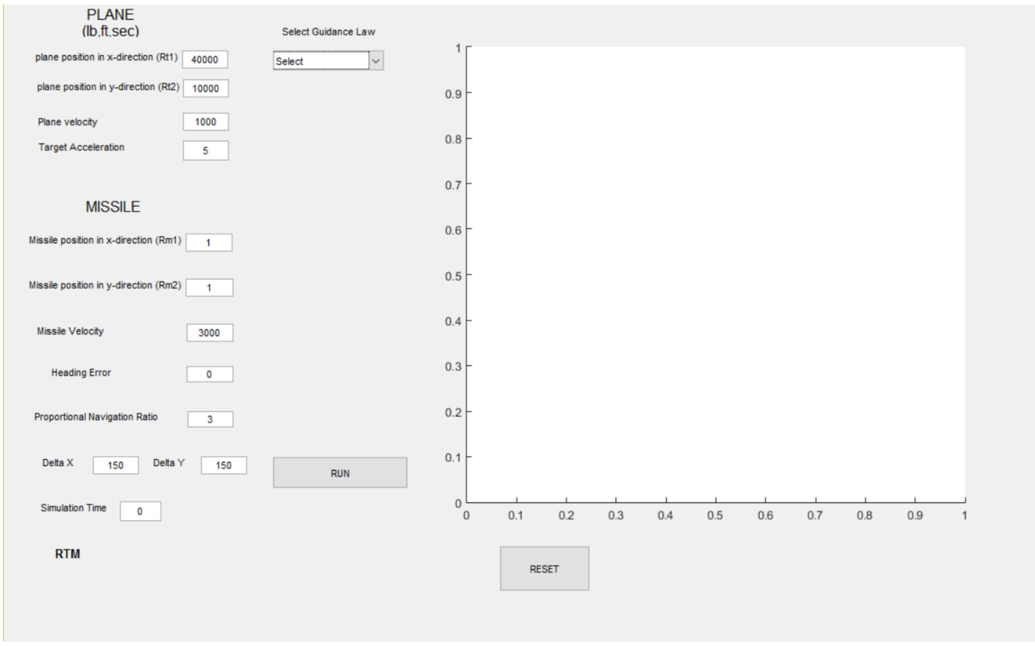

Figure 4.30: Guidance Toolbox

If the user chooses the PN guidance law (Fig.4.31) , there will be more options be available, Now he could select the type of escape maneuver:

- Polynomial
- Trapezoidal
- Symmetric Trapezoidal

and the result will be optimized escape maneuver.

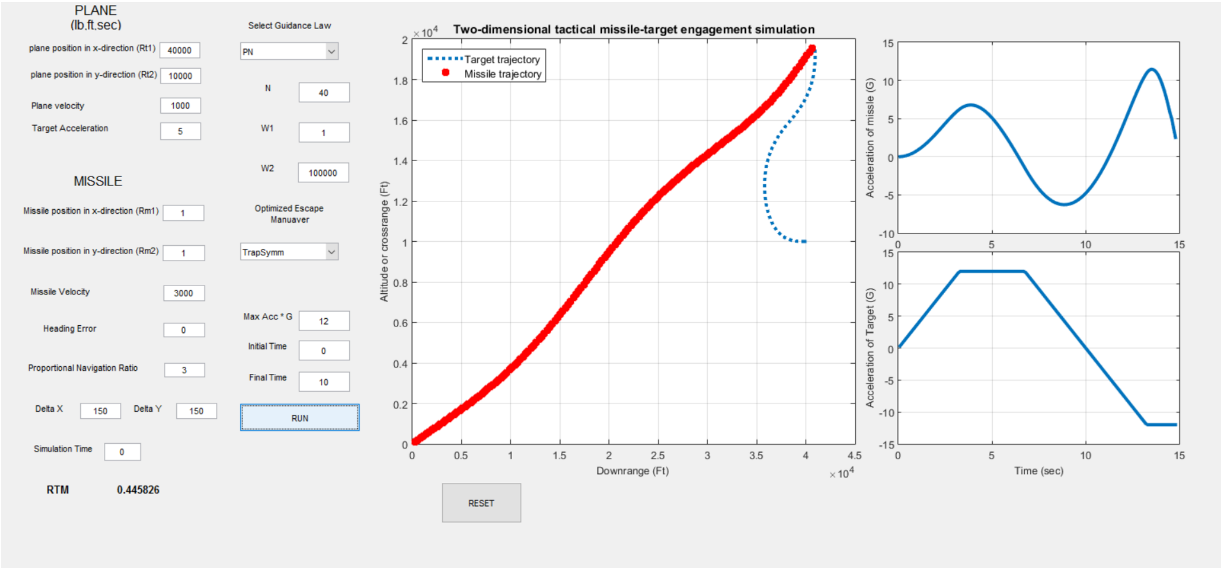

Figure 4.31: Guidance Toolbox options when PN selected

4.3 Genetic Algorithm Solution [using simulink]

In this subsection we will use the power of blocks in Simulink to solve the differential equations in section 3.1.1 in an easy way (Fig. 4.32). We will make these equations as a main block (Fig. 4.33) and as we change the inputs, we get the same results. The advantage of using simulink is to use the main block with an alternative optimization technique (like genetic algorithms) and we will simulate two cases, polynomial and trapezoidal. Now let us have a brief introduction to the genetic algorithm technique.

4.3.1 Introduction to Genetic Algorithm technique

Genetic algorithm is a *stochastic population-based* search method. Genetic Algorithms (GAs) are search algorithms based on the mechanics of the natural selection process (biological evolution). The most basic concept is that the strong tend to adapt and survive while the weak tend to die out. That is, optimization is based on evolution, and the "Survival of the fittest" concept. GAs have the ability to create an initial population of feasible solutions, and then recombine them in a way to guide their search to only the most promising areas of the state space. Each feasible solution is encoded as a chromosome (string) also called a genotype, and each chromosome is given a measure of fitness via a fitness (evaluation or objective) function.

- The fitness of a chromosome determines its ability to survive and produce offspring.
- A finite population of chromosomes is maintained.
- GAs use probabilistic rules to evolve a population from one generation to the next. The generations of the new solutions are developed by genetic recombination operators:
  - Biased Reproduction: selecting the fittest to reproduce.
  - Crossover: combining parent chromosomes to produce children chromosomes.
  - Mutation: altering some genes in a chromosome.

Most Important Parameters in GAs:

- Population Size
- Evaluation Function
- Crossover Method
- Mutation Rate

Use Genetic Algorithms:

- When facing a problem of local minima.
- When a good fitness function is available.
- When a near-optimal, but not optimal solution is acceptable.
- When the state-space is too large for other methods.

4.3.2 COMPONENTS OF GENETIC ALGORITHMS

Representation (definition of individuals):

Objects forming possible solution within original problem context are called phenotypes, their encoding, the individuals within the GA, are called genotypes. The representation step specifies the mapping from the phenotypes onto a set of genotypes. Candidate solution, phenotype and individual are used to denote points of the space of possible solutions. This space is called phenotype space. Chromosome, and individual can be used for points in the genotye space. Elements of a chromosome are called genes. A value of a gene is called an allele. The GA works with a coding of the parameter rather than the actual parameter. Depending on the particular problem, the coding may be Boolean-valued, integer-valued, real-valued, complex-valued, vector-valued, symbolic valued, or multiple-valued.

Evaluation function:

This is just the cost or the objective function which represent what we want to maximize. For minimization problem use the reciprocal (i.e. 1/f).

Population:

The role of the population is to hold possible solutions. A population is a multiset of genotypes. In GA, the population size is (almost always) constant. The bigger the size, the better the final solution, and the larger the execution time.

Parent Selection Mechanism:

The role of parent selection (mating selection) is to distinguish among individuals based on their quality to allow the better individuals to become parents of the next generation. Parent selection is probabilistic. Thus, high quality individuals get a higher chance to become parents than those with low quality. Nevertheless, low quality individuals are often given a small, but positive chance; otherwise the whole search could become too greedy and get stuck in a local optimum.

Variation Operators:

The role of variation operators is to create new individuals from old ones. Variation operators form the implementation of the elementary steps with the search space.

Mutation Operator:

A unary variation operator is called *mutation*. It is applied to one genotype and delivers a modified mutant, the child or *offspring* of it. In general, mutation is supposed to cause a random unbiased change.

Crossover Operator:

A binary variation operator is called recombination or crossover. This operator merges information from two parent genotypes into one or two offspring genotypes. Similarly to mutation, crossover is a stochastic operator: the choice of what parts of each parent are combined, and the way these parts are combined, depend on random drawings. The principle behind crossover is simple: by mating two individuals with different but desirable features, we can produce an offspring which combines both of those features.

Survivor Selection Mechanism:

The role of survivor selection is to distinguish among individuals based on their quality. In GA, the population size is (almost always) constant, thus a choice has to be made on which individuals will be allowed in the next generation. This decision is based on their fitness values, favoring those with higher quality. As opposed to parent selection which is stochastic, survivor selection is often deterministic, for instance, ranking the unified multiset of parents and offspring and selecting the top segment (fitness biased), or selection only from the offspring (age-biased).

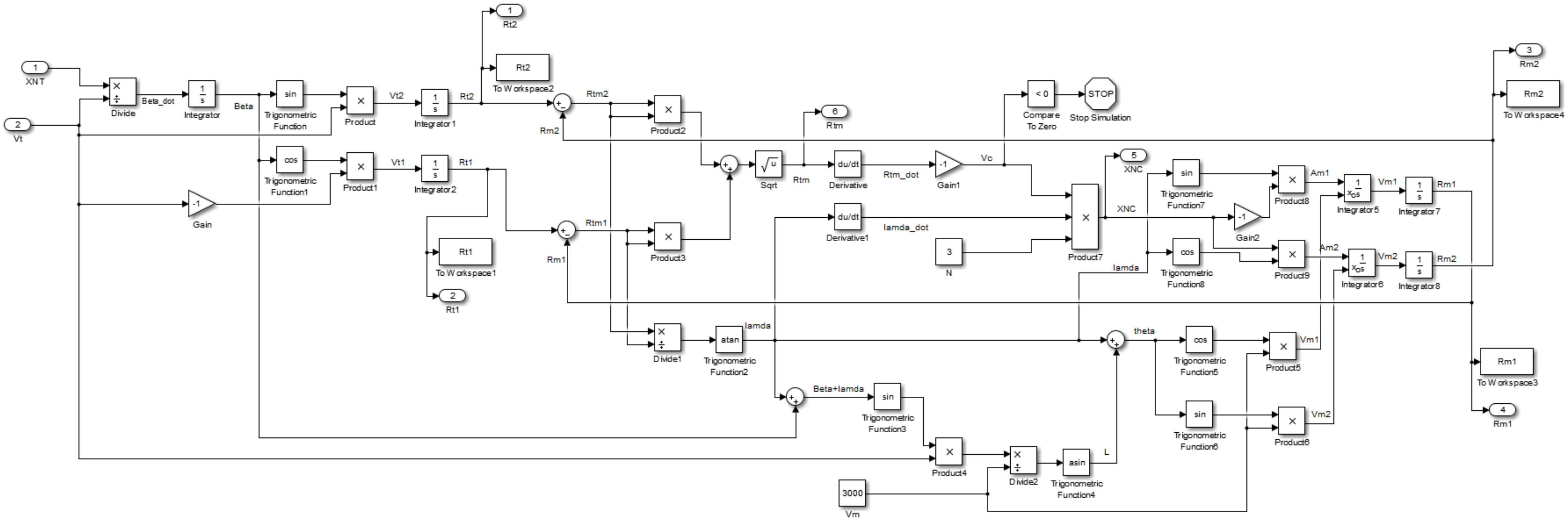

Figure 4.32: The Simulink model for proportional navigation equations in sec 3.1.1

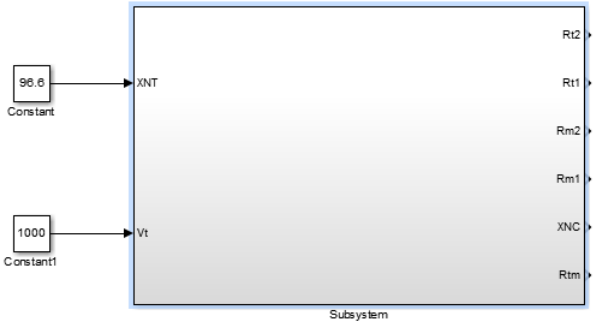

Figure 4.33: The Simulink main block for solving proportional navigation equations in sec 3.1.1

4.3.3 Results

We will use the main block we have created with the genetic algorithm toolbox in MATLAB in the same manner we have done, let the target maneuver unknown, then it is required to find it using genetic algorithm to maximize miss distance and missile acceleration. We have two cases of the target maneuver:

4.3.3.1 Polynomial Target Maneuver

let the target maneuver ba a polynomial with unknown coefficients, then it is required to find the values of these coefficients using genetic algorithm toolbox in Matlab (Fig. 4.34) to maximize miss distance and missile acceleration. The result for the best fitness values are in Fig.4.35. The optimized target acceleration and trajectory simulation are in figures 4.36 and 4.37.

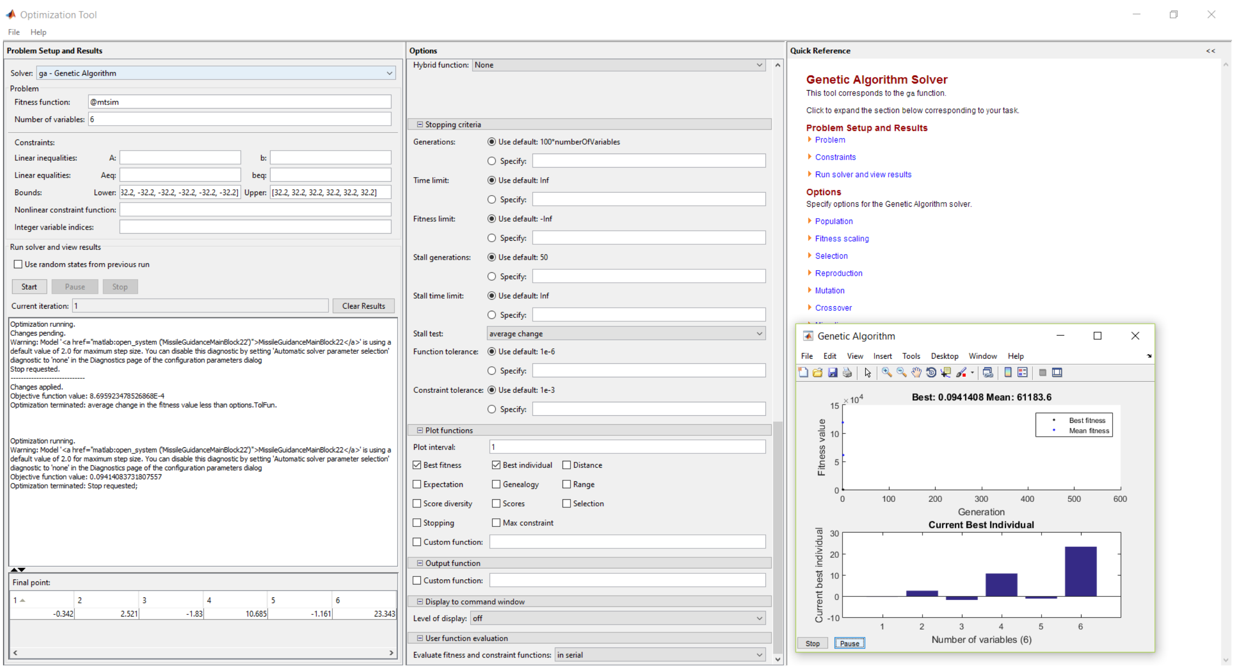

Figure 4.34: Genetic Algorithm Toolbox in Matlab.

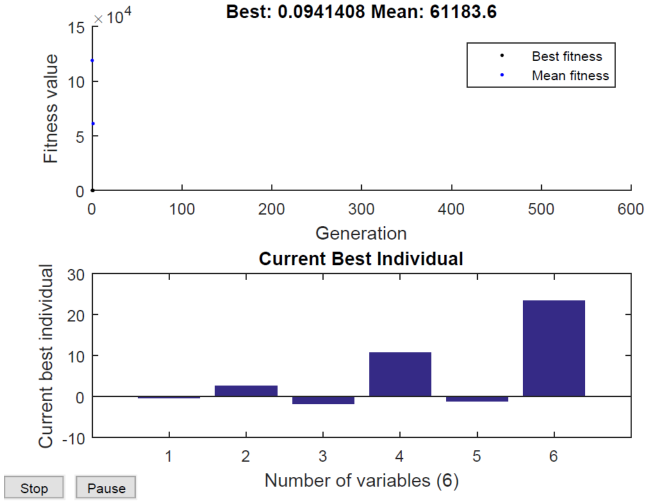

Figure 4.35: Best fitness values

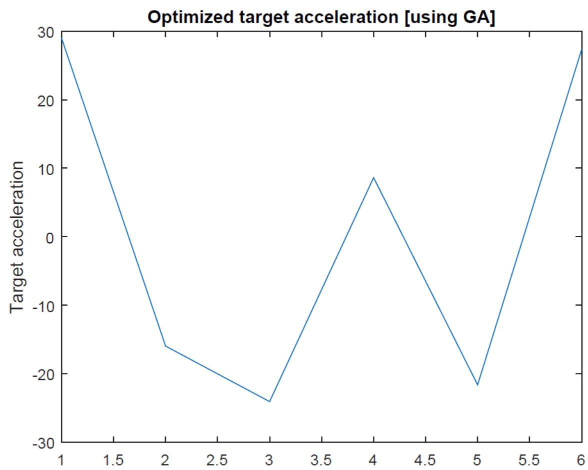

Figure 4.36: Optimized target acceleration using GA.

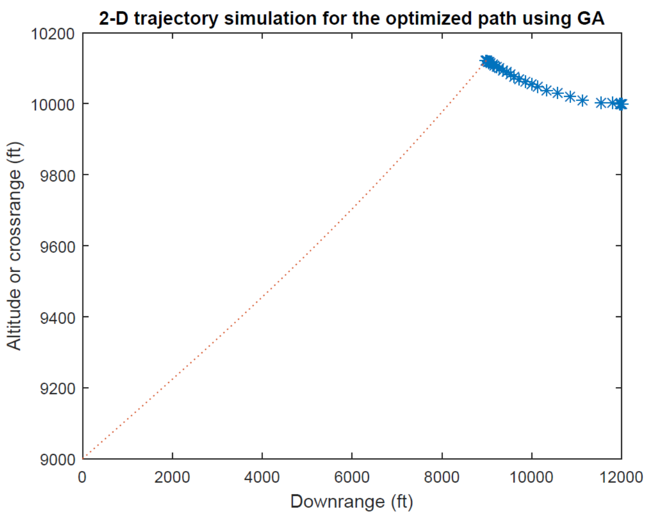

Figure 4.37: Optimized trajectory using GA.

4.3.3.2 Trapezoidal Target Maneuver

Chapter 5: Game

In this chapter we want to have the contribution of the human intelligence in making decisions, so we made a simulation game using *Unity*.

5.1 Introduction to Unity

Unity is a cross-platform game engine (Fig. 5.1) developed by Unity Technologies and used to develop video games for PC, consoles, mobile devices and websites. It is a free software (https://unity3d.com/),working with C# programming language.

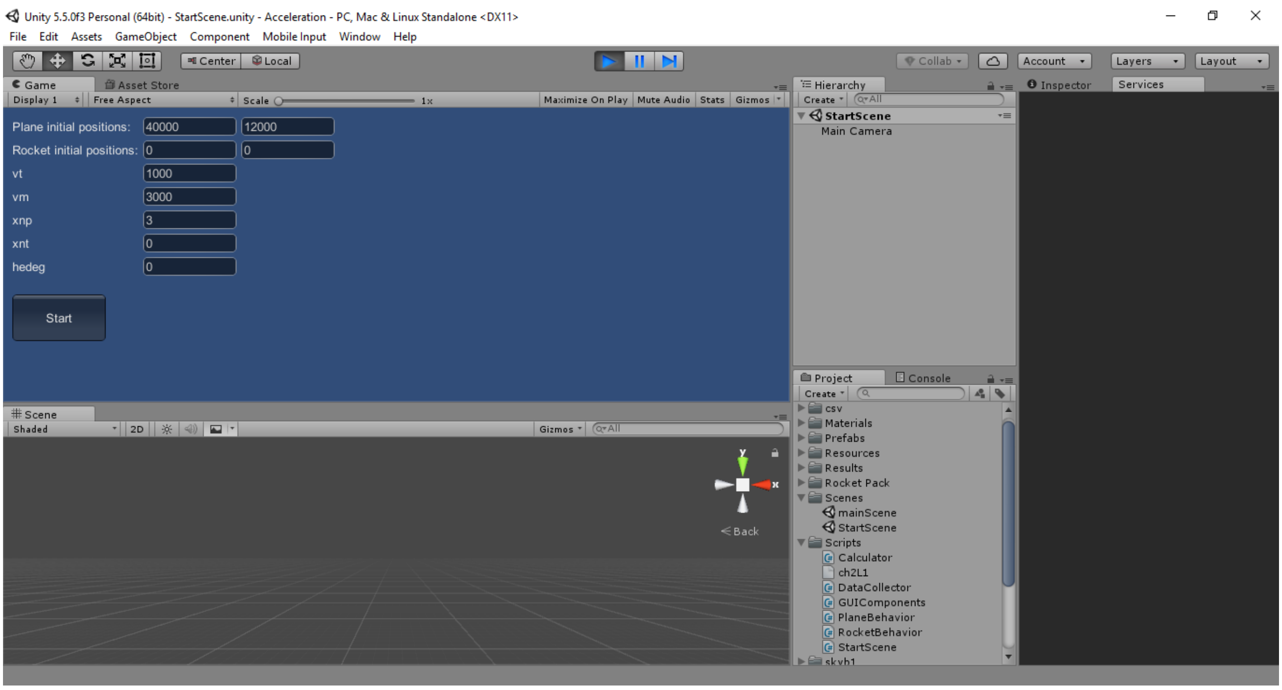

Figure 5.1: Unity game engine interface

5.2 Methodology of the game

The game (Fig. 5.2) consists of two objects: plane (Target) and missile (Attacker). A human player controls the increasing and decreasing of the target acceleration (XNT) by two arrows on the keyboard. The missile object is moving on according to the proportional navigation guidance law (in sec. 3.1).

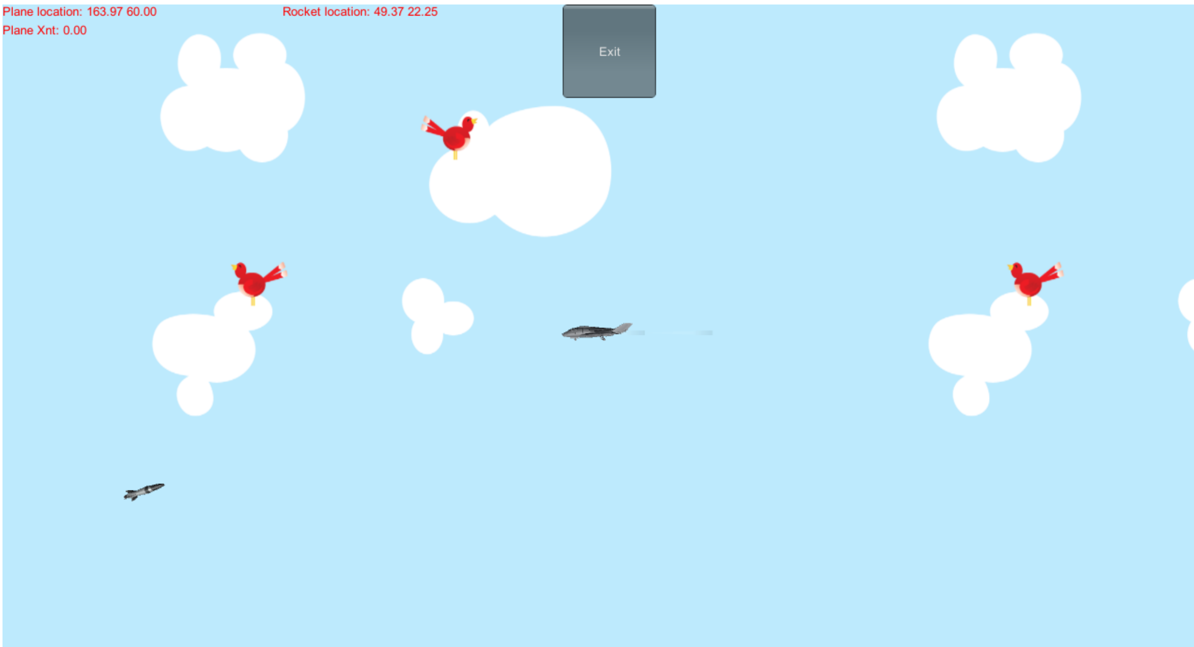

Figure 5.2: Unity game for simulating Target-Attacker engagement

Each game consists of two scenes:

1. Starting scene.
2. Game scene, which updated each frame per second.

In the starting scene there is data fields (position, velocity, ...). After this scene ends, all the data are destroyed, so we save the information we need in file called ”player prefs”.

The game scene consists of some objects, each object has his own script, this script must contain 2 points:

- Start: initialization.
- Updated : every frame.

In our game we have 3 objects:

1. **Plane:** its script contain some commands to control the plane with two arrows in the keyboard, which increase and decrease the target acceleration by upward arrow and downward arrow respectively.
2. **Missile:** it does not contain a script, the equations controlling its behavior is in the script with the ”Data collector” object.
3. **Object ”Data collector”:** its script consists of:
   - Start
     (a) initialization of the variables in the equations.
     (b) set the location of all objects (plane and missile).
   - Update

(a) get plane location.
(b) execute your equations.
(c) update rocket location (according to PN equations).
(d) update informations to be printed to excel.
(e) check the breaking condition, if true, load starting scene.

5.3 Results

Part III

TARGET-ATTACKER-DEFENDER PROBLEM

Chapter 6: TARGET-ATTACKER-DEFENDER PROBLEM

6.1 Problem Statement

6.2 Assumptions, Notation, and Nomenclature

Assumptions

1. The speeds V_T, V_A, and V_D of the Target, Attacker, and Defender are constant.
2. The Attacker missile is faster than the Target aircraft, i.e., $\alpha \equiv \frac{V_T}{V_A} < 1$ (In the case $\alpha \geq 1$, the Target is guaranteed to survive by following an optimal strategy, even without assistance from the Defender).
3. There are three distinct cases for the ratio of the speed of the Attacker to that of the Defender $\gamma = \frac{1}{\beta} = \frac{V_A}{V_D}$
   - $\gamma < 1$ (fast Defender) discussed earlier in Garcia et el. [48], and extended, expounded, simplified and exposed herein.
   - $\gamma = 1$ (same speed Defender) discussed in Garcia et el. [47, 49], and extended, expounded, simplified and exposed herein.
   - $\gamma > 1$ (slow Defender), which is a novel case, discussed herein for the first time, and unified with the two previous cases.
4. The Defender intercepts the Attacker if their separation becomes zero (point capture).
5. The optimal trajectories of the three agents are straight lines.
6. A Cartesian frame is attached to the initial positions A and D of the Attacker and Defender in such a way the X-axis is the infinite extension of the straight segment $\overline{AD}$ and the Y-axis is the perpendicular bisector of $\overline{AD}$.

Notation

- A: Initial position of the Attacker.
- D: Initial position of the Defender.
- T: Initial position of the Target.
- T' Terminal position of the Target, i.e., its position at the time the Defender intercepts the Attacker.

- $\alpha = \dfrac{V_T}{V_A}$ (assumed < 1, otherwise the target trivially survives).

- $\gamma = \dfrac{1}{\beta} = \dfrac{V_A}{V_D}$ (studied for a fast Defender ($\gamma < 1$), a similar Defender ($\gamma = 1$), and a slow Defender ($\gamma > 1$)).

- u, v, w: Aim points on the AD Apollonius circle by the Attacker, Target and Defender, respectively.

Nomenclature

The AD Apollonius circle. The locus of a point such that the ratio of its distance from the initial positions $\boldsymbol{A} = (x_A, 0)$ and $\boldsymbol{D} = (-x_A, 0)$ of the Attacker and Defender, respectively, is a fixed ratio $\gamma = \dfrac{V_A}{V_D}$. This circle degenerates into the perpendicular bisector of $\overline{AD}$ if $\gamma = 1$. Points on the circumference of this circle are reached simultaneously by the Attacker and Defender. For $\gamma < 1$, $\boldsymbol{A}$ belongs to the interior of this circle and points within the circle are reached by the Attacker before the Defender. For $\gamma > 1$, $\boldsymbol{D}$ belongs to the interior of this circle and points within the circle are reached by the Defender before the Attacker. For $\gamma = 1$, the AD circle becomes of infinite radius and degenerates into a straight line, namely the perpendicular bisector of $\overline{AD}$. In this case, $\boldsymbol{A}$ belongs to the R.H.S. of the $XY-$plane where points are reached by the Attacker before the Defender, while $\boldsymbol{D}$ belongs to the L.H.S. of the $XY-$plane where points are reached by the Defender before the Attacker.

The TA Apollonius circle. The locus of a point such that the ratio of its distances from the initial positions $\boldsymbol{T} = (x_T, y_T)$ and $\boldsymbol{A} = (x_A, 0)$, of the Target and Attacker, respectively, is a fixed ratio $\alpha = \dfrac{V_T}{V_A}$ strictly less than 1. Naming of the AD and TA Apollonius circles herein follows a common practice in mathematical circles [72, 73, 74] and is opposite to the style used by Garcia et al. [47, 48, 49].

Region reachable by the Defender before the Attacker (Reachability region R_r):
For $\gamma < 1$, R_r is the exterior of the AD Apollonius circle.
For $\gamma = 1$, R_r is the L.H.S. of the $XY-$plane.
For $\gamma > 1$, R_r is the interior of the AD Apollonius circle.

Figure 6.1 illustrates this region as a shaded region to which point D belongs.

Region of guaranteed Target's escape (Escape region R_e). The escape region R_e is the set of all coordinate pairs (x, y) such that if the Target initial position $\boldsymbol{T} = (x_T, y_T)$ is inside this region, then it is guaranteed to escape the Attacker if both the Target and Defender implement their corresponding optimal strategies. This set is a strict superset of the set of points reachable by the Defender before the Attacker ($R_e \supseteq R_r$). The boundary of this set is called a Voronoi Diagram.

The critical speed ratio $\overline{\alpha}$. A lower limit on the speed ratio $\gamma = \dfrac{V_T}{V_A}$, attained when the TA Apollonius circle is tangent to the AD Apollonius circle (or to the perpendicular bisector of $\overline{AD}$ in the degenerate case $\gamma = 1$).

Escape Condition. For a given speed ratio $\alpha = \dfrac{V_T}{V_A}$ and a given Attacker's initial position $\boldsymbol{A} = (x_A, 0)$, the escape condition is that the TA Apollonius circle (of center O_2 and radius r_2)

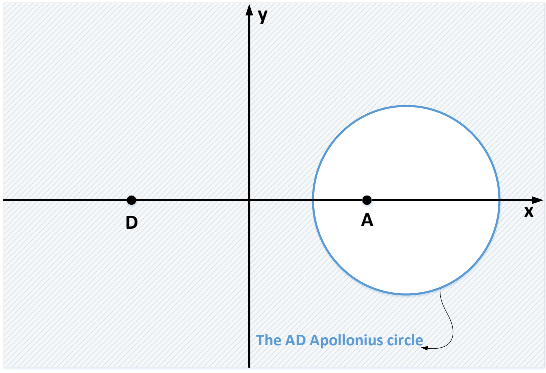

(a) $\gamma < 1$.

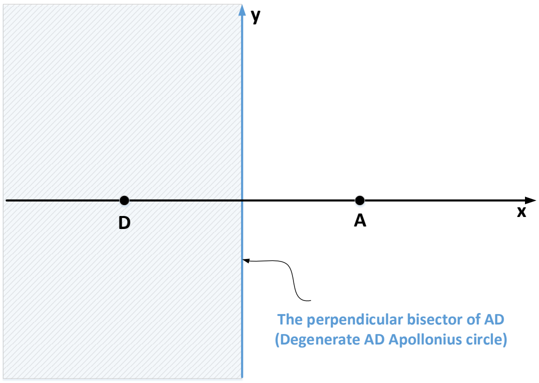

(b) $\gamma = 1$.

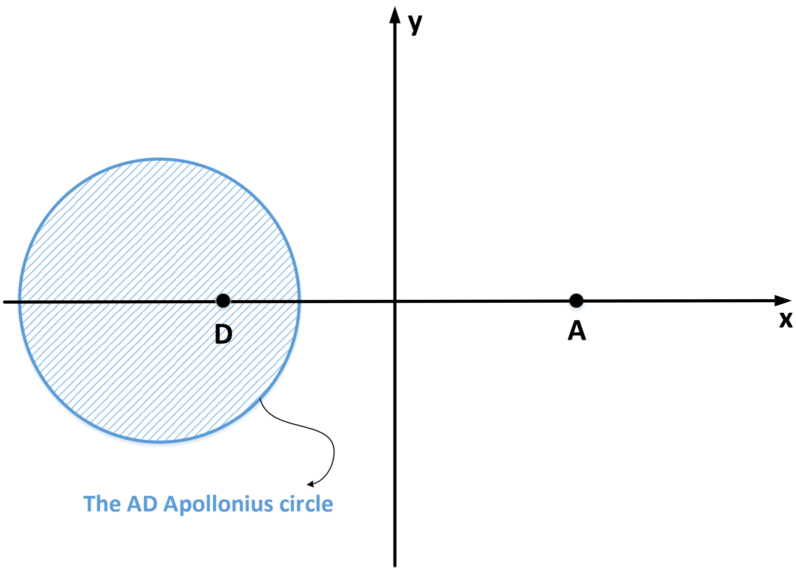

(c) $\gamma > 1$.

Figure 6.1: The reachability region R_r (one including $\boldsymbol{D}$ whose points are reached by the Defender before the Attacker) is shown shaded.

intersects the AD Apollonius circle (of center O_1 and radius r_1). This happens for $\gamma < 1$ when

$$|\boldsymbol{O_1} - \boldsymbol{O_2}| + r_2 > r_1 \tag{6.1}$$

It happens for $\gamma > 1$ when

$$|\boldsymbol{O_1} - \boldsymbol{O_2}| - r_2 < r_1 \tag{6.2}$$

In the degenerate case of $\gamma = 1$, it is required that the TA Apollonius circle intersects the $Y-$axis, i.e.,

$$r_2 > the\ abscissa\ of\ \boldsymbol{O_2} \tag{6.3}$$

6.3 APOLLONIUS CIRCLES PERTAINING TO THE PROBLEM

A circle is the locus moving at a constant distance (called the circle's radius r) from a fixed point (called the circle's centre O). In the limit of an infinite radius ($r \longrightarrow \infty$), the circle degenerates into a straight line. Another definition of the circle is that it is the locus of a point moving such that the ratio of its distances from two fixed points A and B is a constant k. With this definition, the circle is called a circle of Apollonius (in honour of Apollonius of Perga (ca. 262-190 BC), the Great Geometer of Antiquity). In the limit ($k \longrightarrow 1$) this circle degenerates into the perpendicular bisector of $\overline{AD}$, while in the two limits ($k \longrightarrow 0$) and ($k \longrightarrow \infty$), this circle collapses to the two points A and B, respectively.

Two Apollonius circles are studied herein, namely the AD Apollonius circle, and the TA Apollonius circle. The study will be based on simple and intuitive plane-geometric arguments and will avoid the more involved treatment of analytic geometry. Figures 6.2 and 6.3 shows the Apollonius circles for a moving point P such that $\frac{AP}{PB} = k \neq 1$. The case $k > 1$ is shown in Fig. 6.2, while the case $k < 1$ is shwon in Fig. 6.3. The points I and E are the two special cases of P that lie on the straight line extension of the straight segment $\overline{AB}$. These points divide the straight segment $\overline{AB}$ internally and externally in the ratio k ($k \neq 1$), i.e.,

$$\boxed{\frac{AI}{IB} = \frac{AE}{EB} = k,\ \{k \neq 1\}.} \tag{6.4}$$

If we denote the position vector of a point by a bold version of its name, we can rewrite (6.4) in vectorial form as

$$(\boldsymbol{I} - \boldsymbol{A}) = k(\boldsymbol{B} - \boldsymbol{I}), \tag{6.5}$$

$$(\boldsymbol{E} - \boldsymbol{A}) = k(\boldsymbol{E} - \boldsymbol{B}), \tag{6.6}$$

which can be used to express $\boldsymbol{I}$ and $\boldsymbol{E}$ in terms of $\boldsymbol{A}$ and $\boldsymbol{B}$ as

$$\boldsymbol{I} = \frac{1}{k+1}(\boldsymbol{A} + k\boldsymbol{B}), \tag{6.7}$$

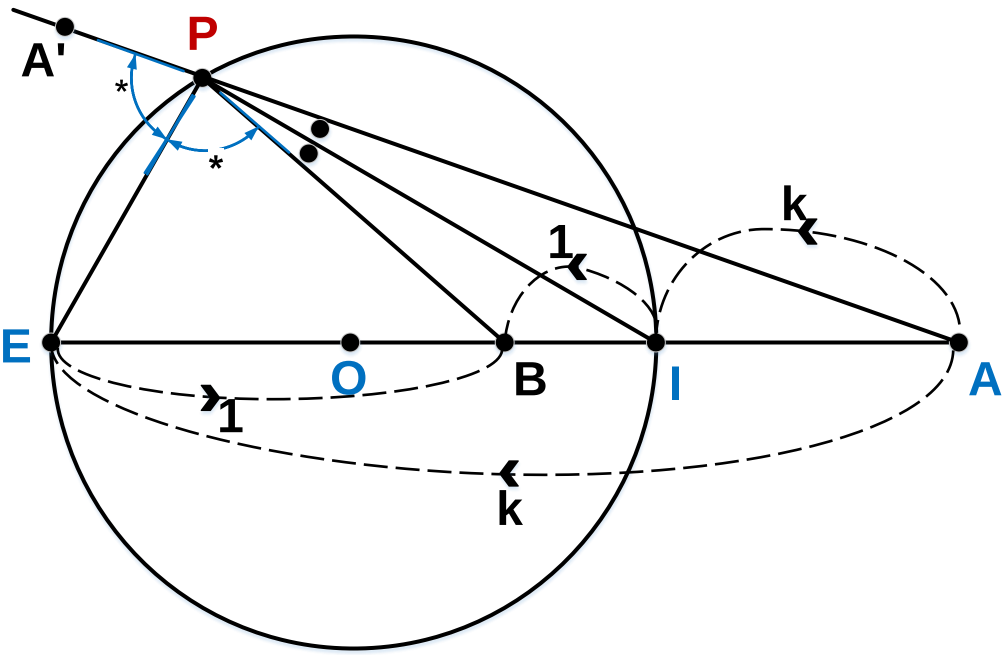

Figure 6.2: Apollonius circle for a moving point P such that $\dfrac{AP}{PB} = k > 1$. Here $m\angle API = m\angle BPI$ and $m\angle A'PE = m\angle BPE$.

$$\boldsymbol{E} = \frac{1}{k-1}(-\boldsymbol{A} + k\boldsymbol{B}). \tag{6.8}$$

The Apollonius circle is easily characterized by the points $\boldsymbol{I}$ and $\boldsymbol{E}$, since they are the two end points of one of the its diameters. The center of the circle is the midpoint of points $\boldsymbol{I}$ and $\boldsymbol{E}$, namely:

$$\begin{aligned}
\boldsymbol{O} &= \frac{1}{2}(\boldsymbol{I} + \boldsymbol{E}) \\
&= \frac{1}{2}[(\frac{1}{k+1} - \frac{1}{k-1})]\boldsymbol{A} + k(\frac{1}{k+1} + \frac{1}{k-1})\boldsymbol{B} \\
&= -\frac{1}{k^2-1}\boldsymbol{A} + \frac{k^2}{k^2-1}\boldsymbol{B},
\end{aligned} \tag{6.9}$$

while the radius of the circle is half the length of the displacement from $\boldsymbol{I}$ to $\boldsymbol{E}$,

$$\begin{aligned}
r &= \frac{1}{2}|\boldsymbol{I} - \boldsymbol{E}| \\
&= \frac{1}{2}|(\frac{1}{k+1} + \frac{1}{k-1})\boldsymbol{A} + k(\frac{1}{k+1} - \frac{1}{k-1})\boldsymbol{B}| \\
&= |\frac{k}{k^2-1}\boldsymbol{A} - \frac{k}{k^2-1}\boldsymbol{B}| \\
&= |\frac{k}{k^2-1}||\boldsymbol{A} - \boldsymbol{B}| = \frac{k}{k^2-1}(AB).
\end{aligned} \tag{6.10}$$

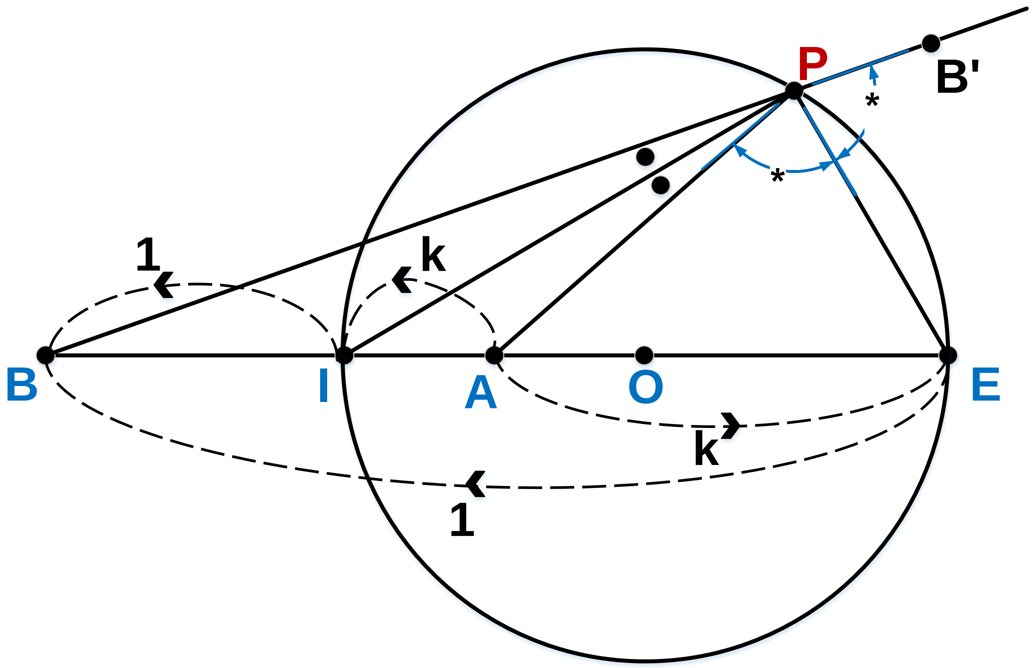

Figure 6.3: Apollonius circle for a moving point P such that $\dfrac{AP}{PB} = k < 1$. Here $m\angle API = m\angle BPI$ and $m\angle APE = m\angle B'PE$.

It is clear from (6.9) and (6.10) that $\lim_{k\to 1}|\boldsymbol{O}| \to \infty$ and $\lim_{k\to 1} r \to \infty$, and hence for $k = 1$, the Apollonius circle degenerates into a straight line, namely the perpendicular bisector of the straight segment $\overline{AB}$ (Fig. 6.4).

6.3.1 The *AD* Apollonius circle

For the AD Apollonius circle, the two fixed points are the initial positions of the Attacker $\boldsymbol{A} = (x_A, 0)$ and the initial position of the defender $\boldsymbol{D} = (-x_A, 0)$. The fixed ratio of the circle k is replaced by the following dimensionless ratio which is the Attacker's speed normalized w.r.t the Defender speed:

$$\gamma = \frac{V_A}{V_D}. \tag{6.11}$$

We will consider the three cases of

1. $\gamma < 1$ (fast Defender) discussed in Garcia et al. [48].

2. $\gamma = 1$ (same-speed Defender) discussed in Garcia et al. [47, 49].

3. $\gamma > 1$ (slow Defender), which is a novel case.

Substituting the values of $\boldsymbol{A}$ and $\boldsymbol{D}$ above for $\boldsymbol{A}$ and $\boldsymbol{B}$ in (6.7),(6.8),(6.9) and (6.10), respectively, and replacing k therein by γ we obtain for $\gamma \neq 1$,

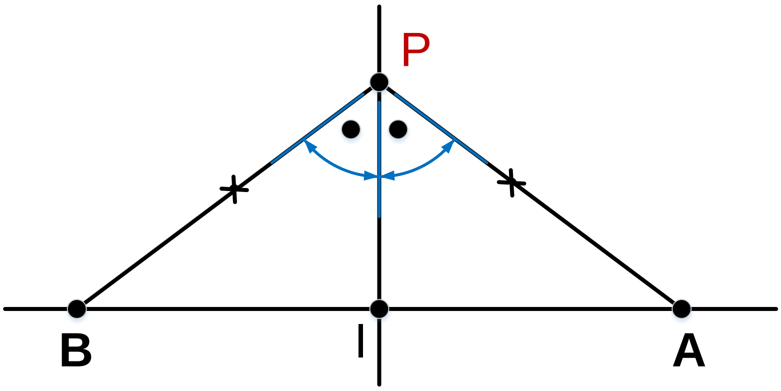

Figure 6.4: For $k = 1$, the Apollonius circle in figures 6.2 or 6.3 degenerates into the perpendicular bisector of the straight segment $\overline{AB}$. The point E disappears in this figure as it goes to ∞

$$\begin{aligned}
\boldsymbol{I_1} &= (\frac{1-\gamma}{1+\gamma}x_A, 0), && (6.12)\\
\boldsymbol{E_1} &= (\frac{1+\gamma}{1-\gamma}x_A, 0), && (6.13)\\
\boldsymbol{O_1} &= (\frac{1+\gamma^2}{1-\gamma^2}x_A, 0), && (6.14)\\
r_1 &= \frac{2\gamma}{|1-\gamma^2|}x_A. && (6.15)
\end{aligned}$$

Three interesting sets of limits are now considered. The first set of limits are those when $(\gamma \to 1)$, namely

$$\begin{aligned}
\lim_{\gamma\to 1} \boldsymbol{I}_1 &= (0,0), && (6.16)\\
\lim_{\gamma\to 1} \boldsymbol{E}_1 &= (\mp\infty, 0), && (6.17)\\
\lim_{\gamma\to 1} \boldsymbol{O}_1 &= (\mp\infty, 0), && (6.18)\\
\lim_{\gamma\to 1} r_1 &= \infty, && (6.19)
\end{aligned}$$

which means that the AD Apollonius circle degenerates in the limit $(\gamma \to 1)$ to a circle of an infinite radius with center still on the $x-$axis but infinitely distant from the origin. More precisely, this limit is identified as a straight line, namely the perpendicular bisector of the straight-line segment $\overline{AD}$.

The second set of limits are those when $(\gamma \to 0)$, namely

$$
\begin{aligned}
\lim_{\gamma\to 0} \boldsymbol{I}_1 &= (x_A, 0), &(6.20)\\
\lim_{\gamma\to 0} \boldsymbol{E}_1 &= (x_A, 0), &(6.21)\\
\lim_{\gamma\to 0} \boldsymbol{O}_1 &= (x_A, 0), &(6.22)\\
\lim_{\gamma\to 0} r_1 &= 0, &(6.23)
\end{aligned}
$$

which means that the AD Apollonius circle collapses in the limit ($\gamma \to 0$) to a single point, namely the initial position of the Attacker $\boldsymbol{A} = (x_A, 0)$.

The third set of limits are those when ($\gamma \to \infty$), namely

$$
\begin{aligned}
\lim_{\gamma\to \infty} \boldsymbol{I}_1 &= (-x_A, 0), &(6.24)\\
\lim_{\gamma\to \infty} \boldsymbol{E}_1 &= (-x_A, 0), &(6.25)\\
\lim_{\gamma\to \infty} \boldsymbol{O}_1 &= (-x_A, 0), &(6.26)\\
\lim_{\gamma\to \infty} r_1 &= 0, &(6.27)
\end{aligned}
$$

which means that the AD Apollonius circle collapses in the limit ($\gamma \to \infty$) to a single point, namely the initial position of the Defender $\boldsymbol{D} = (-x_A, 0)$.

6.3.2 The TA Apollonius circle

For the TA Apollonius circle, the two fixed points are the initial position of the Target $\boldsymbol{T} = (x_T, y_T)$ and the initial position of the Attacker $\boldsymbol{A} = (x_A, 0)$. Again, the fixed ratio of the circle k is replaced by a dimensionless quantity, namely the Target's speed normalized w.r.t. the Attacker's speed:

$$\alpha = \frac{V_T}{V_A}. \tag{6.28}$$

Here, we will consider only the case $\alpha < 1$, since for $\alpha \geqslant 1$, the Target always survives, even without any assistance from the Defender.

Now, we substitute the values of $\boldsymbol{T}$ and $\boldsymbol{A}$ above for $\boldsymbol{A}$ and $\boldsymbol{B}$ in (6.7),(6.8),(6.9) and (6.10), respectively, and replace k therein by α to obtain:

$$\boldsymbol{I_2} = \frac{1}{1+\alpha}(\boldsymbol{T} + \alpha \boldsymbol{A}) = \frac{1}{1+\alpha}(x_T + \alpha x_A, y_T), \tag{6.29}$$

$$\boldsymbol{E_2} = \frac{1}{\alpha - 1}(-\boldsymbol{T} + \alpha \boldsymbol{A}) = \frac{1}{1-\alpha}(x_T - \alpha x_A, y_T), \tag{6.30}$$

$$\boldsymbol{O_2} = \frac{1}{1-\alpha^2}(\boldsymbol{T} - \alpha^2 \boldsymbol{A}) = \frac{1}{1-\alpha^2}(x_T - \alpha^2 x_A, y_T), \tag{6.31}$$

$$r_2 = \frac{\alpha}{1-\alpha^2}(TA) = \frac{\alpha d}{1-\alpha^2}, \tag{6.32}$$

where $d = TA$ = the initial distance between the target and Attacker, namely

$$d = \sqrt{(x_T - x_A)^2 + y_T{}^2}. \tag{6.33}$$

Chapter 7: CRITICAL SPEED RATIO

Target survival is guaranteed if there is an overlapping of the region reachable by the Target before the Attacker (the interior of the TA Apollonius circle) and the region R_r reachable by the Defender before the Attacker (Fig. 6.1), since within this overlapping, the Defender can perform its intended role of intercepting the Attacker before the Attacker captures the Target. Target survival is critical when the aforementioned overlapping diminishes into a single point at which the aforementioned two regions barely touch, or are tangent to one another. For this situation, the normalized Target speed (the speed ratio) $\alpha = \dfrac{V_T}{V_A}$ attains its minimal or critical value $\overline{\alpha}$. Now, we consider three cases, in which the TA-Apollonius circle is tangent from outside to the boundary of the shaded region R_r. An implicit assumption throughout the forthcoming analysis is that $\boldsymbol{T} = (x_T, Y_T)$ is outside R_r.

7.1 The case $\gamma < 1$ (fast defender)

The critical speed ratio $\overline{\alpha}$, occurs when the TA Apollonius circle is *internally* tangent to the AD Apollonius circle, i.e., when the centers $\boldsymbol{O_2}$ and $\boldsymbol{O_1}$ of these two circles and their tangency point $\boldsymbol{C}$ are collinear (Fig. **??**). This happens when

$$r_1 - r_2 = |\boldsymbol{O_1} - \boldsymbol{O_2}|. \tag{7.1}$$

Substituting for r_1,r_2,$\boldsymbol{O_1}$and $\boldsymbol{O_2}$ from (6.15), (6.32), (6.15) and (6.31) respectively, and noting that $\gamma < 1$, one obtains

$$\begin{aligned} \frac{2\gamma}{1-\gamma^2}x_A - \frac{\alpha}{1-\alpha^2}d &= |(\frac{1+\gamma^2}{1-\gamma^2}x_A, 0) - \frac{1}{1-\alpha^2}(x_T - \alpha^2 x_A, y_T)| \\ &= [(\frac{1+\gamma^2}{1-\gamma^2}x_A - \frac{1}{1-\alpha^2}(x_T - \alpha^2 x_A))^2 + \frac{1}{(1-\alpha^2)^2}y_T^2]^{\frac{1}{2}}. \end{aligned} \tag{7.2}$$

In (7.2), we deliberately replaced $|1-\gamma^2|$ by $(1-\gamma^2)$ because $\gamma < 1$. We now square both sides of (7.2) to obtain:

$$\begin{aligned} \frac{4\gamma^2}{(1-\gamma^2)^2}x_A^2 + \frac{\alpha^2}{(1-\alpha^2)^2}d^2 - \frac{4\gamma\alpha d}{(1-\gamma^2)(1-\alpha^2)}x_A = \\ = \frac{(1+\gamma^2)^2}{(1-\gamma^2)^2}x_A^2 + \frac{x_T^2 - 2\alpha^2 x_T x_A + \alpha^4 x_A^2}{(1-\alpha^2)^2} - \frac{2(1+\gamma^2)(x_T - \alpha^2 x_A)x_A}{(1-\gamma^2)(1-\alpha^2)} + \frac{1}{(1-\alpha^2)^2}y_T^2. \end{aligned} \tag{7.3}$$

By squaring both sides of equation (7.2), the cardinality of the solution set for equation (7.2) is doubled. This means that when we solve the resulting equation, half of the resulting solutions will be extraneous or irrelevant and have to be rejected. Fortunately, we will have genuine reasons that enable us to identify such solutions, and compel us to reject them. The solutions retained after such a rejection are the correct solutions of (7.1) We now use (6.33) to replace y_T^2 by $(d^2 - x_A^2 - x_T^2 - 2x_A x_T)$ and rearrange terms in (7.3) to obtain

$$
\begin{aligned}
&[\frac{4\gamma^2}{(1-\gamma^2)^2}-\frac{(1+\gamma^2)^2}{(1-\gamma^2)^2}-\frac{\alpha^4}{(1-\alpha^2)^2}-\frac{2\alpha^2(1+\gamma^2)}{(1-\gamma^2)(1-\alpha^2)}+\frac{1}{(1-\alpha^2)^2}]x_A^2\\
&\qquad+[\frac{\alpha^2}{(1-\alpha^2)^2}-\frac{1}{(1-\alpha^2)^2}]d^2\\
&\qquad-\frac{4\gamma\alpha x_A d}{(1-\gamma^2)(1-\alpha^2)}+[\frac{-1}{(1-\alpha^2)^2}+\frac{1}{(1-\alpha^2)^2}]x_T^2\\
&\qquad+[\frac{2\alpha^2}{(1-\alpha^2)^2}+\frac{2(1+\gamma^2)}{(1-\gamma^2)(1-\alpha^2)}-\frac{2}{(1-\alpha^2)^2}]x_T x_A=0
\end{aligned}
\tag{7.4}
$$

The coefficient of x_A^2 in (7.4) is

$$
\begin{aligned}
&\frac{4\gamma^2}{(1-\gamma^2)^2}-\frac{(1+\gamma^2)^2}{(1-\gamma^2)^2}-\frac{\alpha^4}{(1-\alpha^2)^2}-\frac{2\alpha^2(1+\gamma^2)}{(1-\gamma^2)(1-\alpha^2)}+\frac{1}{(1-\alpha^2)^2}\\
&=\frac{4\gamma^2-1-\gamma^4-2\gamma^2}{(1-\gamma^2)^2}+\frac{(1-\alpha^4)}{(1-\alpha^2)^2}-\frac{2\alpha^2(1-\gamma^2)}{(1-\gamma^2)(1-\alpha^2)}\\
&=-1+\frac{1+\alpha^2}{(1-\alpha^2)}-\frac{2\alpha^2(1+\gamma^2)}{(1-\gamma^2)(1-\alpha^2)}\\
&=\frac{2\alpha^2}{(1-\alpha^2)}-\frac{2\alpha^2(1+\gamma^2)}{(1-\gamma^2)(1-\alpha^2)}\\
&=\frac{2\alpha^2}{(1-\alpha^2)}[1-\frac{(1+\gamma^2)}{(1-\gamma^2)}]=\frac{2\alpha^2}{(1-\alpha^2)}(\frac{-2\gamma^2}{(1-\gamma^2)})\\
&=\frac{-4\alpha^2\gamma^2}{(1-\alpha^2)(1-\gamma^2)},
\end{aligned}
\tag{7.5}
$$

and the coefficient of d^2 in (7.4) is

$$
\frac{\alpha^2}{(1-\alpha^2)^2}-\frac{1}{(1-\alpha^2)^2}=\frac{-(1-\alpha^2)}{(1-\alpha^2)^2}=-\frac{1}{(1-\alpha^2)},
\tag{7.6}
$$

while the coefficient of $x_T x_A$ in (7.4) is

$$
\begin{aligned}
&\frac{2\alpha^2}{(1-\alpha^2)^2}+\frac{2(1+\gamma^2)}{(1-\gamma^2)(1-\alpha^2)}-\frac{2}{(1-\alpha^2)^2}\\
&=\frac{2(\alpha^2-1)}{(1-\alpha^2)^2}+\frac{2(1+\gamma^2)}{(1-\gamma^2)(1-\alpha^2)}\\
&=-\frac{2}{(1-\alpha^2)}+\frac{2(1+\gamma^2)}{(1-\gamma^2)(1-\alpha^2)}\\
&=\frac{2}{(1-\alpha^2)}[-1+(\frac{1+\gamma^2}{1-\gamma^2})]=\frac{2}{(1-\alpha^2)}(\frac{2\gamma^2}{1-\gamma^2})\\
&=\frac{4\gamma^2}{(1-\alpha^2)(1-\gamma^2)}
\end{aligned}
\tag{7.7}
$$

This means that equation (7.4) can be simplified considerably to the equivalent form

$$\frac{-4\alpha^2\gamma^2}{(1-\alpha^2)(1-\gamma^2)}x_A^2 - \frac{1}{1-\alpha^2}d^2 - \frac{4\gamma\alpha x_A d}{(1-\gamma^2)(1-\alpha^2)} + \frac{4\gamma^2}{(1-\alpha^2)(1-\gamma^2)}x_T x_A \tag{7.8}$$

Now, we multiply (7.8) by $[-(1-\alpha^2)(1-\gamma^2)]$ noting that $\alpha \neq 1$ and $\gamma \neq 1$, to obtain

$$(4\gamma^2 x_A^2)\alpha^2 + (4\gamma x_A d)\alpha + (1-\gamma^2)d^2 - 4\gamma^2 x_T x_A = 0 \tag{7.9}$$

or equivalently

$$\boxed{\alpha^2 + \frac{d}{\gamma x_A}\alpha + [(\frac{1-\gamma^2}{4\gamma^2})(\frac{d}{x_A})^2 - \frac{x_T}{x_A}] = 0} \tag{7.10}$$

Equation (7.10) is an improvement of equation (36) in [49]. while (7.10) is a quadratic equation in α, equation (36) in [49] is a quartic in α that has the same two roots of (7.10) in addition to the two irrelevant roots $\alpha \mp 1$. As a bonus, equation (7.10) is written in a self-verifying dimensionless form.

7.2 The case $\gamma = 1$ (similar Defender)

The critical speed ratio $\overline{\alpha}$ occurs when the TA Apollonius circle touches the $L.H.S.$ of the $XY-$plane (Fig. **??**), i.e., when

$$r_2 = Absicessa\ of\ \boldsymbol{O_2}. \tag{7.11}$$

i.e., thanks to (6.31) and (6.32) when:

$$\frac{\alpha d}{1-\alpha^2} = \frac{x_T - \alpha^2 x_A}{1-\alpha^2}. \tag{7.12}$$

Multiplying (7.12) by $(1-\alpha^2)$ (thanks to the fact that $\alpha \neq 1$), and rearranging, one obtains the following quadratic equation in α

$$x_A\alpha^2 + d\alpha - x_T = 0, \tag{7.13}$$

which is equation (12) in [3]. It is interesting to note that equation (7.12) is the special case ($\gamma = 1$) of (7.10), though (7.10) was derived under the assumption $\gamma \neq 1$.

7.3 The case $\gamma > 1$ (Slow Defender)

The critical speed ratio $\overline{\alpha}$ occurs when the TA Apollonius circle is *externally* tangent to the AD Apollonius circle, i.e., when the centre $\boldsymbol{O_2}$, the tangency point $\boldsymbol{C}$ and the centre $\boldsymbol{O_1}$ are collinear(Fig. **??**), i.e., when

$$r_1 + r_2 = |\boldsymbol{O_1} - \boldsymbol{O_2}| \tag{7.14}$$

Since $\gamma > 1$, we write

$$r_1 + r_2 = \frac{2\gamma}{|1-\gamma^2|} + \frac{\alpha}{1-\alpha^2}d = \frac{-2\gamma}{1-\gamma^2} + \frac{\alpha}{1-\alpha^2}d. \tag{7.15}$$

The above expression for $(r_1 + r_2)$ is exactly the negative of $(r_1 - r_2)$ in (7.2). Hence, squaring of (7.14) results in (7.3), and consequently lead to (7.4) and (7.8), and finally to (7.9) and (7.10). Equation (7.10) is thereby shown to hold for a slow Defender besides being true for a fast one.

Therefore, we will use the quadratic formula (7.10) for all values of γ, and will solve it to obtain $\overline{\alpha}$ for any γ as

$$\begin{aligned}\overline{\alpha} &= \frac{1}{2}[-\frac{d}{\gamma x_A} \pm [(\frac{d}{\gamma x_A})^2 - 4(\frac{1-\gamma^2}{4\gamma^2})(\frac{d}{x_A})^2 + \frac{4x_T}{x_A}]^{1/2}] \\ &= \frac{1}{2\gamma x_A}[-d \mp \gamma\sqrt{d^2 + 4x_T x_A}] \\ &= \frac{1}{2\gamma x_A}[-\sqrt{(x_A - x_T)^2 + y^2} + \gamma\sqrt{(x_A + x_T)^2 + y_T^2}]\end{aligned} \tag{7.16}$$

Equation (7.16) was derived in [49] for $\gamma < 1$ and in [47] for $\gamma = 1$, provided $x_T > 0$. It is shown herein to hold for all values in γ, including $\gamma > 1$. Note that $\overline{\alpha}$ is definitely nonnegative and hence the minus sign in the solution for $\overline{\alpha}$ is rejected. The question remains whether (7.16) yields a non-negative value for $\overline{\alpha}$ when the positive sign is chosen in (7.16). It could be argued that (7.16) should be used (with the positive sign, of course) as long as it yields a nonnegative value for $\overline{\alpha}$, and otherwise $\overline{\alpha}$ should be set to zero. For example, if $\gamma = 1$ and $x_T < 0$, equation (7.16) yields a negative value for $\overline{\alpha}$ which need to be rejected and replaced by zero. Physically, the situation $\gamma = 1, x_T < 0$ is one in which the Target is initially in the region reachable by the Defender before the Attacker, i.e., it is within the effective protection of the Defender, even if it does not move itself at all. Therefor, we rewrite (7.16) in the following dimensionless form:

$$\overline{\alpha} = \frac{1}{2\gamma}[-\sqrt{(1 - \frac{x_T}{x_A})^2 + (\frac{y_T}{x_A})^2} + \gamma\sqrt{(1 + \frac{x_T}{x_A})^2 + (\frac{y_T}{x_A})^2}\ ] \tag{7.17}$$

provided that

$$\gamma\ \sqrt{(1 + \frac{x_T}{x_A})^2 + (\frac{y_T}{x_A})^2}\ >\ \sqrt{(1 - \frac{x_T}{x_A})^2 + (\frac{y_T}{x_A})^2} \tag{7.18}$$

and whenever (7.18) is not valid, we simply set

$$\overline{\alpha} = 0. \tag{7.19}$$

Figures 7.2 to 7.4 plot α as a function of $(\frac{x_T}{x_A})$ with $(\frac{y_T}{x_A})$ as a parameter for the specific γ values of 0.8, 1.0, and 1.25 respectively.

We pay a special attention to the special case when the Target is initially on the x-axis (i.e., when the Target, Attacker. and Defender are initially collinear). In this case, equation (7.17) reduces to

$$\overline{\alpha} = \frac{1}{2\gamma}[-\sqrt{(1 - \frac{x_T}{x_A})^2} + \gamma\sqrt{(1 + \frac{x_T}{x_A})^2}\ ], \tag{7.20}$$

care must be taken that the $\sqrt{\ }$ sign indicates the principal branch of the inverse square

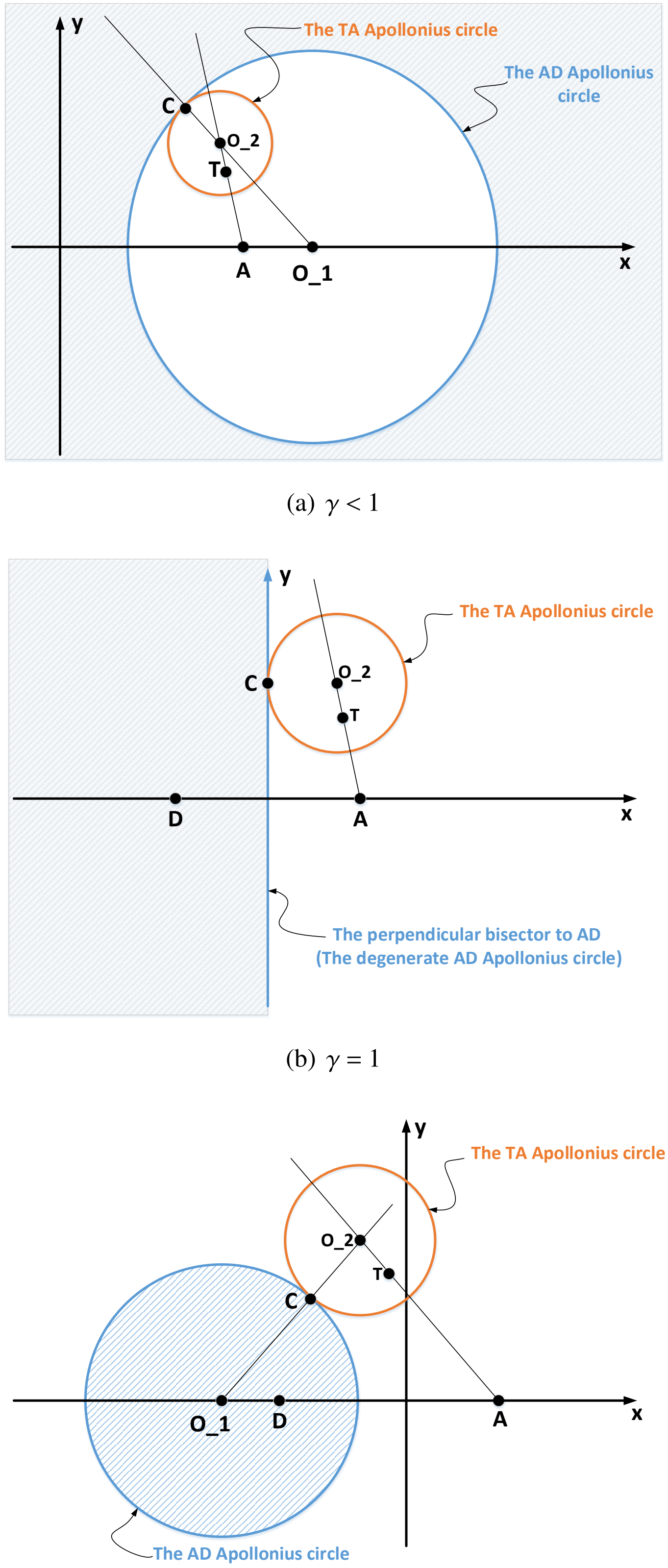

(a) $\gamma < 1$

(b) $\gamma = 1$

(c) $\gamma > 1$

Figure 7.1: The critical speed ratio $\overline{\alpha}$ is obtained when the TA Apollonius circle is tangent to the boundary of the shaded region R_r which is the region reachable by the Defender befor the Attacker.

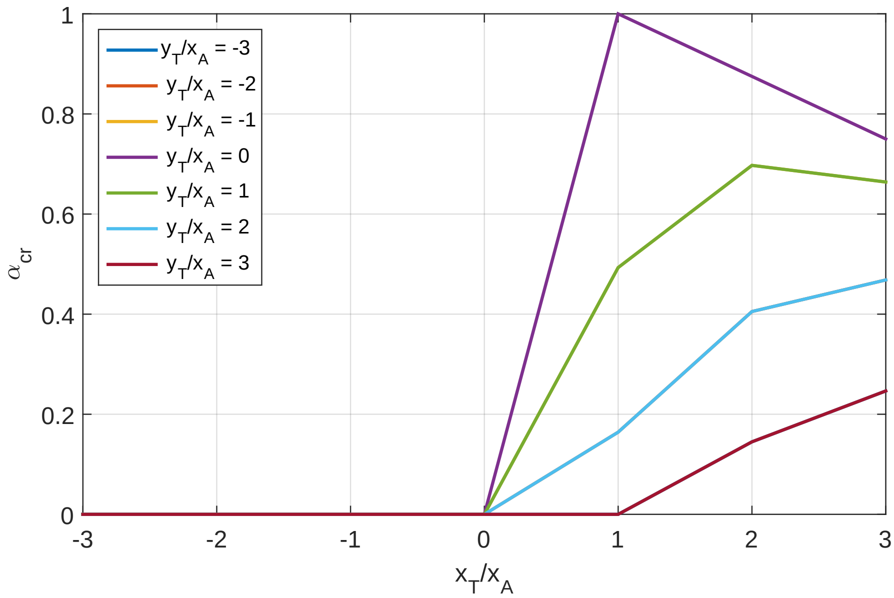

Figure 7.2: The critical normalized speed $\overline{\alpha}$ or α_{cr} as a function of $(\frac{x_T}{x_A})$ with $(\frac{y_T}{x_A})$ as a parameter when $\gamma = 0.8$ (fast defender).

function. i.e.,

$$\sqrt{y^2} = |y| \tag{7.21}$$

Therefore, we write

$$\sqrt{(1-\frac{x_T}{x_A})^2} = \begin{cases} 1-\frac{x_T}{x_A}, & \frac{x_T}{x_A} \leq 1 \\ \frac{x_T}{x_A} - 1, & \frac{x_T}{x_A} > 1, \end{cases} \tag{7.22}$$

$$\sqrt{(1+\frac{x_T}{x_A})^2} = \begin{cases} 1+\frac{x_T}{x_A}, & \frac{x_T}{x_A} \geq -1 \\ -1-\frac{x_T}{x_A}, & \frac{x_T}{x_A} < -1, \end{cases} \tag{7.23}$$

We now consider the three specific values of γ considered in Figs. 7.2 to 7.4 , namely $\gamma = 0.8, \gamma = 1$, and $\gamma = 1.25$.

For $\gamma = 0.8$

$$\overline{\alpha} = \frac{1}{1.6}[-\sqrt{(1-\frac{x_T}{x_A})^2} + 0.8\sqrt{(1+\frac{x_T}{x_A})^2}]. \tag{7.24}$$

For $(\frac{x_T}{x_A}) < -1$

$$\overline{\alpha} = \frac{1}{1.6}[-(1-\frac{x_T}{x_A}) + 0.8(-1-\frac{x_T}{x_A})] = \frac{1}{1.6}[-1.8+0.2\frac{x_T}{x_A}] = \frac{1}{8}(-9+\frac{x_T}{x_A})$$

which is definitely negative, and hence

$$\overline{\alpha} = 0, \quad (\frac{x_T}{x_A}) < -1, \quad \gamma = 0.8 \tag{7.25}$$

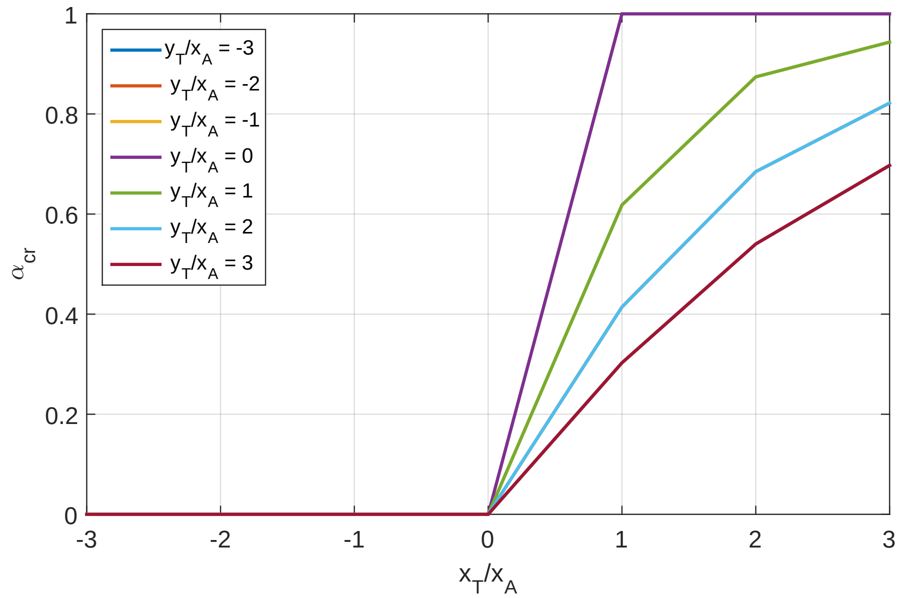

Figure 7.3: The critical normalized speed $\overline{\alpha}$ or α_{cr} as a function of $(\frac{x_T}{x_A})$ with $(\frac{y_T}{x_A})$ as a parameter when $\gamma = 1$ (similar defender).

For $-1 \le (\frac{x_T}{x_A}) \le 1$

$$\overline{\alpha} = \frac{1}{1.6}[-(1 - \frac{x_T}{x_A}) + 0.8(1 + \frac{x_T}{x_A})] = \frac{1}{1.6}[-0.2 + 1.8\frac{x_T}{x_A}] = \frac{1}{8}(-1 + 9\frac{x_T}{x_A})$$

The above $\overline{\alpha}$ is negative when $(-1 + 9\frac{x_T}{x_A})$ is negative and hence we again set

$$\overline{\alpha} = 0, \quad -1 \le (\frac{x_T}{x_A}) < \frac{1}{9}, \quad \gamma = 0.8. \tag{7.26}$$

while $\overline{\alpha}$ increases linearly from 0 to 1 in $\frac{x_T}{x_A} \in [\frac{1}{9}, 1]$

$$\overline{\alpha} = \frac{1}{8}(-1 + 9\frac{x_T}{x_A}), \quad \frac{1}{9} \le (\frac{x_T}{x_A}) \le 1, \quad \gamma = 0.8 \tag{7.27}$$

Finally, when $(\frac{x_T}{x_A}) > 1$

$$\overline{\alpha} = \frac{1}{1.6}[-(\frac{x_T}{x_A} - 1) + 0.8(\frac{x_T}{x_A} + 1)] = \frac{1}{1.6}[1.8 - 0.2(\frac{x_T}{x_A})] = \frac{1}{8}(9 - \frac{x_T}{x_A}). \tag{7.28}$$

This means that after peaking at 1 when $(\frac{x_T}{x_A}) = 1$, the value of $\overline{\alpha}$ starts to decrease linearly to be 0 at $(\frac{x_T}{x_A}) = 9$ and then it remains 0 (rather than becoming negative), i.e.,

$$\overline{\alpha} = \frac{1}{8}(9 - \frac{x_T}{x_A}), \quad 1 < (\frac{x_T}{x_A}) \le 9, \quad \gamma = 0.8, \tag{7.29}$$

$$\overline{\alpha} = 0, \quad (\frac{x_T}{x_A}) > 9, \quad \gamma = 0.8. \tag{7.30}$$

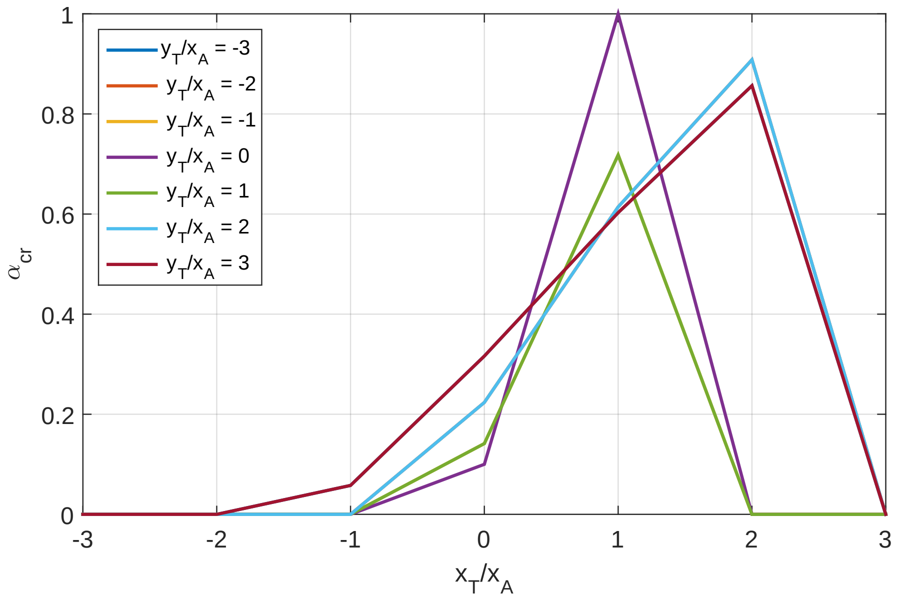

Figure 7.4: The critical normalized speed $\overline{\alpha}$ or α_{cr} as a function of $(\frac{x_T}{x_A})$ with $(\frac{y_T}{x_A})$ as a parameter when $\gamma = 1.25$ (slow defender).

For $\gamma = 1$

$$\overline{\alpha} = \frac{1}{2}[-\sqrt{(1-\frac{x_T}{x_A})^2} + \sqrt{(1+\frac{x_T}{x_A})^2}\ ]. \tag{7.31}$$

For $(\frac{x_T}{x_A}) < -1$

$$\overline{\alpha} = \frac{1}{2}[-(1-\frac{x_T}{x_A}) + (-1-\frac{x_T}{x_A})] = -1.$$

Set

$$\overline{\alpha} = 0, \quad (\frac{x_T}{x_A}) < -1, \quad \gamma = 1 \tag{7.32}$$

For $-1 \leq (\frac{x_T}{x_A}) \leq 1$

$$\overline{\alpha} = \frac{1}{2}[-(1-\frac{x_T}{x_A}) + (1+\frac{x_T}{x_A})]$$

$$\overline{\alpha} = (\frac{x_T}{x_A}), \quad -1 \leq (\frac{x_T}{x_A}) \leq 1, \quad \gamma = 1 \tag{7.33}$$

For $-1 \leq (\frac{x_T}{x_A}) < 0$, $\overline{\alpha}$ is again negative and is to be set to 0

$$\overline{\alpha} = (\frac{x_T}{x_A}), \quad 0 \leq (\frac{x_T}{x_A}) \leq 1, \quad \gamma = 1 \tag{7.34}$$

and hence $\overline{\alpha}$ increases linearly from 0 at $(\frac{x_T}{x_A}) = 0$ to 1 at $(\frac{x_T}{x_A}) = 1$

For $(\frac{x_T}{x_A}) > 1$

$$\overline{\alpha} = \frac{1}{2}[-(\frac{x_T}{x_A} - 1) + (1 + \frac{x_T}{x_A})] = 1, \quad (\frac{x_T}{x_A}) > 1, \quad \gamma = 1 \tag{7.35}$$

Note that the situation of ($\gamma = 1$) differs significantly from that of ($\gamma = 0.8$). For ($\gamma = 1$), $\overline{\alpha}$ increases from 0 to 1 and remains so indefinitely, but for ($\gamma = 0.8$), $\overline{\alpha}$ increases from 0 to 1 and immediately decreases again to 0.

For $\gamma = 1.25$

$$\overline{\alpha} = \frac{1}{2.5}[-\sqrt{(1 - \frac{x_T}{x_A})^2} + 1.25\sqrt{(1 + \frac{x_T}{x_A})^2}] \tag{7.36}$$

For $(\frac{x_T}{x_A}) < -1$

$$\overline{\alpha} = \frac{1}{2.5}[-(1 - \frac{x_T}{x_A}) + 1.25(-1 - \frac{x_T}{x_A})] = \frac{1}{2.5}[-2.25 - 0.25\frac{x_T}{x_A}] = \frac{1}{10}(-9 - \frac{x_T}{x_A}),$$

which results in setting

$$\overline{\alpha} = 0, \quad -9 \le (\frac{x_T}{x_A}) < -1, \quad \gamma = 1.25, \tag{7.37}$$

$$\overline{\alpha} = \frac{1}{10}(-9 - \frac{x_T}{x_A}), \quad (\frac{x_T}{x_A}) < -9, \quad \gamma = 1.25. \tag{7.38}$$

For $-1 \le (\frac{x_T}{x_A}) \le 1$

$$\overline{\alpha} = \frac{1}{2.5}[-(1 - \frac{x_T}{x_A}) + 1.25(1 + \frac{x_T}{x_A})] = \frac{1}{2.5}[0.25 + 2.25(\frac{x_T}{x_A})] = \frac{1}{10}[1 + 9\frac{x_T}{x_A}],$$

which reduces to

$$\overline{\alpha} = 0, \quad -1 \le \frac{x_T}{x_A} < -\frac{1}{9}, \quad \gamma = 1.25, \tag{7.39}$$

$$\overline{\alpha} = \frac{1}{10}(1 + 9\frac{x_T}{x_A}), \quad -\frac{1}{9} \le \frac{x_T}{x_A} \le 1, \quad \gamma = 1.25. \tag{7.40}$$

While $\overline{\alpha}$ remains 0 for $(\frac{x_T}{x_A}) \in [-9, -\frac{1}{9})$ it starts to increase linearly to 1 for $(\frac{x_T}{x_A}) \in [-\frac{1}{9}, 1)$.

Finally, when $(\frac{x_T}{x_A}) > 1$

$$\overline{\alpha} = \frac{1}{2.5}[-(\frac{x_T}{x_A} - 1) + 1.25(\frac{x_T}{x_A} + 1)] = \frac{1}{2.5}[2.25 + 0.25\frac{x_T}{x_A}] = \frac{1}{10}[9 + \frac{x_T}{x_A}], \tag{7.41}$$

which means that $\overline{\alpha}$ increases linearly. Note that equations (7.38) and (7.41) predict values of $\overline{\alpha}$ exceeding 1, a phenomenon taking place in the current analysis only when $\gamma > 1$, i.e., for a slow defender.

Chapter 8: ESCAPE REGION AND VORONOI DIAGRAM

In this chapter, we develop a novel analytic expression for the pursuit-evasion Voronoi diagram [47] that marks or borders the "safe" or "escape" region R_e for the Target, i.e., the region defined by the set of all coordinate points (x, y) such that if the target's initial position (x_T, y_T) is inside this region, then the target is guaranteed to survive (to escape the Attacker) provided both the Target and Defender implement their optimal strategies, and regardless of the policy adopted by the Attacker, whether optimal or not. The Voronoi diagram obtaind divides the $XY-$plane, into two regions

- a safe or escape region R_e to which the Defender's initial position $\boldsymbol{D}$ belongs.
- a *potentially* unsafe region to which the Attacker's initial position $\boldsymbol{A}$ belongs.

Garcia et al. [47] treated this problem for $\gamma = 1$ only using some involved arguments with inequalities developed from scratch, and without due reference to their earlier analysis concerning the critical speed ratio.

A very important *insight* that markedly simplifies our work is to note that required Voronoi diagram is simply a rephrasing of the criticality equation (7.10) for any value of γ including the cases $\gamma > 1$ or $\gamma < 1$ and $\gamma = 1$, viewed as a relation between y_T and x_T rather than a polynomial in α. Working with equalities is definitely simpler than working with inequalities, and it specifies a Voronoi diagram that divides the whole plane into two distinct parts, namely: the safe region and the (potentially) unsafe region. The safe region is then identified simply as the region to which $\boldsymbol{D}$ belongs. Note that the set of points of the safe regions R_e is a superset of the points reachable by the Defender before the Attacker R_r, i.e., $R_e \supseteq R_r$. The two regions R_e and R_r are identical if the Target does not move at all ($\alpha = 0$), a situation in which the Target does not exert any own effort to secure its survival and relies solely on the Defender's helping efforts. The family of Voronoi diagrams for various values of the normalized speed α will be bounded by the one for $\alpha = 0$, which is the border of R_r (Fig. 6.1).
Now, we obtain the general Voronoi diagram by rewriting the critically equation (7.10) or (7.9) as a relation between y_T and x_T. This is achieved via (6.33) to substitute $(x_A^2 + x_T^2 - 2x_A x_T + y_T^2)$ for d^2. To avoid mistakes in the manipulations, one must make sure that the pertinent equation at every step is dimensionally homogeneous. From (7.9), we write

$$(4\gamma\alpha x_A)d = -(1-\gamma^2)d^2 + 4\gamma^2 x_A x_T - 4\gamma^2\alpha^2 x_A^2 \tag{8.1}$$

Now, we square both sides of (8.1) to obtain

$$\begin{aligned} 16\gamma^2\alpha^2 x_A^2(x_A^2 + x_T^2 - 2x_A x_T + y_T^2) &= [-(1-\gamma^2)(x_A^2 + x_T^2 - 2x_A x_T + y_T^2) + 4\gamma^2 x_A x_T - 4\gamma^2\alpha^2 x_A^2]^2 \\ &= [-(1-\gamma^2)(x_A^2 + x_T^2 + y_T^2) + 2(1+\gamma^2)x_A x_T - 4\gamma^2\alpha^2 x_A^2]^2 \end{aligned} \tag{8.2}$$

Now we rearrange (8.2) as a quartic equation (forth-degree polynomial) in x_T and y_T, namely

$$
\begin{aligned}
p(x_T, y_T) = {} & 16\gamma^2\alpha^2 x_A^4 \\
& + 16\gamma^2\alpha^2 x_A^2 x_T^2 \\
& - 32\gamma^2\alpha^2 x_A^3 x_T \\
& + 16\gamma^2\alpha^2 x_A^2 y_T^2 \\
& - (1-\gamma^2)^2[x_A^4 + x_T^4 + y_T^4 + 2x_A^2x_T^2 + 2x_A^2y_T^2 + 2x_T^2y_T^2] \\
& - (1+\gamma^2)^2 * 4x_A^2x_T^2 \\
& - 16\gamma^4\alpha^4x_A^4 \\
& + 2(1-\gamma^4)(2x_A^3x_T + 2x_Ax_T^3 + 2x_Ax_Ty_T^2) \\
& - 8\gamma^2(1-\gamma^2)\alpha^2(x_A^4 + x_A^2x_T^2 + x_A^2y_T^2) \\
& + 16\gamma^2(1+\gamma^2)\alpha^2x_A^3x_T
\end{aligned}
\tag{8.3}
$$

Equation (8.3) is satisfied by the required Voronoi diagram. The quartic polynomial $p(x_t, y_T)$ satisfies

$$p(x_T, -y_T) = p(x_T, y_T), \tag{8.4}$$

since it has even powers only for y_T. This means $p(x_T, y_T)$ is an even function in y_T and its graph in the $x_T - y_T$ plane is *symmetric* w.r.t. the x_T-axis.

Though (8.3) is a quartic equation, the actual Voronoi diagram is expected to be a quadratic curve and not a quartic curve. Note that we performed a squaring operation in obtaining (7.9) and hence for obtaining (8.3), which doubled the pertinent degree from two to four. Hence, the Voronoi diagram is just a second-degree factor, part or branch of the fourth-degree curve depicted by (8.3). We will be able to identify the correct Voronoi diagram by rejecting any part of the curve that lies in R_r, i.e., the correct Voronoi diagram should define the border of R_e such that $R_e \supseteq R_r$.

Note that (8.3) is the general equation for the Voronoi diagram in our current TAD problem and it appears here for the first time. As a check on its correctness, we use it to produce the correct curve for $\gamma = 1$, earlier obtained by Garcia et al. [49], namely

$$16x_A^2[-(1-\alpha^2)x_T^2 + \alpha^2y_T^2] = -16x_A^4\alpha^2(1-\alpha^2), \tag{8.5}$$

or equivalently

$$\frac{x_T^2}{\alpha^2x_A^2} - \frac{y_T^2}{(1-\alpha^2)x_A^2} = 1. \tag{8.6}$$

Equation (8.5) represents a hyperbola which is an open curve of two branches. Interestingly enough the term hyperbola is believed to have been coined by our old friend Apollonius of Perga in his work on conic sections. This hyperbola is represented in Fig. 8.1 and has the following properties:

- The hyperbola has two focal points $\boldsymbol{F_1} = (c, 0)$ and $\boldsymbol{F_2} = (-c, 0)$, where

$$c^2 = \alpha^2x_A^2 + (1-\alpha^2)x_A^2 = x_A^2, \tag{8.7}$$

i.e. the focal points coincide with the initial positions of the Attacker $\boldsymbol{A} = (x_A, 0)$ and the Defender $\boldsymbol{D} = (-x_A, 0)$. Note that these two focal points are shared by an infinite set of curves for various values of α ($0 < \alpha < 1$).

- The line joining the focal points, i.e., the *transverse axis* coincides with the x_T-axis. The midpoint of the two focal points, i.e., the *center* of the hyperbola, is the origin (0,0). The conjugate axis (the line perpendicular to the hyperbola's transverse axis through its center) is the y_T-axis.

- The eccentricity of the hyperbola e is

$$e = \frac{c}{\alpha x_A} = \frac{1}{\alpha} > 1, \tag{8.8}$$

where the fact that $e > 1$ distinguishes the hyperbola from other conic sections, namely the ellipse (of $e < 1$) and the parabola (of $e = 1$). Note that the eccentricity e equals the ratio of the distance PF_i from a point P on the hyperbola to one focus F_i to the distance of the point to the corresponding directrix PQ_i, i.e.

$$PF_i = e\, PQ_i, \quad i = 1, 2, \tag{8.9}$$

- The vertices of the hyperbola (its intersections with the x_T-axis) are at $(\alpha x_A, 0)$ and $(-\alpha x_A, 0)$, and hence approach the two focal points as α tends to 1 (from below).

- Perpendicular to the transverse axis are the two directrices D_1 and D_2 given by

$$x_T = \mp\frac{\alpha x_A}{e} = \mp\alpha^2 x_A \tag{8.10}$$

These directrices also approach the focal points when $\alpha \to 1$.

- The hyperbola has two asymptotes that intersect at its center, and are given by

$$y_T = \mp\left(\frac{\sqrt{1-\alpha^2}}{\alpha}\right)x_T. \tag{8.11}$$

For $0 < \alpha < 1$, the magnitude of the slope for an asymptote increases as α decreases and vice verse. Unlike the vertices and directrices, the asymptotes are independent of x_A.

- As a special case of the polynomial $p(x_T, y_T)$, in (8.3) the hyperbola (8.6) is an even function of y_T and hence is symmetric about the x_T-axis, Incidently the hyperbola is also even in x_T and hence its two branches are symmetric about the y_T-axis but this observation is irrelevant since only one branch is retained in further study.

- In the limit ($\alpha \to 0$), the hyperbola (8.6) degenerates into the y_T-axis.

- In the limit ($\alpha \to 1$), the right branch or the hyperbole (8.6) degenerates into a ray emanating from $\boldsymbol{A}$ in the positive direction of the x_T-axis, while its left branch degenerates into a ray emanating from $\boldsymbol{D}$ in the opposite direction.

In passing, we note that though equation (8.6) was obtained herein as the special case ($\gamma = 1$) of equation (8.3), we have first obtained it by a rephrasing of the criticality condition

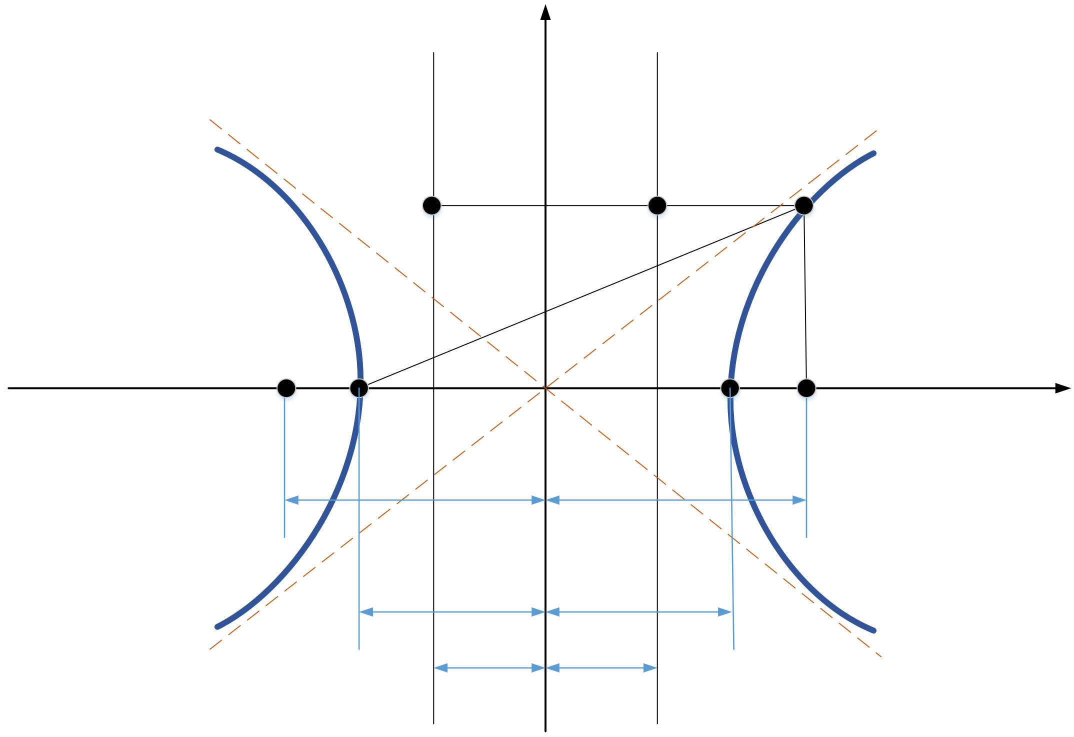

Figure 8.1: Graph and features of the hyperbola $\dfrac{x_T^2}{\alpha^2 x_A^2} - \dfrac{y_T^2}{(1-\alpha^2)x_A^2} = 1$

(7.13) which holds for $\gamma = 1$.

Now we note that the left branch of the hyperbola lies entirely in R_r and hence it is rejected. The right branch of the hyperbola is the required Voronoi diagram, and it is bordering the escape region R_e which extends to its left. Clearly, it is an enlargement of the reachability region R_r. Likewise, we expect the escape region to be a subset of the AD Apollonius circle in Fig. **??** where $\gamma < 1$, and to be a superset of this circle in Fig. **??** where $\gamma > 1$.

Figure 8.2 is a sketch of the hyperbola (8.6) for $\alpha = 0.25$. the figure stresses that the right branch of the hyperbola is accepted as a Voronoi diagram while the left branch is rejected as such. Figure 5.3 is computer generated Voronoi diagrams for $\gamma = 1$ and α varying from 0 (the y_T-axis) to slightly less than 1 (the straight-line ray emanating from $\boldsymbol{A}$ and coinciding with the x_T-axis).

Now, we come to a novel and really important contribution of this thesis, where we visualize the escape regions in the case of a fast Defender and a slow Defender. Figure 8.4 shows the AD-Apollonius circle for $\gamma = 0.8$ and $x_A = 4$ for which $\boldsymbol{I_1} = (0.444, 0)$, $\boldsymbol{E_1} = (36, 0)$, $\boldsymbol{O_1} = (18.22, 0)$, and $r_1 = 17.78$. Imposed on this circle is the quartic curve given by (8.3) which consists of two closed curves. There is one closed curve entirely outside the AD-Apollonius circle, i.e., entirely inside the Reachability region R_r and hence is rejected. The other closed curve is entirely inside the AD-Apollonius circle, i.e., the reachability region R_r and hence it is accepted as the Voronoi diagram. The escape region (safe region) is the *unshaded* area in this figure. Figure 5.5 generalizes Fig. 8.4 by demonstrating various accepted branches of the Voronoi diagram for $\gamma = 0.8$ and α as s parameter ranging from 0 (the AD-Apollonius circle) to a value approaching 1 from below (a closed curve collapsing to one barely encircling point A). This means that as α increases from 0 to 1, the safe or escape region expands from the exterior of the AD-Apollonius circle to almost the whole $x_T - y_T$ plane (excluding point A).

Now, we discuss the strikingly similar or dual case of a slow Defender. Figure 8.6 shows the AD-Apollonius circle for $\gamma = 1.25$ and $x_A = 4$ for which $\boldsymbol{I_1} = (-0.444, 0)$, $\boldsymbol{E_1} = (-36, 0)$, $\boldsymbol{O_1} = (-18.22, 0)$, $r_1 = 17.78$. Imposed on this circle is the quartic curve given by (8.3). Note that the whole graph in Fig. 8.6 is a *mirror image* of that in Fig. 8.4. The quartic curve again consists of two closed curves. There is one closed curve entirely inside the AD-Apollonius circle. i.e., entirely inside the Reachability region R_r and hence is rejected. The other closed curve is entirely outside the AD-Apollonius circle, i.e., entirely outside the Reachability region R_r, and hence is accepted as the Voronoi diagram. The escape region (safe region) is the *shaded* area in this figure. Figure 5.7 generalizes Fig. 8.6 by demonstrating various accepted branches of the Voronoi diagram for $\gamma = 1.25$ and α as a parameter ranging from 0 (the AD-Apollonius circle) to a value approaching 1 from below.

In passing, we discuss the situation of $\gamma = 0$ (when the Target does not move at all). In this case the TA circle collapse into a single point $\boldsymbol{T}$ and the critically condition (7.9) reduces to

$$(1 - \alpha^2)d^2 = 4\gamma^2 x_T x_A \tag{8.12}$$

which can readily be written as

$$(x_T - (\frac{1+\gamma^2}{1-\gamma^2})x_A)^2 + (y_T - 0)^2 = (\frac{2\gamma x_A}{1-\gamma^2})^2 \tag{8.13}$$

an equation that can be identified as the equation of the AD Apollonius circle in the $Y_T - X_T$ coordinates. This circle serves as the Voronoi diagram for $\alpha = 0$, a fact confirming our assertion that the escape region R_e reduces to the reachability region R_r when $\alpha = 0$. Likewise, when $\gamma = 1$, imposing the condition $\alpha = 0$ on the condition (7.13) results in

$$x_T = 0 \tag{8.14}$$

which means that the right branch of the hyperbolic Voronoi diagram (8.6) degenerates into the y_T−axis (the perpendicular bisector of $\overline{AD}$) and again the region R_e concides with the region R_r in this case.

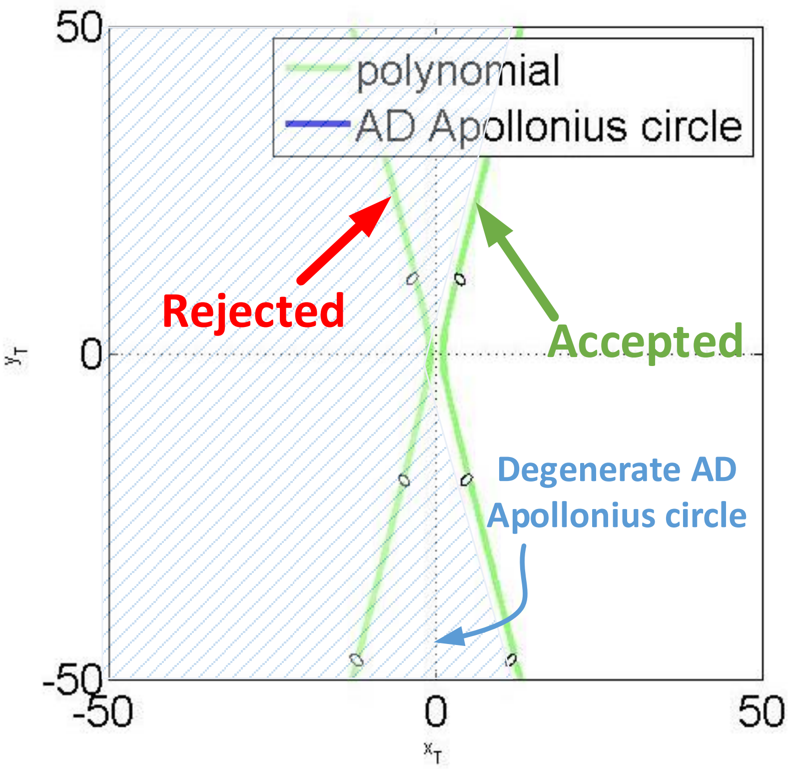

Figure 8.2: Generated computer output for the Voronoi diagram bordering the safe region for $x_A = 4,\ \alpha = 0.25,\ \gamma = 1$ (the safe region is the shaded area)

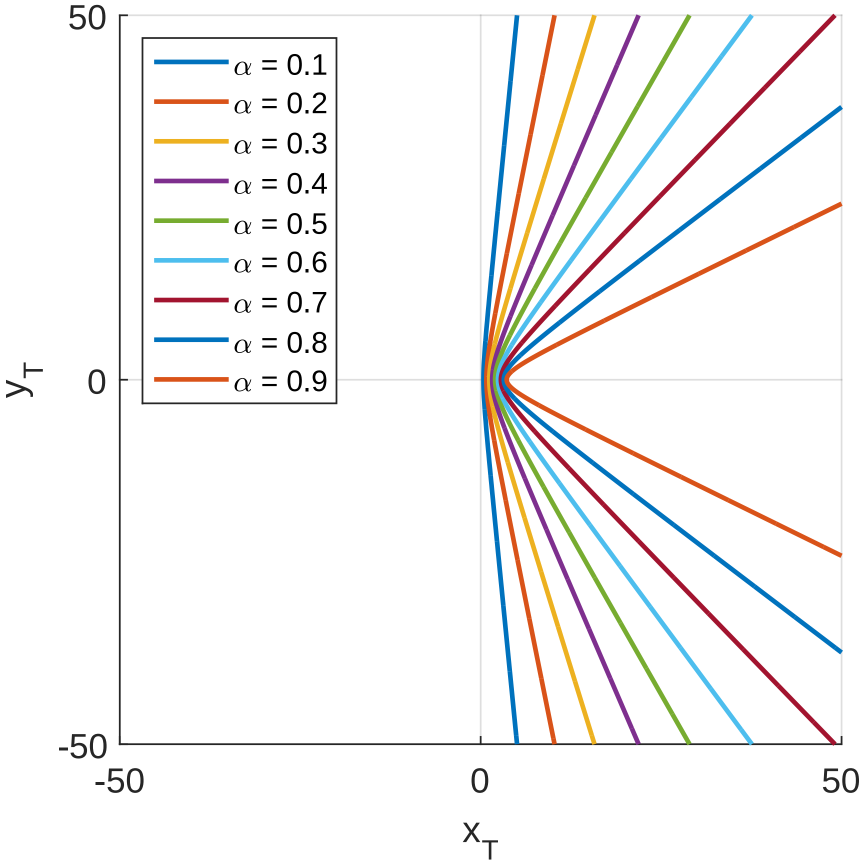

Figure 8.3: Various accepted branches of the voronoi diagram for $\gamma = 1$ and α as a parameter ranging from 0 to 1. These curves are computer generated from (8.3) and (8.6)

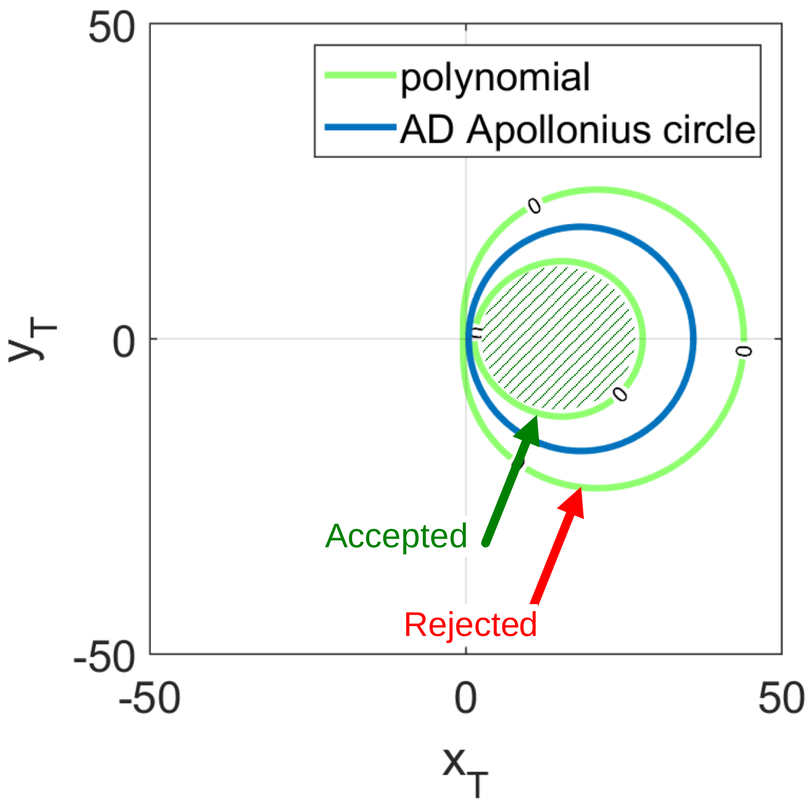

Figure 8.4: generated computer output for the Voronoi diagram bordering the safe region for $x_A = 4$, $\alpha = 0.25$, $\gamma = 0.8$ (the safe region is the unshaded area) the quartic in (8.2) or (8.3) produces two closed curves: one outside the AD-Apollonius circle (rejected) and the other inside the circle (accepted as the Voronoi diagram)

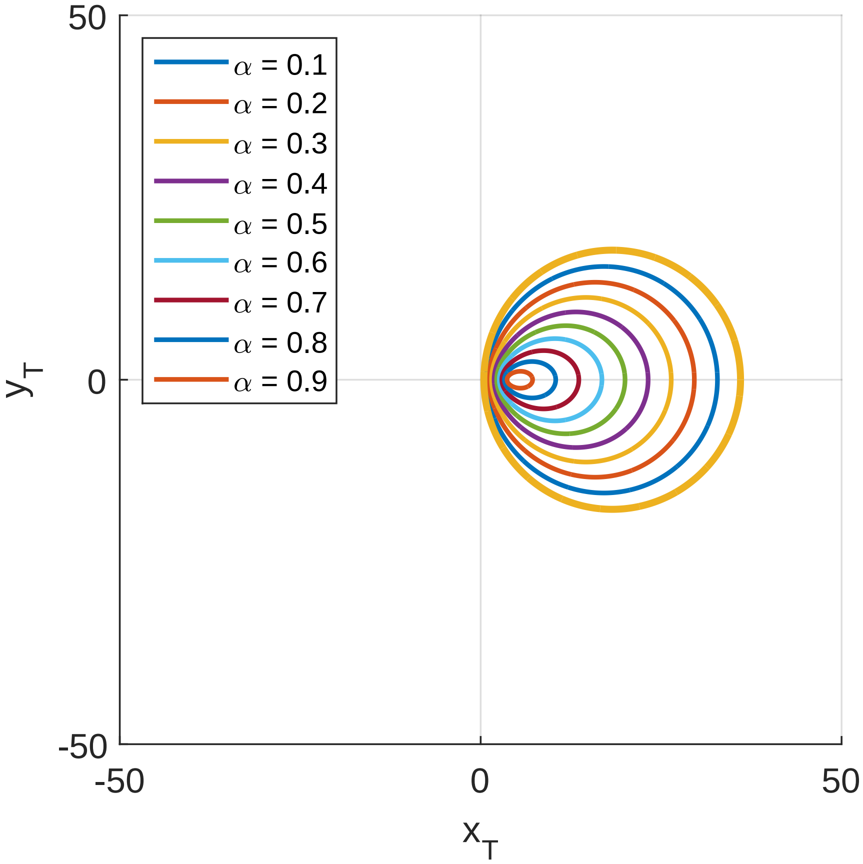

Figure 8.5: Various accepted branches of the voronoi diagram for $\gamma = 0.8$ and α as a parameter ranging from 0 to 1. These curves are computer generated from (8.3) and (8.6)

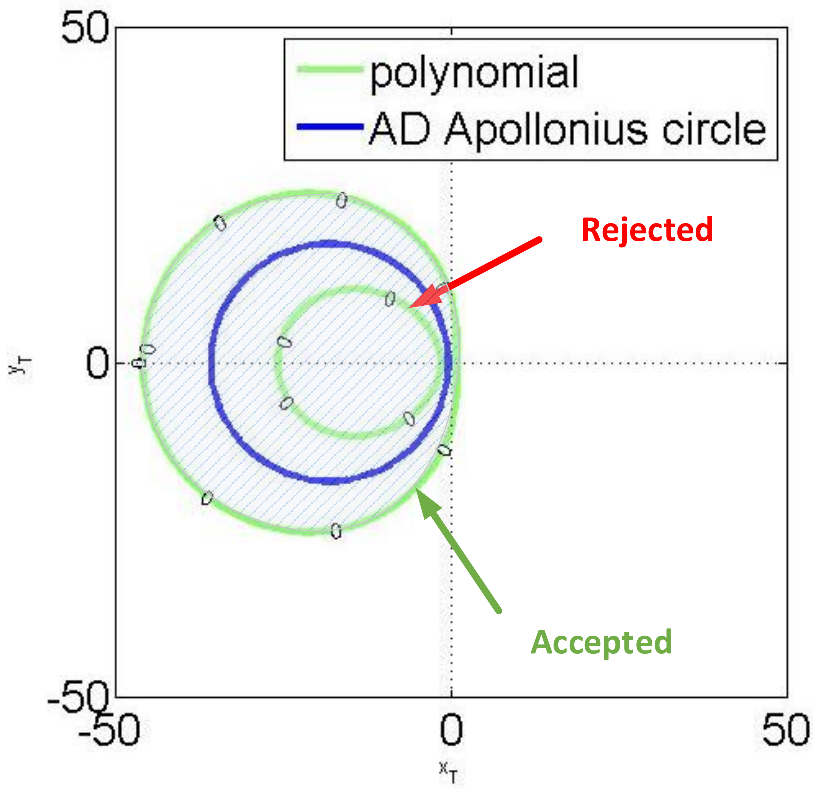

Figure 8.6: generated computer output for the Voronoi diagram bordering the safe region for $x_A = 4,\ \alpha = 0.25,\ \gamma = 1.25$ (the safe region is the shaded area) the quartic in (8.2) or (8.3) produces two closed curves: one inside the AD-Apollonius circle (rejected) and the other outside the circle (accepted as the Voronoi diagram)

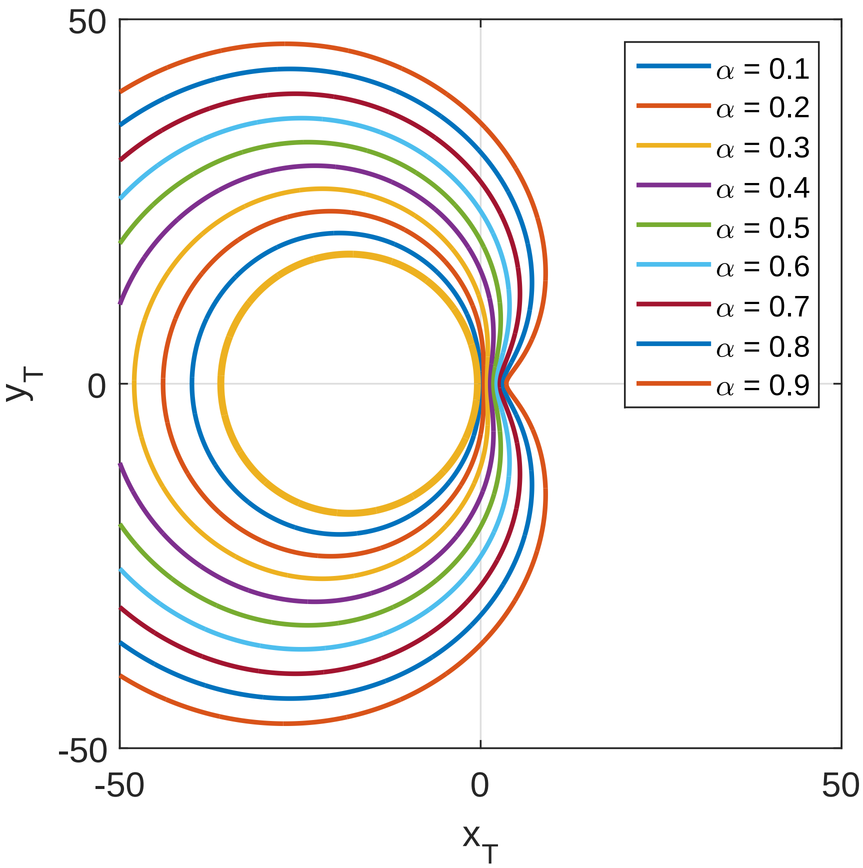

Figure 8.7: Various accepted branches of the voronoi diagram for $\gamma = 1.25$ and α as a parameter ranging from 0 to 1. These curves are computer generated from (8.3) and (8.6)

Chapter 9: OPTIMAL STRATEGIES

The TAD pursuit-evasion differential game is discussed and solved herein to obtain the optimal heading angels for the Target and the Defender team to maximize the terminal separation between the Target and Attacker, and also to obtain the optimal heading angle for the Attacker to minimize this distance. In the following sections, we discuss a variety of cases differing according to the initial position of the Target $\boldsymbol{T} = (x_T, y_T)$ relative to the AD-Apollonius circle, and also according to whether the Defender is fast ($\gamma < 1$), similar ($\gamma = 1$) or slow ($\gamma > 1$).

9.1 Target initial position is outside the AD Apollonius circle, and $\gamma < 1$

Assume that the Target, Attacker, and Defender aim at points v, u and w on the AD Apollonius circle. While the Attacker and Defender try to go to points u and w, the Target tries to run away from the point u. These three agents try collectively to solve the minmax optimization problem.

$$min_u \; max_{v,w} \; J(u, v, w) \tag{9.1}$$

where the cost/payoff function $J(u, v, w)$ is the final separation, i.e., the distance between the Target terminal position T' and the point C on the AD Apollonius circle where the Defender intercepts the Attacker, i.e.,

$$\begin{aligned} J(u, v, w) &= CT' = CT + TT' \\ &= CT + \alpha\, AC \\ &= [(x_C - x_T)^2 + (y_C - y_T)^2]^{\frac{1}{2}} + \alpha[(x_A - x_C)^2 + y_C^2]^{\frac{1}{2}} \\ &= J(x_C, y_C) \end{aligned} \tag{9.2}$$

Note that the Target is initially outside the AD-Apollonius circle, i.e., it is within the Reachability Region R_r whose points are reachable by the Defender before the Attacker. Hence, the Defender can help the Target regardless of the effort contributed by the Target, i.e., regardless of the speed ratio α ($0 \le \alpha < 1$). This means that the critical speed ratio in this case $\overline{\alpha} = 0$. The Defender's optimal policy is to choose its aim point w as w^* such that:

$$w^*(u, v) = u, \tag{9.3}$$

in order to guarantee interception of the Attacker (which is aiming at u). The cost/payoff function $J(u, v, w)$ can now be viewed as $J(u, v)$, i.e., a function of u and v only. Gaecia, et al. [48] assert also the solution of the optimization problem (9.1) is such that

$$u^* = v^*. \tag{9.4}$$

The point C chosen in (9.2) is in fact the common optimal aim points (according to (9.3) and (9.4)), i.e.,

$$C = u^* = v^* = w^*, \tag{9.5}$$

which means that the statement made in (9.2) is indeed correct. Hence the optimization problem (9.1) is replaced by

$$min_{(x_C,y_C)} J(x_C, y_C) \;\; subject\ to\ (x_C, y_C)\ being\ on\ the\ AD\ circle \tag{9.6}$$

With angle ϕ defined as the complement to the polar angle of position vector of C w.r.t. the centre of the AD Apollonius circle and the angle λ defined as the complement to the polar angle of the position vector of T w.r.t. that center (Fig. 9.1), the *constrained* optimization in (9.6) is replaced by the *unconstrained* optimization [48] with a single independent variable ϕ,

$$min_{\phi} J(\phi) \tag{9.7}$$

where

$$J(\phi) = [r_1^2 + N^2 - 2Nr_1\cos(\phi - \lambda)]^{\frac{1}{2}} + \alpha[r_1^2 + M^2 - 2Mr_1\cos\phi]^{\frac{1}{2}} \tag{9.8}$$

where by view of (6.15) and (6.15), we have

$$r_1 = \frac{2\gamma}{1-\gamma^2} x_A, \tag{9.9}$$

$$M = AO_1 = (\frac{1+\gamma^2}{1-\gamma^2})x_A - x_A = \frac{2\gamma^2}{1-\gamma^2} x_A = \gamma r_1, \tag{9.10}$$

$$N = O_1T = [(\frac{1+\gamma^2}{1-\gamma^2} x_A - x_T)^2 + y_T^2]^{\frac{1}{2}}, \tag{9.11}$$

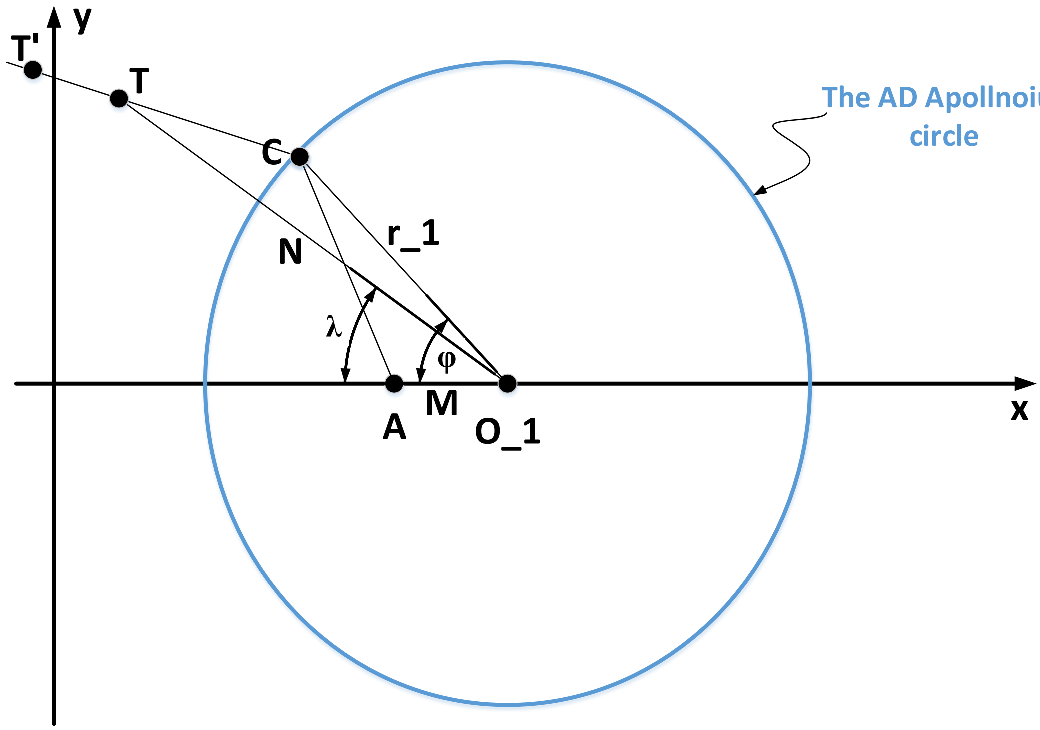

Figure 9.1: Pertaining to expressing the final separation in terms of shown distances and angles

We now solve (9.7) by setting $\dfrac{dJ(\phi)}{d\phi}$ to zero, thereby obtaining

$$Nr_1\sin(\phi-\lambda)[r_1^2+N^2-2Nr\cos(\phi-\lambda)]^{\frac{-1}{2}} = -\alpha M r_1 \sin\phi[r_1^2+M^2-2Mr\cos\phi]^{\frac{-1}{2}} \quad (9.12)$$

which is squared and simplified via (9.10) to obtain:

$$N^2 r_1^2 \sin^2(\phi-\lambda)[1+\gamma^2-2\gamma\cos\phi] = \alpha^2 M^2 \sin^2\phi[r_1^2+N^2-2Nr_1\cos(\phi-\lambda)] \quad (9.13)$$

Note that both sides of (9.13) now have the dimension of $(length)^4$. Now, we substitute for $\sin\phi, \cos\phi, \sin(\phi-\lambda), \cos(\phi-\lambda)$ by their exponential expressions

$$\sin\phi = \tfrac{1}{2j}[e^{j\phi}-e^{-j\phi}],$$

$$\cos\phi = \tfrac{1}{2}[e^{j\phi}+e^{-j\phi}],$$

$$\sin(\phi-\lambda) = \tfrac{1}{2j}[e^{j(\phi-\lambda)}-e^{-j(\phi-\lambda)}]$$

,

$$\cos(\phi-\lambda) = \tfrac{1}{2}[e^{j(\phi-\lambda)}+e^{-j(\phi-\lambda)}] = \tfrac{1}{2}[e^{j\phi}l^{-1}+e^{-j\phi}l],$$

to obtain

$$\sin^2\phi = -\tfrac{1}{4}[e^{j(2\phi)} + e^{-j(2\phi)} - 2]$$

$$\sin^2(\phi-\lambda) = -\tfrac{1}{4}[e^{j(2\phi)}e^{-j(2\lambda)} + e^{-j(2\phi)}e^{j(2\lambda)} - 2] = -\tfrac{1}{4}[e^{j(2\phi)}l^{-2} + e^{-j(2\phi)}l^2 - 2]$$

$$\begin{aligned} &N^2r_1^2[e^{j(2\phi)}l^{-2} + e^{-j(2\phi)}l^2 - 2][1+\gamma^2-\gamma(e^{j\phi}+e^{-j\phi})] \\ &= \alpha^2M^2[e^{j(2\phi)}+e^{-j(2\phi)}-2][r_1^2+N^2-Nr_1(e^{j\phi}l^{-1}+e^{-j\phi}l)] \end{aligned} \tag{9.14}$$

where $l = e^{j\lambda}$

$$\begin{aligned} &[-N^2r_1^2l^{-2}\gamma + Nr_1l^{-1}\alpha^2M^2]e^{j(6\phi)} \\ &+[N^2r_1^2l^{-2}(1+\gamma^2) - \alpha^2M^2(r_1^2+N^2)]e^{j(5\phi)} \\ &+[-N^2r_1^2l^{-2}\gamma + 2\gamma N^2r_1^2 + \alpha^2M^2Nr_1l - 2\alpha^2M^2Nr_1l^{-1}]e^{j(4\phi)} \\ &+[-2N^2r_1^2(1+\gamma^2) + 2\alpha^2M^2(r_1^2+N^2)]e^{j(3\phi)} \\ &+[-N^2r_1^2l^2\gamma + 2N^2r_1^2\gamma + \alpha^2M^2Nr_1l^{-1} - 2\alpha^2M^2Nr_1l]e^{j(2\phi)} \\ &+[N^2r_1^2l^2(1+\gamma^2) - \alpha^2M^2(r_1^2+N^2)]e^{j\phi} \\ &+[-N^2r_1^2l^2\gamma + \alpha^2M^2Nr_1l] = 0 \end{aligned} \tag{9.15}$$

Now, we rewrite (9.15) in the following form (in an attempt to make it resemble equation (41) in [48]) by invoking (9.10) and dividing by $\alpha^2M^2 = \alpha M\gamma r_1$.

$$\begin{aligned} &\frac{Nr_1}{l}(1-\frac{N}{\alpha^2Ml})e^{j(6\phi)} \\ &+[(\frac{N}{\alpha Ml})^2(r_1^2+M^2) - (r_1^2+N^2)]e^{j(5\phi)} \\ &+Nr_1[\frac{N}{\alpha^2Ml^2}(2l^2-1) + (l-\frac{2}{l})]e^{j(4\phi)} \\ &+2[r_1^2+N^2-(\frac{N}{\alpha M})^2(r_1^2+M^2)]e^{j(3\phi)} \\ &+Nr_1[(\frac{N}{\alpha^2M})(2-l^2) - 2l + \frac{1}{l}]e^{j(2\phi)} \\ &+[(\frac{Nl}{\alpha M})^2(r_1^2+M^2) - (r_1^2+N^2)]e^{j\phi} \\ &+Nr_1l(1-\frac{Nl}{\alpha^2M}) = 0 \end{aligned} \tag{9.16}$$

Equation (9.16) is a sixth-degree polynomial in $e^{j\phi}$ that has six roots. Each of these roots should be substituted in the expression (9.8) for $J(\phi)$ to determine which root yields the minimal value of $J(\phi)$.

9.2 Target initial position is inside the AD-Apollonius circle, and $\gamma < 1$

Again, the Target, Attacker, and Defender aim at points u, v and W on the AD-Apollonius circle, but now each of them is going toward its respective aim. The three agents now try to collectively solve the *maxmin* optimization problem

$$max_{v,w}\ min_u\ J(u,v,w) \tag{9.17}$$

Garcia et al. [48] use arguments similar to those of Sec. 6.1 to deduce conditions similar to (9.3) - (9.5), and then reduce to (9.17) to a form similar to that of (9.6) [albeit with minimization replaced by maximization]

$$max_{(x_c,y_c)}\ J(x_c,y_c) \quad subject\ to\ (x_c,y_c)\ being\ on\ the\ AD\ circle, \tag{9.18}$$

where

$$\begin{aligned} J(x_c,y_c) &= CT' = TT' - CT \\ &= \alpha\ AC - CT \\ &= \alpha[(x_A - x_c)^2 + y_c^2]^{\frac{1}{2}} - [(x_c - x_T)^2 + (y_c - y_T)^2]^{\frac{1}{2}} \end{aligned} \tag{9.19}$$

Again, the constrained optimization (9.18) can be replaced by constrained optimization of single-variable cost/payoff function, $J(\phi)$, namely

$$max_\phi\ J(\phi), \tag{9.20}$$

where

$$J(\phi) = \alpha[r_1^2 + M^2 - 2r_1 M\cos\phi]^{\frac{1}{2}} - [r_1^2 + N^2 - 2r_1 N\cos(\lambda - \phi)]^{\frac{1}{2}}. \tag{9.21}$$

where, again, $M = AO_1$ and $N = TO_1$. Equation (9.21) differs from (9.8) in the sign of one of its two terms. Setting $\dfrac{dJ(\phi)}{d(\phi)}$ to zero results in an equation that has a sign difference from (9.12) which is lost upon squaring to obtain (9.13).

Therefore, (9.14)-(9.16) are obtained in this case also. Again, one has to obtain each of the six roots of (9.16), but now he has to substitute it in the expression (9.21) for $J(\phi)$ to determine which root yields the maximal (rather than the minimal) value for $J(\phi)$.

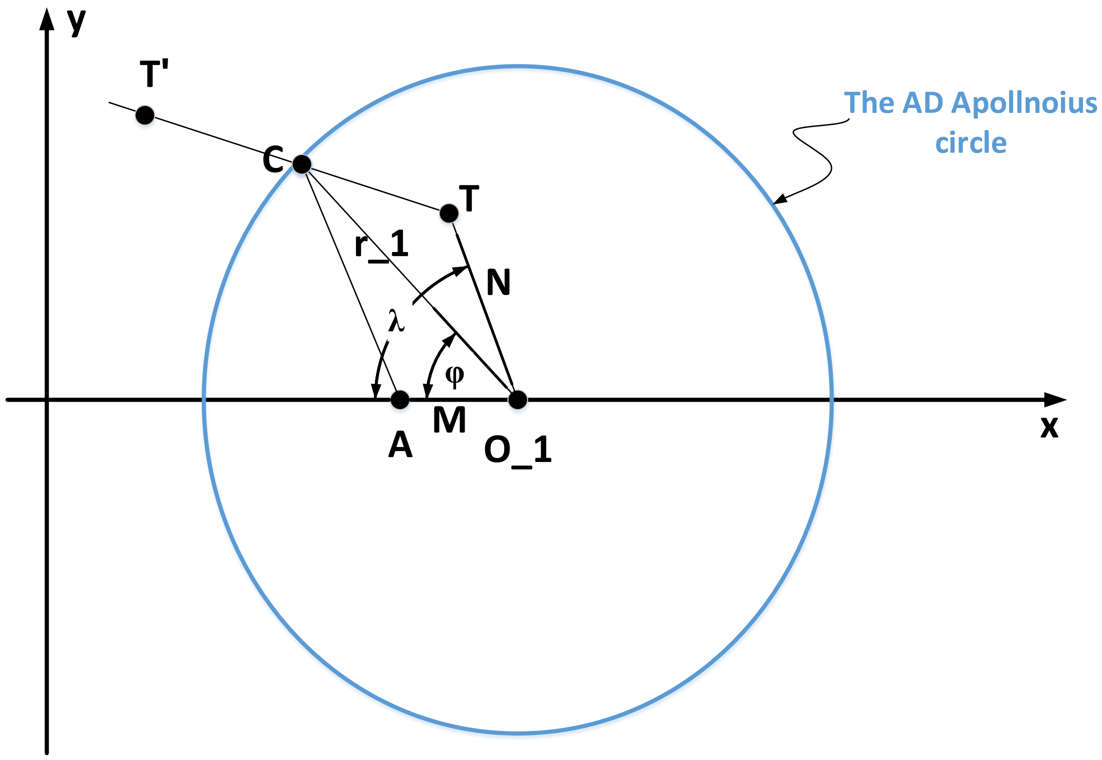

Figure 9.2: Pertaining to expressing the final separation in terms of the shown distance and angles for $\gamma < 1$ and T inside the AD Apollonius circle, i.e., outside R_r.

9.3 Target initial position is in the R.H.S. of the XY-plane, and $\gamma = 1$

This case, which appears here for the first time, resembles that of Sec. 6.1, with the exception that the condition $\gamma = 1$ makes the AD-Apollonius circle degenerate into the perpendicular bisector or the Y-axis (Fig. 9.4). Now the cost/payoff function is replaced by

$$\begin{aligned} J(y_c) &= CT' = CT + TT' \\ &= CT + \alpha\, AC \\ &= [x_T^2 + (y_c - y_T)^2]^{\frac{1}{2}} + \alpha[x_A^2 + y_c^2]^{\frac{1}{2}}. \end{aligned} \tag{9.22}$$

and one has to solve a single-variable unconstrained minimization problem.

$$min_{y_c}\ J(y_c) \tag{9.23}$$

by setting $\dfrac{dJ(y_c)}{dy_c}$ to zero, i.e.,

$$\frac{dJ(y_c)}{dy_c} = \frac{(y_c - y_T)}{[x_T^2 + (y_c - y_T)^2]^{\frac{1}{2}}} + \frac{\alpha y_c}{[x_A^2 + y_c^2]^{\frac{1}{2}}} = 0. \tag{9.24}$$

which can be arranged as

$$(y_c - y_T)(x_A^2 + y_c^2)^{\frac{1}{2}} = -\alpha y_c (x_T^2 + (y_c - y_T)^2)^{\frac{1}{2}} \tag{9.25}$$

Equation (9.25) can be squared to yield the following quartic (fourth-degree) real equation in y_c.

$$(y_c^2 - 2y_c y_T + y_T^2)(x_A^2 + y_c^2) = \alpha^2 y_c^2 [x_T^2 + y_c^2 + y_T^2 - 2y_c y_T] \tag{9.26}$$

or

$$(1-\alpha^2)y_c^4 - 2(1-\alpha^2)y_T y_c^3 + [(1-\alpha^2)y_T^2 + x_A^2 - \alpha^2 x_T^2]y_c^2 - 2x_A^2 y_T y_c + x_A^2 y_T^2 = 0 \tag{9.27}$$

Equation (9.27) yields four roots (expected to ba all real, or to have two real and two complex conjugate roots). Each of the real roots is substituted into $J(y_c)$ given by (9.22) to select the one minimizing it.

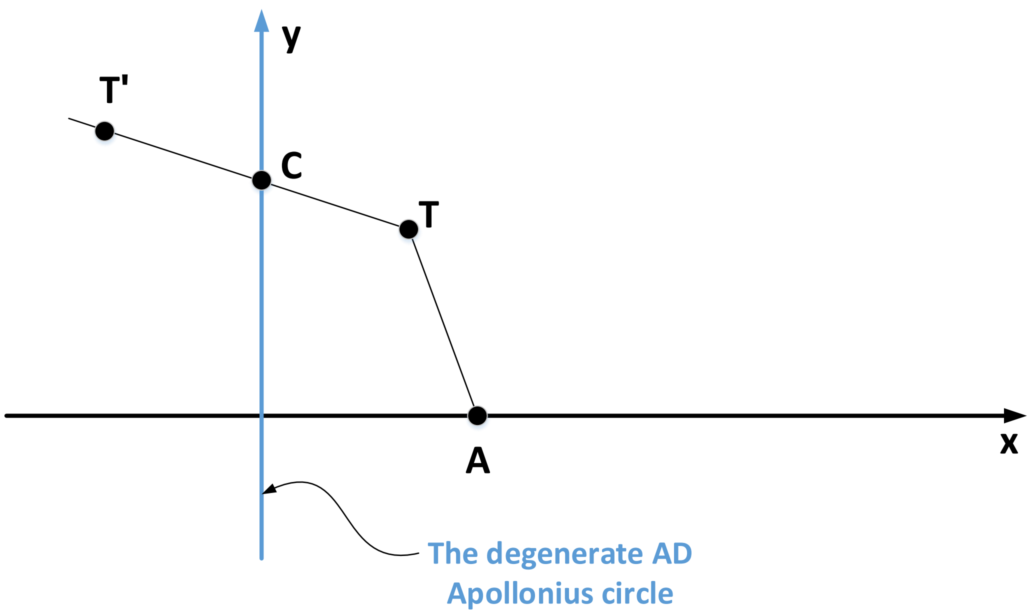

Figure 9.3: Pertaining to expressing the final separation CT' when $\gamma = 1$ and T is in the R.H.S. of the Y-plane, i.e., outside R_r.

9.4 Target initial position is in the L.H.S. of the XY-plane, and $\gamma = 1$

This case was discussed previously by Garcia et al. [], and resemble that of Sec. 6.1, with the exception that the condition $\gamma = 1$ makes the AD-Apollonius circle degenerate into the perpendicular bisector or the Y-axis (Fig. 9.3). The current case is also similar to the case in Sec. 6.3, with the exception that $\boldsymbol{T}$ is in the L.H.S. rather than the R.H.S. of the Y-plane. Now, the cost/payoff function is replaced by

$$\begin{aligned} J(y_c) &= CT' = TT' - CT \\ &= \alpha\, AC - CT \\ &= \alpha[x_A^2 + y_c^2]^{\frac{1}{2}} - [x_T^2 + (y_c - y_T)^2]^{\frac{1}{2}}, \end{aligned} \tag{9.28}$$

and one has to solve a single-variable unconstrained maximization problem

$$max_{y_c}\ J(y_c) \tag{9.29}$$

by setting $\dfrac{dJ(y_c)}{dy_c}$ to zero, i.e.,

$$\frac{dJ(y_c)}{dy_c} = \frac{\alpha y_c}{[x_A^2 + y_c^2]^{\frac{1}{2}}} - \frac{(y_c - y_T)}{[x_T^2 + (y_c - y_T)^2]^{\frac{1}{2}}} \tag{9.30}$$

Equation (9.30) can be rearranged and then squared to yield (9.26) and consequently (9.27). Each of the real roots or the quartic equation (9.27) should be substituted into $J(y_c)$ given by (9.28) to decide which of them maximize $J(y_c)$

9.5 Target initial position is inside the AD Apollonius circle, and $\gamma > 1$

Again, the case discussed in this section has not appear earlier in the open literature. This case resembles the cases in sections 6.1 and 6.3 in the fact that it deals with a Target initially within R_2. The current situation is depicted in Fig. 9.5, in which the distances M, N and angels ϕ and λ are defined. Note that the angles ϕ and λ are the polar angles (rather than complements thereof) for the position vector of C and T w.r.t. the center O_1 of the AD Apollonius circle. The distance $N = O_1T$ is still given by (9.11), while $M = AO_1$ is given by

$$\begin{aligned} M + AO_1 &= x_A - \frac{1+\gamma^2}{1-\gamma^2} x_A \\ &= \frac{-2\gamma^2}{1-\gamma^2} x_A = \frac{2\gamma^2}{\gamma^2 - 1} x_A \\ &= \gamma r_1, \end{aligned} \tag{9.31}$$

a result that can be unified with (9.10) in the form

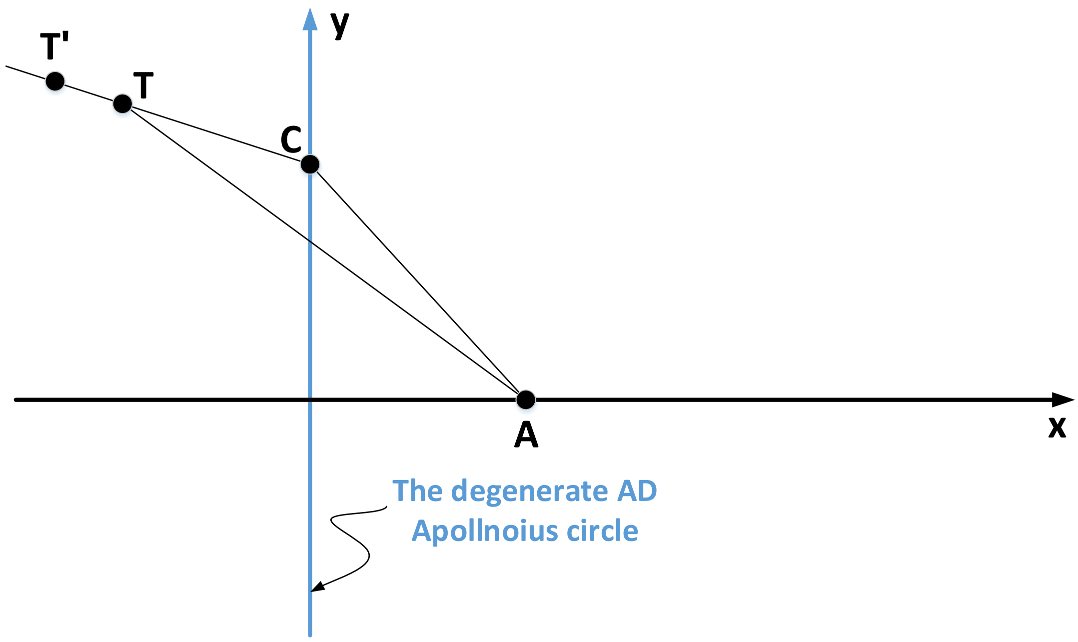

Figure 9.4: Pertaining to expressing the final separation CT' when $\gamma = 1$ and T is in the L.H.S. of the Y-plane, i.e., within R_r.

$$M = \frac{2\gamma^2}{|1-\gamma^2|} x_A = \gamma r_1. \tag{9.32}$$

with these minor observations, we can easily verify that equations (9.1)-(9.16) are still valid in the current case.

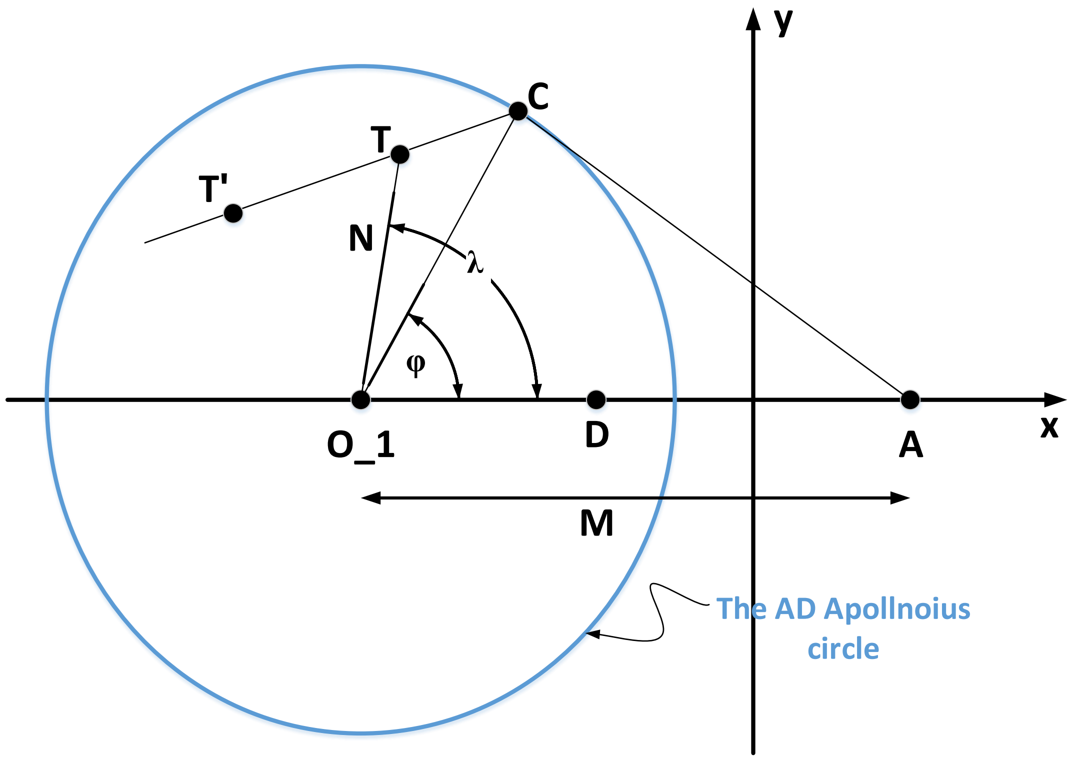

Figure 9.5: Pertaining to expressing the final separation in terms of the shown distance and angles for $\gamma > 1$ and T inside the AD Apollonius circle, i.e., within R_r.

9.6 Target initial position is outside the *AD* Apollonius circle, and $\gamma > 1$

This case is again a novel case. It resembles the cases in the Sections 6.2 and 6.4 in the fact that it deals with a Target initially outside R_r. It is similar to the case in the previous section (Sec. 6.5) as both sections deals with a slow Defender. The situation is demonstrated by Fig. 9.6, which has similarities and differences with Fig. 9.2 and Fig. 9.5. We can easily verify that equations (9.18)-(9.21), and consequently equations (9.14)-(9.16) are still valid in the current case.

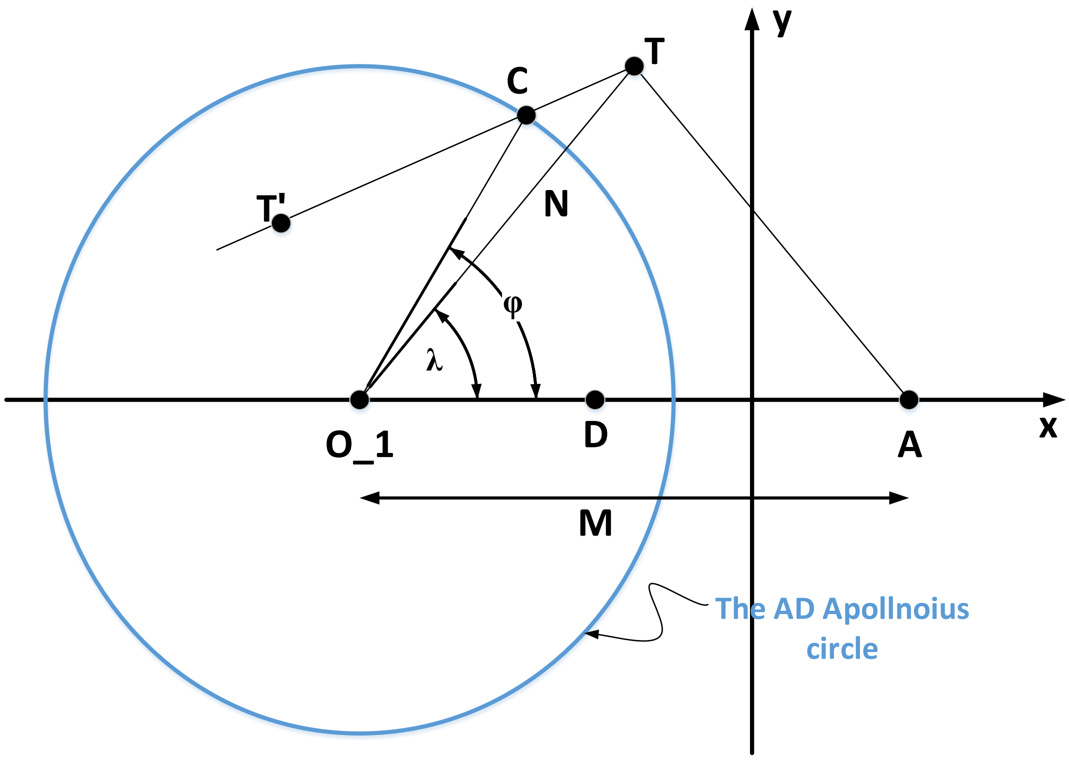

Figure 9.6: Pertaining to expressing the final separation in terms of the shown distance and angles for $\gamma > 1$ and T outside the AD Apollonius circle, i.e., outside R_r.

9.7 Numerical Results

We study the optimal values of ϕ or y_c for $x_A = 4,\ \alpha = 0.25$ and the following choices of γ and (x_T, y_T)

9.7.1 $\gamma = 0.8,\ x_T = 1.0,\ y_T = 20.0$

This is the case in Sec. 6.1, and is handled by obtaining six roots via (9.16) and selecting the one which minimizes $J(\phi)$ in (9.8). Results are shown in Table 6.1 and the optimal value of ϕ is $\phi_{optimal} =$

i	$\phi_i = Root \neq i$ of (9.16)	$J(\phi_i)$ in (9.8) [choose minimum]
1		
2		
3		
4		
5		
6		

9.7.2 $\gamma = 0.8,\ x_T = 20.0,\ y_T = 1.0$

This is the case in Sec. 6.2, and is handled by obtaining six roots via (9.16) and selects the one that maximizes $J(\phi)$ in (9.21). Results are shown in Table 6.2, and the optimal value of ϕ is $\phi_{optimal} =$

i	$\phi_i = Root \neq i$ of (9.16)	$J(\phi_i)$ in (9.21) [choose minimum]
1		
2		
3		
4		
5		
6		

9.7.3 $\gamma = 1.0,\ x_T = -1.0,\ y_T = 1.0$

This is the case in Sec. 6.3, and is handled by obtaining four roots via (9.27) and selecting the one that *minimizes* $J(\phi)$ in (9.24). Results are shown in Table 6.3, and the optimal value of $y_c =$

i	$\phi_i = Root \neq i$ of (9.21)	$J(\phi_i)$ in (9.24) [choose minimum]
1		
2		
3		
4		

9.7.4 $\gamma = 1.0,\ x_T = 1.0,\ y_T = 1.0$

This is the case in Sec. 6.4, and is handled by obtaining four roots via (9.27) and selecting the one that maximizes $J(y_c)$ in (9.28). Results are shown in Table 6.4, and the optimal value of $y_c =$

i	$y_i = Root \neq i$ of (9.27)	$J(\phi_i)$ in (9.28) [choose minimum]
1		
2		
3		
4		

9.7.5 $\gamma = 1.25,\ x_T = -20.0,\ y_T = 1.0$

This is the case in Sec. 6.5, and is handled by obtaining six roots via (9.16) and selecting the one that *minimizes* $J(\phi)$ in (9.8). Results are shown in Table 6.5 and the optimal value of ϕ is $\phi_{optimal} =$

i	$\phi_i = Root \neq i$ of (9.16)	$J(\phi_i)$ in (9.8) [choose minimum]
1		
2		
3		
4		
5		
6		

9.7.6 $\gamma = 1.25,\ x_T = -1.0,\ y_T = 20.0$

This is the case in Sec. 6.6, and is handled by obtaining six roots via (9.16) and selecting the one that maximizes $J(\phi)$ in (9.21). Results are shown in Table 6.6, and the optimal value of ϕ is $\phi_{optimal} =$

i	$\phi_i = Root \neq i$ of (9.16)	$J(\phi_i)$ in (9.21) [choose minimum]
1		
2		
3		
4		
5		
6		

Chapter 10: OPTIMAL HEADING ANGLE SIMULATION

In this chapter, we address the active target defense differential game where an Attacker missile pursues a Target aircraft. A Defender missile is fired by the Targets wingman in order to intercept the Attacker before it reaches the aircraft. Thus, a team is formed by the Target and the Defender which cooperate to maximize the distance between the Target aircraft and the point where the Attacker missile is intercepted by the Defender missile, while the Attacker tries to minimize said distance. The results shown here extend previous work. We consider here the case where the Defender is faster than the Attacker. The solution to this differential game provides optimal heading angles for the Target and the Defender team to maximize the terminal separation between Target and Attacker and it also provides the optimal heading angle for the Attacker to minimize the said distance.

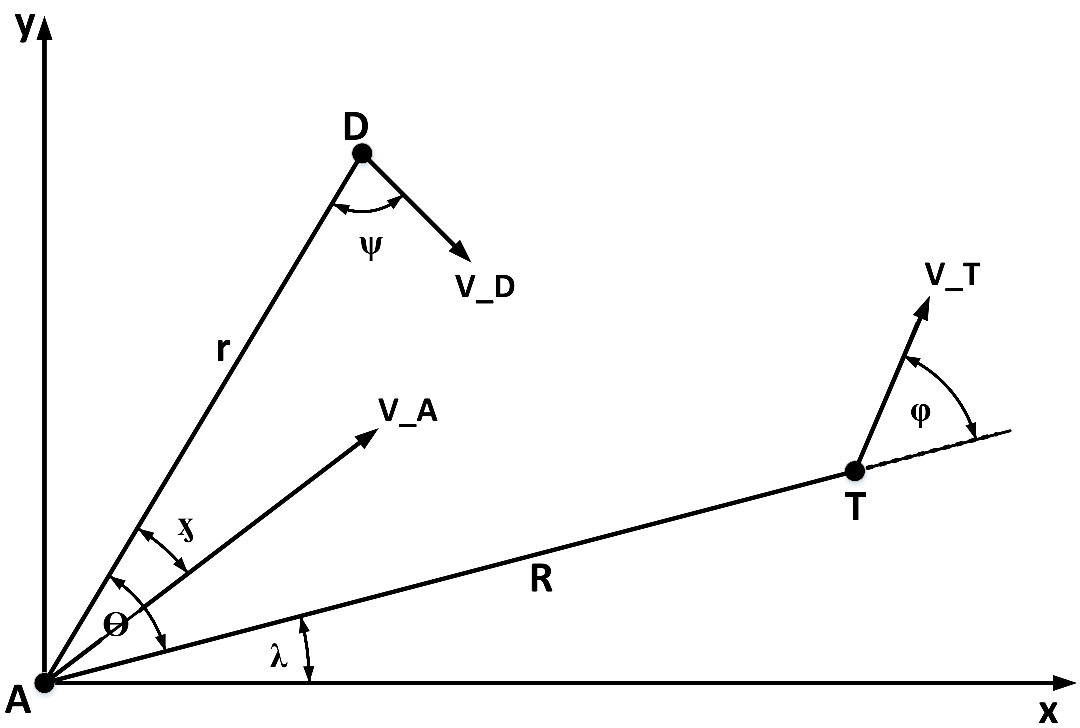

Figure 10.1: State space for the Attacker (A), Target (T), and Defender (D). The origin is arbitrary situated at the Attacker position (A). In polar coordinates with respect to arbitrary coordinates (x, y), the various positions and speeds are

Figure 10.1 illustrates the state space for the ATD game. The variables R and r are the separations between the Target and Attacker, respectively, and hence denote the radial polar coordinates of the Target and Defender when the origin of coordinates is arbitrarily situated at the position of the Attacker, The speeds of the Attacker, Target and Defender are denoted by $\boldsymbol{V_A}$, $\boldsymbol{V_T}$, $\boldsymbol{V_D}$ with corresponding magnitudes V_A, V_T and V_D, and polar angles

$$Ang\ \boldsymbol{V_A} = \hat{\chi} = \lambda + \theta - \chi \tag{10.1}$$

$$Ang\ \boldsymbol{V_T} = \hat{\phi} = \lambda + \phi \tag{10.2}$$

$$Ang\ \boldsymbol{V_D} = \hat{\psi} = \lambda + \theta - (\pi - \psi) \tag{10.3}$$

The derivatives $\dot{R}$ and $\dot{r}$ can be obtained as differences in radial speeds, while $\dot{\theta}$ can be obtained in terms of the difference in circumferential speeds. The end points of the distance R are moving at a speed V_T at an angle ϕ with respect to the radial directions and a speed V_A at an angle $(\theta - \chi)$ with respect to the radial directions. Hence;

$$\begin{aligned} \dot{R} &= V_t \cos\phi - V_A \cos(\theta - \chi) \\ &= V_A(\alpha \cos\phi - \cos(\theta - \chi)) \end{aligned} \tag{10.4}$$

Similarly, we obtain

$$\begin{aligned} \dot{r} &= -V_A \cos\chi - V_D \cos\psi \\ &= V_A(-\cos\chi - \gamma \cos\psi) \end{aligned} \tag{10.5}$$

In the following, we will deliberately differ from Garcia et.al. [] We will not use <u>reduced</u> equations in which $V_A = V_D = 1$. Our equations will look dimensionally homogeneous to any reader, and we will allow $\gamma = \dfrac{V_D}{V_A}$ to differ from 1.

The circumferential speeds are

$$\begin{aligned} R\dot{\lambda} &= V_T \sin\phi - V_A \sin(\theta - \chi) \\ \dot{\lambda} &= V_A[\frac{\alpha}{R}\sin\phi - \frac{1}{R}\sin(\theta - \chi)] \\ r(\theta + \lambda)^{\cdot} &= -V_D \sin\psi + V_A \sin\chi \end{aligned}$$

Hence, one obtains

$$\dot{\lambda} = V_A[\frac{\alpha}{R}\sin\phi - \frac{1}{R}\sin(\theta - \chi)] \tag{10.6}$$

$$\dot{\theta} + \dot{\lambda} = V_A[-\frac{\gamma}{r}\sin\psi + \frac{1}{r}\sin\chi] \tag{10.7}$$

Now, subtract (10.7) minus (10.6) to obtain

$$\dot{\theta} = V_A[-\frac{\alpha}{R}\sin\phi + \frac{1}{R}\sin(\theta - \chi) - \frac{\gamma}{r}\sin\psi + \frac{1}{r}\sin\chi] \tag{10.8}$$

Equations (10.4), (10.5), (10.8) reduce to equations (10.6) of Garcia et.al [] when we set both V_A and $\gamma = \dfrac{V_D}{V_A}$ equal to 1.

The system dynamics are given by (10.4), (10.5), and (10.8) for $0 \leqslant t \leqslant t_f$, together with the initial conditions

$$R(t_0) = R_0,$$
$$r(t_0) = r_0,$$
$$\theta(t_0) = \theta_0,$$

The objective of the Target-Defender team is to maximize the separation between the Target and the Attacker at the interception time $R(t_f)$, where the terminal time t_f is free, such that $r(t_f) = r_c$. The objective of the Attacker is to minimize the same distance $R(t_f)$. This can be expressed as

$$max_{\phi,\psi}\ min_{\chi}\ J = \int_{t_0}^{t_f} \dot{R}\, dt$$

The Hamiltonian is

$$\begin{aligned} H =& \cos(\theta-\chi) - \alpha\cos\phi \\ &+ [\alpha\cos\phi - \cos(\theta-\chi)]\ \lambda_R \\ &- [\cos\chi + \cos\psi]\ \lambda_r \\ &+ [-\frac{\alpha}{R}\sin\phi + \frac{1}{R}\sin(\theta-\chi) - \frac{1}{r}\sin\psi + \frac{1}{r}\sin\chi]\ \lambda_\theta \end{aligned} \tag{10.9}$$

$$\begin{aligned} H =& -(1-\lambda_R)[\alpha\cos\phi - \cos(\theta-\chi)] \\ &- [\cos\chi + \beta\cos\psi]\ \lambda_R \\ &+ [-\frac{\alpha}{R}\sin\phi + \frac{1}{R}\sin(\theta-\chi) - \frac{\beta}{r}\sin\psi + \frac{1}{r}\sin\chi]\ \lambda_\theta \end{aligned}$$

We now find the optimal heading angles ψ^*, ϕ^* and χ^*. Since these angles are known to be positive or negative angles (ranging from $\frac{-\pi}{2}$ to $\frac{\pi}{2}$), it suffices to determine the tangent $\tan a$ of each angle a and then determine the cosine and sine from

$$\cos a = [1 + \tan^2 a]^{\frac{-1}{2}} \tag{10.10}$$

$$\sin a = \tan a[1 + \tan^2 a]^{\frac{-1}{2}} \tag{10.11}$$

We obtain ψ^* by partially differentiating the Hamiltonian (10.9) w.r.t. ψ and equating the derivative $\frac{\partial H}{\partial \psi}$ to zero, namely

$$\frac{\partial H}{\partial \psi} = \beta\lambda_r \sin\psi - \frac{\beta}{r}\lambda_\theta \cos\psi = 0 \tag{10.12}$$

Hence the optimal heading ψ^* is given by:

$$\tan\psi^* = \frac{\lambda_\theta / r}{\lambda_r} \tag{10.13}$$

Figure 10.5 shows that ψ^* is a (positive or negative) acute angle in a right-angled triangle

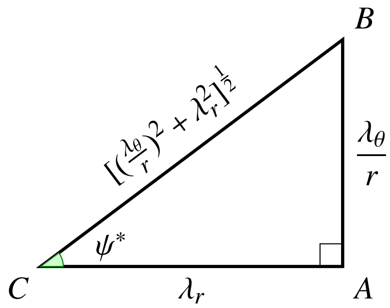

Figure 10.2: Defender

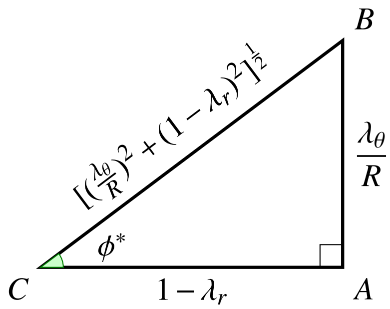

Figure 10.3: Target

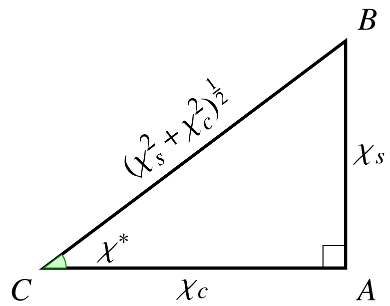

Figure 10.4: Attacker

Figure 10.5: Right-angled triangles that define the optimal headings ψ^*, ϕ^* and χ^* for the Defender, Target, and Attacker, respectively

with an opposite side equal to (λ_θ/r), an adjacent side equal to λ_r and a hypotenuse equal to $[(\frac{\lambda_\theta}{r})^2 + \lambda_r^2]^{\frac{1}{2}}$. Using Fig.10.5 or relations (10.10) and (10.11) one obtains

$$\cos\psi^* = \lambda_r[(\frac{\lambda_\theta}{r})^2 + \lambda_r^2]^{\frac{-1}{2}} = \frac{r\lambda_r}{\sqrt{\lambda_\theta^2 + r^2\lambda_r^2}} \tag{10.14}$$

$$\sin\psi^* = (\frac{\lambda_\theta}{r})[(\frac{\lambda_\theta}{r})^2 + \lambda_r^2]^{\frac{-1}{2}} = \frac{\lambda_\theta}{\sqrt{\lambda_\theta^2 + r^2\lambda_r^2}} \tag{10.15}$$

We further compute the second partial derivative of the Hamiltonian w.r.t. ψ, that is

$$
\begin{aligned}
\frac{\partial^2 H}{\partial \psi^2} &= \beta\lambda_r \cos\psi + \beta\frac{\lambda_\theta}{r}\sin\psi \\
&= [\beta r\lambda_r^2 + \beta\frac{\lambda_\theta^2}{r}][\lambda_\theta^2 + r^2\lambda_r^2]^{\frac{-1}{2}} > 0
\end{aligned}
\tag{10.16}
$$

The fact that $\frac{\partial^2 H}{\partial \psi^2} > 0$ means that the extremum obtained by (10.12) is a minimum, i.e., the optimal value ψ^* minimizes the cost $(-J)$.

We now obtain ϕ^* by partially differentiating Hamiltonian (10.9) w.r.t. ϕ and equating the partial derivative $\frac{\partial H}{\partial \phi}$ to zero, namely

$$
\frac{\partial H}{\partial \phi} = \alpha(1-\lambda_R)\sin\phi - \frac{\alpha}{R}\lambda_\theta\cos\phi = 0 \tag{10.17}
$$

Hence the optimal heading ϕ^* is given by

$$
\tan\phi^* = \frac{(\lambda_\theta/R)}{1-\lambda_R} \tag{10.18}
$$

Figure 10.5 shows that ϕ^* is a positive or negative acute angle in a right-angled triangle with an opposing side of length (λ_θ/R), an adjacent side of length $(1-\lambda_R)$, and a hypotenuse of length $[(\lambda_\theta/R)^2 + (1-\lambda_R)^2]^{\frac{1}{2}}$.

Using Fig.10.5 or relations (10.10) and (10.11), we obtain

$$
\cos\phi^* = (1-\lambda_R)[(\lambda_\theta/R)^2 + (1-\lambda_R)^2]^{\frac{-1}{2}} = \frac{R(1-\lambda_R)}{\sqrt{\lambda_\theta^2 + R^2(1-\lambda_R)^2}} \tag{10.19}
$$

$$
\sin\phi^* = (\lambda_\theta/R)[(\lambda_\theta/R)^2 + (1-\lambda_R)^2]^{\frac{-1}{2}} = \frac{\lambda_\theta}{\sqrt{\lambda_\theta^2 + R^2(1-\lambda_R)^2}} \tag{10.20}
$$

The second partial derivative of the Hamiltonian w.r.t. ϕ is given by

$$
\begin{aligned}
\frac{\partial^2 H}{\partial \phi^2} &= \alpha(1-\lambda_R)\cos\phi + \frac{\alpha}{R}\lambda_\theta\sin\phi \\
&= [\alpha R(1-\lambda_R)^2 + \frac{\alpha}{R}\lambda_\theta^2][\lambda_\theta^2 + R^2(1-\lambda_R)^2]^{\frac{-1}{2}} > 0
\end{aligned}
\tag{10.21}
$$

The fact that $\frac{\partial^2 H}{\partial \phi^2} > 0$ means that the extrema obtained by (10.17) is minimum, i.e., the optimal heading ϕ^* minimizes the cost $(-J)$.

Finally, we obtain the optimal heading χ^* by partially differentiating the Hamiltonian (10.9) w.r.t. χ and equating the partial derivative $\frac{\partial H}{\partial \chi}$ to zero, namely

$$
\frac{\partial H}{\partial \chi} = (1-\lambda_R)\sin(\theta-\chi) + \lambda_r\sin\chi - \frac{\lambda_\theta}{R}\cos(\theta-\chi) + \frac{\lambda_\theta}{r}\cos\chi = 0 \tag{10.22}
$$

Using the trigonometric expansions:

$$
\sin(\theta-\chi) = \sin\theta\,\cos\chi - \cos\theta\,\sin\chi \tag{10.23}
$$

$$\cos(\theta-\chi) = \cos\theta\ \cos\chi + \sin\theta\ \sin\chi \tag{10.24}$$

We can rewrite (10.22) in the form

$$\frac{\partial H}{\partial \chi} = \chi_s \cos\chi - \chi_c \sin\chi = 0 \tag{10.25}$$

where

$$\chi_s = (1-\lambda_R)\sin\theta - \frac{\lambda_\theta}{R}\cos\theta + \frac{\lambda_\theta}{r} \tag{10.26}$$

$$\chi_c = (1-\lambda_R)\cos\theta + \frac{\lambda_\theta}{R}\sin\theta - \lambda_r \tag{10.27}$$

The optimal heading χ^* is obtained from (10.25) as

$$\tan\chi^* = \frac{\chi_s}{\chi_c} \tag{10.28}$$

Figure 10.5 shows that χ^* is a positive or negative acute angle in a right-angled triangle with an opposing leg of length χ_s, an adjacent leg of length χ_c, and a hypotenuse of length $[\chi_s^2+\chi_c^2]^{\frac{1}{2}}$. Using Fig. 10.5 or relations (10.10) and (10.11), we obtain

$$\cos\chi^* = \chi_c\ [\chi_s^2+\chi_c^2]^{\frac{-1}{2}} = \frac{\chi_c}{\sqrt{\chi_s^2+\chi_c^2}} \tag{10.29}$$

$$\sin\chi^* = \chi_s\ [\chi_s^2+\chi_c^2]^{\frac{-1}{2}} = \frac{\chi_s}{\sqrt{\chi_s^2+\chi_c^2}} \tag{10.30}$$

The second derivative of the Hamiltonian w.r.t. χ is obtained from (10.25) as

$$\begin{aligned}\frac{\partial^2 H}{\partial \chi^2} &= -\chi_s \sin\chi - \chi_c \cos\chi \\ &= -[\chi_s^2+\chi_c^2](\chi_s^2+\chi_c^2)^{\frac{-1}{2}} \\ &= -(\chi_s^2+\chi_c^2)^{\frac{1}{2}} > 0\end{aligned} \tag{10.31}$$

Equation (10.31) demonstrates definitely that $\frac{\partial^2 H}{\partial \chi^2}$ is negative. The corresponding claim via Eq.(28) of Garcia et. al. [] is not complete. The fact that $\frac{\partial^2 H}{\partial \chi^2} < 0$ means that the extremum obtained via (10.25) is a maximum, i.e., the optimal heading χ^* maximizes the cost $(-J)$.

In passing, we note that (10.22) can be simplified via (10.14), (10.15), (10.19) and (10.20) to give:

$$\begin{aligned}\frac{\partial H}{\partial \chi} &= [(\frac{\lambda_\theta}{R})^2+(1-\lambda_R)^2]^{\frac{1}{2}}[\cos\phi\sin(\theta-\chi)-\sin\phi\cos(\theta-\chi)]+[(\frac{\lambda_\theta}{r})^2+\lambda_r^2]^{\frac{1}{2}}[\cos\psi\sin\chi+\sin\psi\cos\chi] \\ &= [(\frac{\lambda_\theta}{R})^2+(1-\lambda_R)^2]^{\frac{1}{2}}\sin(\theta-\chi-\phi)+[(\frac{\lambda_\theta}{r})^2+\lambda_r^2]^{\frac{1}{2}}\sin(\chi+\psi) = 0\end{aligned} \tag{10.32}$$

The expressions for the optimal heading angles (10.13), (10.18), and (10.28) are to be used in the numerical solution of the Two-Point Boundary Value Problem (TPBVP). That solution is found by substituting the optimal headings into the state equations (), and the co-state rquations () with the terminal conditions ().

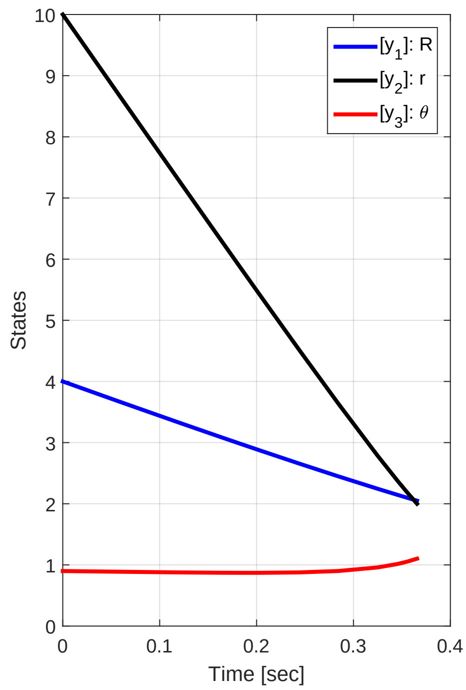

Figure 10.6: States

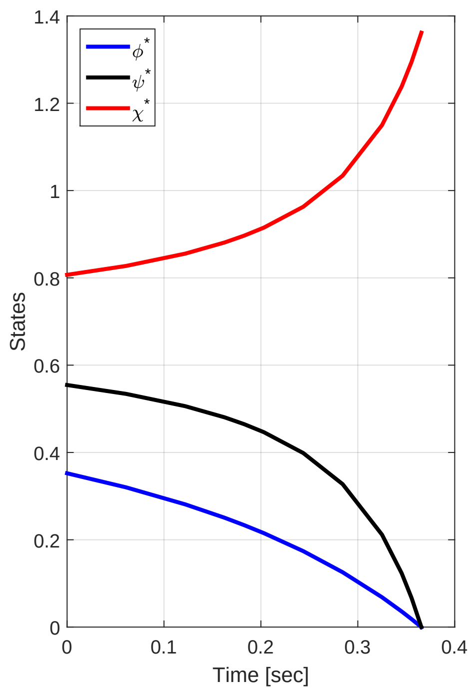

Figure 10.7: Optimal heading angles

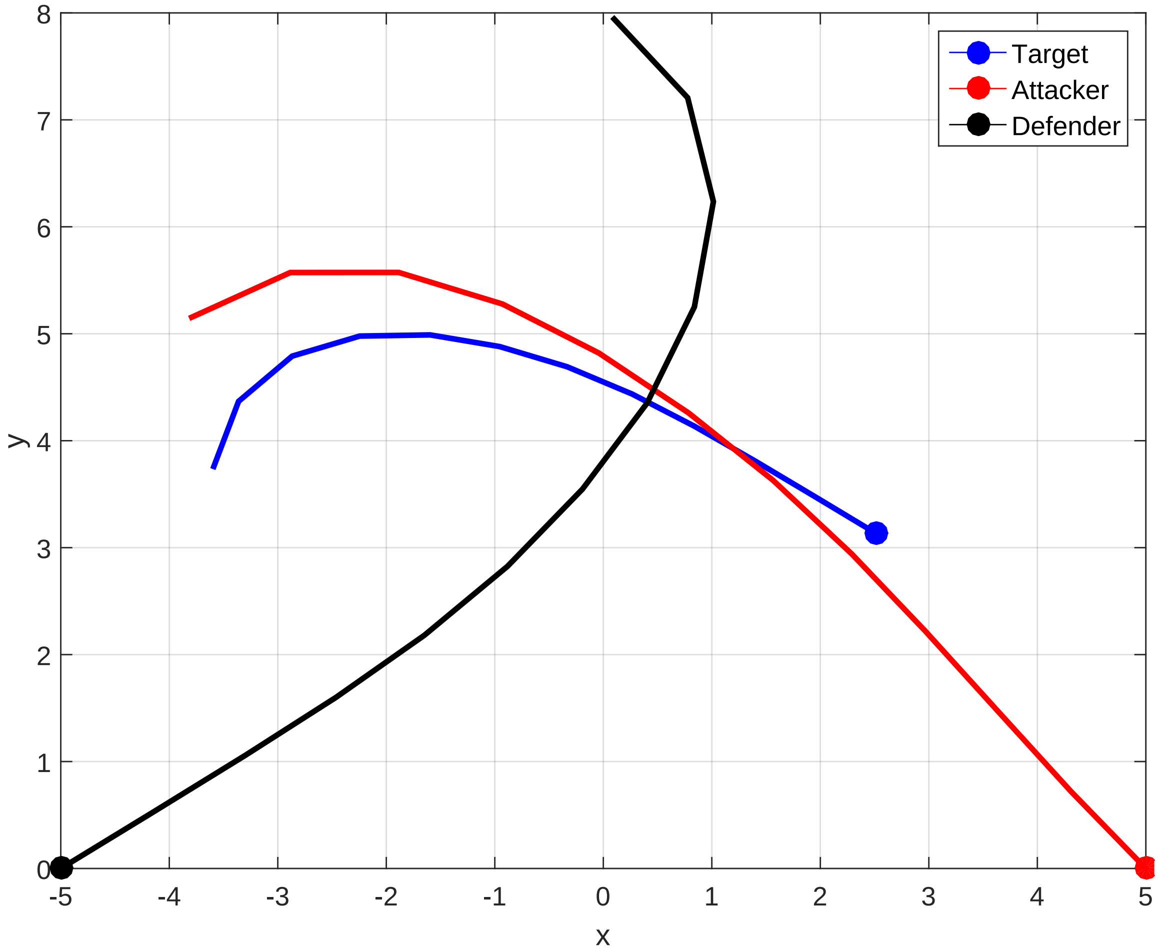

Figure 10.8: Optimal trajectories

Part IV

CONCLUSION AND FUTURE WORK

Chapter 11: CONCLUSION AND FUTURE WORK

This thesis offered a unified analytic solution of the TAD problem in which an Attacker is pursuing a Target while attempting to evade a Defender. The thesis reviews and extends the work that has recently appeared in [47, 48, 49], beside making the following new contributions:

1. The thesis covers all cases for the ratio γ of the Attacker's speed w.r.t the Defender's speed. It treats the case of a slow Defender $\gamma > 1$ for the first time, and presents this case along with the case of a fast Defender ($\gamma < 1$) discussed in [48] and the case of a similar Defender ($\gamma = 1$), discussed earlier in [47, 49].

2. The thesis demonstrates a striking increase in complexity when $\gamma \neq 1$ compared with the case $\gamma = 1$. It also demonstrates some sort of *duality* between the two cases of ($\gamma < 1$) and ($\gamma > 1$).

3. The thesis develops novel analytic expressions for the Voronoi diagrams for bordering the escape regions when ($\gamma < 1$) or ($\gamma > 1$). These expressions are more complex than the ones obtained in [3] for ($\gamma = 1$), and reduce to it as a limiting case.

4. The thesis offers a tutorial exposition of the TAD problem, uses simple arguments of plane geometry to develop the necessary Apollonius circle, utilizes equalities rather than inequalities in developing Voronoi diagram, and pays careful attention to the inadvertent inclusion of extraneous solutions so as to justify their subsequent rejection.

5. The thesis supplements its analysis with extensive computations for the critical speed ratio, Voronoi diagrams, and the optimal interception points. The results obtained encompass all possible values of γ, and they reduce to the already available results for $\gamma = 1$. Results for the trajectories and optimal interception points obtained agree with those obtained by the numerical solution of a two-point boundary value problem (TPBVP) utilizing Pontryagin's Maximum Principle [48].

Some possible extensions of the current work that warrant further exploration include:

1. Further analysis of the quartic equation obtained for the Voronoi diagram when $\gamma \neq 1$, with an aim to *split* it into two factors representing the rejected and accepted branches of the diagram.

2. Investigation of the sixth-degree complex polynomial equation for the optimal interception angle to get some *insight* about its six roots, and to find a better way for *selecting* desirable root.

3. Relaxation of some of the assumption used in this study. In particular, it is very interesting to consider the possibility of *variable* rather than constant speeds the three agents.

4. Addition of an element of *uncertainty* to the computation. For example, we might assume that the initial positions of the three agents are not deterministic but *stochastic* or *fuzzy*.

5. Extension of the current work to a more general situation involving several Targets, several Attackers and/or several Defenders.

Bibliography

[1] Adler, F. P., 1956, “Missile guidance by three-dimensional proportional navigation,” *Journal of Applied Physics*, vol. 27, no. 5, pp. 500–507.

[2] Becker, K., 1990, “Closed-form solution of pure proportional navigation,” *IEEE Transactions on Aerospace and Electronic Systems*, vol. 26, no. 3, pp. 526–533.

[3] Ghose, D., 1994, “On the generalization of true proportional navigation,” *IEEE Transactions on Aerospace and Electronic Systems*, vol. 30, no. 2, pp. 545–555.

[4] Gutman, S., 2012, “On optimal guidance for homing missiles,” *Journal of Guidance, Control, and Dynamics*.

[5] Shinar, J. and Gutman, S., 1980, “Three-dimensional optimal pursuit and evasion with bounded controls,” *IEEE Transactions on Automatic Control*, vol. 25, no. 3, pp. 492–496.

[6] Nesline, F. W. and Zarchan, P., 2012, “A new look at classical vs modern homing missile guidance,” *Journal of Guidance, Control, and Dynamics*.

[7] Anderson, G. M., 2012, “Comparison of optimal control and differential game intercept missile guidance laws,” *Journal of Guidance, Control, and Dynamics*.

[8] Pastrick, H., Seltzer, S., and Warren, M., 2012, “Guidance laws for short-range tactical missiles,” *Journal of Guidance, Control, and Dynamics*.

[9] Rodin, E., 1987, “A pursuit-evasion bibliographyversion 1,” *Computers & Mathematics with Applications*, vol. 13, no. 1, pp. 275–340.

[10] Rodin, E., 1989, “A pursuit-evasion bibliographyversion 2,” *Computers & Mathematics with Applications*, vol. 18, no. 1-3, pp. 245–320.

[11] Lin, C.-F., *Modern navigation, guidance, and control processing*, vol. 2. Prentice Hall Englewood Cliffs, 1991.

[12] Cochran, J., No, T., and Thaxton, D., 1991, “Analytical solutions to a guidance problem,” *Journal of Guidance, Control, and Dynamics*, vol. 14, no. 1, pp. 117–122.

[13] Lê, N.-M., 1998, “On determining optimal strategies in pursuit games in the plane,” *Theoretical computer science*, vol. 197, no. 1-2, pp. 203–234.

[14] Creaser, P. A., 1998, “Generation of missile guidance algorithms,”

[15] Siouris, G. M., *Missile guidance and control systems*. Springer Science & Business Media, 2004.

[16] Lechevin, N. and Rabbath, C., 2004, “Lyapunov-based nonlinear missile guidance,” *Journal of guidance, control, and dynamics*, vol. 27, no. 6, pp. 1096–1102.

[17] Lee, J.-I., Jeon, I.-S., and Tahk, M.-J., 2007, “Guidance law to control impact time and angle,” *IEEE Transactions on Aerospace and Electronic Systems*, vol. 43, no. 1.

[18] Breivik, M. and Fossen, T. I., 2008, “Guidance laws for planar motion control,” in *Decision and Control, 2008. CDC 2008. 47th IEEE Conference on*, pp. 570–577, IEEE.

[19] Rusnak, I., 2008, “Guidance laws in defense against missile attack,” in *Electrical and Electronics Engineers in Israel, 2008. IEEEI 2008. IEEE 25th Convention of*, pp. 090–094, IEEE.

[20] Shinar, J. and Turetsky, V., 2009, “Meeting the challenges of modern interceptor guidance by non-conventional approaches,” in *Control and Automation, 2009. MED’09. 17th Mediterranean Conference on*, pp. 1563–1568, IEEE.

[21] Lin, Y.-P., Tsao, L.-P., and Lin, C.-L., 2010, “Development of three-dimensional aiming point guidance law,” *International Journal of Systems Science*, vol. 41, no. 11, pp. 1353–1362.

[22] Shneydor, N. A., *Missile guidance and pursuit: kinematics, dynamics and control*. Elsevier, 1998.

[23] Pham, T.-D., Tran, Q., and Vu, D.-V., 2012, “Fuzzy guidance law for surface-to-air missile in the command control systems,” in *Control, Automation and Information Sciences (ICCAIS), 2012 International Conference on*, pp. 317–322, IEEE.

[24] White, B., *Advances in missile guidance, control, and estimation*. CRC Press, 2012.

[25] Li, C., Sun, Y., Lv, T., Ma, G., and Xiao, J., 2014, “A fuzzy guidance law design with terminal-angle constraint,” in *Control Conference (CCC), 2014 33rd Chinese*, pp. 749–753, IEEE.

[26] Cho, H., Ryoo, C.-K., Tsourdos, A., and White, B., 2014, “Optimal impact angle control guidance law based on linearization about collision triangle,” *Journal of Guidance, Control, and Dynamics*, vol. 37, no. 3, pp. 958–964.

[27] Grinfeld, N. and Ben-Asher, J. Z., 2015, “Minimal-jerk missile guidance law,” *Journal of Guidance, Control, and Dynamics*, vol. 38, no. 8, pp. 1520–1525.

[28] Zarchan, P., 1999, “Ballistic missile defense guidance and control issues,” *Science & Global Security*, vol. 8, no. 1, pp. 99–124.

[29] Zarchan, P., 2000, “Tracking and intercepting spiraling ballistic missiles,” in *Position Location and Navigation Symposium, IEEE 2000*, pp. 277–284, IEEE.

[30] Zarchan, P., 2011, “Kill vehicle guidance and control sizing for boost-phase intercept,” *Journal of Guidance, Control, and Dynamics*, vol. 34, no. 2, pp. 513–521.

[31] Pearce, J. R., 2013, "Tactical and strategic missile guidance–sixth edition: Progress in aeronautics and astronautics–vol 239 p. zarchan. american institute of aeronautics and astronautics, 1801 alexander bell drive, suite 500, reston, va 20191-4344, usa. 2012. distributed by transatlantic publishers group, 97 greenham road, london, n10 1ln (tel: 020-8815 5994; e-mail: mark. chaloner@ tpgltd. co. uk). 1027pp. illustrated.£ 107.50 (20% discount available to raes members on request). isbn 978-1-60086-894-8. advances in missile guidance, control and estimation edited by sn balakrishnan et al. crc press, taylor & francis group, 6000 broken sound parkway nw, suite 300, boca raton, fl, 33487-2742, usa. 2012. distributed by taylor & francis group, 2 park square, milton park, abingdon, ox14 4rn. 682pp. illustrated.£ 99. isbn 978-1-4200-8313-2.," *The Aeronautical Journal*, vol. 117, no. 1187, pp. 90–92.

[32] Chung, T. H., Hollinger, G. A., and Isler, V., 2011, "Search and pursuit-evasion in mobile robotics," *Autonomous robots*, vol. 31, no. 4, p. 299.

[33] Weiss, M., Shima, T., Castaneda, D., and Rusnak, I., 2017, "Combined and cooperative minimum-effort guidance algorithms in an active aircraft defense scenario," *Journal of Guidance, Control, and Dynamics*.

[34] Garcia, E., Casbeer, D., and Pachter, M., 2017, "Optimal guidance for active aircraft defense against homing missiles," in *AIAA Guidance, Navigation, and Control Conference*, p. 1017.

[35] Flood, M. M., 1972, "The hide and seek game of von neumann," *Management Science*, vol. 18, no. 5-part-2, pp. 107–109.

[36] Turetsky, V. and Shinar, J., 2003, "Missile guidance laws based on pursuit–evasion game formulations," *Automatica*, vol. 39, no. 4, pp. 607–618.

[37] Gutman, S. and Goldan, O., 2010, "3d differential game guidance," *Applied Mathematics and Computation*, vol. 217, no. 3, pp. 1077–1084.

[38] Ho, Y.-C., Bryson, A. E., and Baron, S., (1965), "Differential games and optimal pursuit-evasion strategies," in *Joint Automatic Control Conference*, no. 3, pp. 37–40.

[39] Isaacs, R., *Differential games III*. Wiley, (1954).

[40] Meier, L., 1969, "A new technique for solving pursuit-evasion differential games," in *Joint Automatic Control Conference*, no. 7, pp. 514–521.

[41] Hsueh, M.-H., Huang, C.-I., and Fu, L.-C., (2007), "A differential game based guidance law for the interceptor missiles," in *Industrial Electronics Society, 2007. IECON 2007. 33rd Annual Conference of the IEEE*, pp. 665–670.

[42] Yi, L., Yan, Y., Tian, G., and Zhanrong, J., (2010), "An improved terminal guidance algorithm based on differential game theory," in *Intelligent System Design and Engineering Application (ISDEA), 2010 International Conference on*, vol. 1, pp. 250–254.

[43] Bressan, A., (2010), "Noncooperative differential games. a tutorial," *Department of Mathematics, Penn State University*.

[44] Perelman, A., Shima, T., and Rusnak, I., (2011), “Cooperative differential games strategies for active aircraft protection from a homing missile,” *Journal of Guidance, Control, and Dynamics*, vol. 34, no. 3, pp. 761–773.

[45] Battistini, S. and Shima, T., (2014), “Differential games missile guidance with bearings-only measurements,” *Aerospace and Electronic Systems, IEEE Transactions on*, vol. 50, no. 4, pp. 2906–2915.

[46] Yavin, Y. and Pachter, M., *Pursuit-evasion differential games*. Elsevier, (2014).

[47] Meir, P., Garcia, E., and Casbeer, D. W., (2014), “Active target defense differential game,” in *Proceedings of the 2014 IEEE 52nd Annual Allerton Conference on Communication, Control, and Computing*, pp. 46–53.

[48] Garcia, E., Casbeer, D. W., and Pachter, M., (2015), “Active target defense differential game with a fast defender,” *arXiv preprint arXiv:1502.02747*.

[49] Garcia, E., Casbeer, D. W., and Pachter, M., (2015), “Escape regions of the active target defense differential game,” *arXiv preprint arXiv:1504.07900*.

[50] Garcia, E., Casbeer, D. W., Pham, K., and Pachter, M., (2014), “Cooperative aircraft defense from an attacking missile,” in *Decision and Control (CDC), 2014 IEEE 53rd Annual Conference on*, pp. 2926–2931.

[51] Garcia, E., Casbeer, D. W., Pham, K., and Pachter, M., (2015), “Cooperative aircraft defense from an attacking missile using proportional navigation,” in *2015 AIAA Guidence, Navigation, and Control Conference*, pp. 2015–0337.

[52] Garcia, E., Casbeer, D. W., and Pachter, M., (2015), “Cooperative strategies for optimal aircraft defense from an attacking missile,” *Journal of Guidance, Control, and Dynamics*, pp. 1–11.

[53] Boyell, R., 1976, “Defending a moving target against missile or torpedo attack,” *Aerospace and Electronic Systems, IEEE Transactions on*, no. 4, pp. 522–526.

[54] Shneydor, N., 1977, “Comments on” defending a moving target against missile or topedo attack”,” *IEEE Transactions on Aerospace and Electronic Systems*, vol. 3, no. AES-13, p. 321.

[55] Rusnak, I., (2005), “The lady, the bandits, and the bodyguards–a two team dynamic game,” in *Proceedings of the 16th World IFAC Congress*.

[56] de Lope, J., Maravall, D., and others,, (2010), “Analysis and solution of a predator–protector–prey multi-robot system by a high-level reinforcement learning architecture and the adaptive systems theory,” *Robotics and Autonomous Systems*, vol. 58, no. 12, pp. 1266–1272.

[57] Rusnak, I., Weiss, H., and Hexner, G., (2011), “Guidance laws in target-missile-defender scenario with an aggressive defender,” in *Proceedings of the 18th IFAC World Congress*, vol. 18, pp. 9349–9354, International Federation of Automatic Control Laxenburg, Austria.

[58] Fuch, Z. E. and Khargonekar, P. P., (2011), "Encouraging attacker retreat through defender cooperation," in *Decision and Control and European Control Conference (CDC-ECC), 2011 50th IEEE Conference on*, pp. 235–242.

[59] Scott, W. and Leonard, N. E., (2013), "Pursuit, herding and evasion: A three-agent model of caribou predation," in *American Control Conference (ACC), 2013*, pp. 2978–2983.

[60] Rubinsky, S. and Gutman, S., (2013), "Three-player pursuit and evasion conflict," *Journal of Guidance, Control, and Dynamics*, vol. 37, no. 1, pp. 98–110.

[61] Oyler, D. W., Kabamba, P. T., and Girard, A. R., (2014), "Pursuit-evasion games in the presence of a line segment obstacle," in *Decision and Control (CDC), 2014 IEEE 53rd Annual Conference on*, pp. 1149–1154.

[62] Anderson, G., 1978, "A model for the bat versus moth pursuit-evasion problem," *The Journal of the Acoustical Society of America*, vol. 64, no. S1, pp. S88–S88.

[63] Miller, G. F. and Cliff, D., *Co-evolution of pursuit and evasion I: Biological and game-theoretic foundations*. University of Sussex, School of Cognitive and Computing Sciences, (1994).

[64] Cliff, D. and Miller, G. F., (1995), "Co-evolution of pursuit and evasion ii: Simulation methods and results,"

[65] Pekalski, A., (2004), "A short guide to predator-prey lattice models," *Computing in Science and Engineering*, vol. 6, no. 1, pp. 62–66.

[66] Zarchan, P., (2012), "Tactical and strategic missile guidance," *Progress in astronautics and aeronautics*.

[67] Hagedorn, P. and Breakwell, J., 1976, "A differential game with two pursuers and one evader," *Journal of Optimization Theory and Applications*, vol. 18, no. 1, pp. 15–29.

[68] Kim, H., *Multiagent pursuit-evasion games: algorithms and experiments*. (2001).

[69] Fuchs, Z. E., Khargonekar, P. P., and Evers, J., (2010), "Cooperative defense within a single-pursuer, two-evader pursuit evasion differential game," in *Decision and Control (CDC), 2010 49th IEEE Conference on*, pp. 3091–3097.

[70] Pan, S., Huang, H., Ding, J., Zhang, W., Stipanovic, D. M., and Tomlin, C. J., (2012), "Pursuit, evasion and defense in the plane," in *American Control Conference (ACC), 2012*, pp. 4167–4173.

[71] Ragesh, R., Ratnoo, A., and Ghose, D., (2014), "Analysis of evader survivability enhancement by decoy deployment," in *American Control Conference (ACC), 2014*, pp. 4735–4740.

[72] Ayoub, A. B., (2003), "Proving the circle of apollonius theorem," *The Mathematics Teacher*, pp. 400–401.

[73] Ayoub, A. B., (2006), "On the circle of apollonius.," *Mathematics and Computer Education*, vol. 40, no. 3, pp. 198–204.

[74] Partensky, M. B., (2008), "The circle of apollonius and its applications in introductory physics," *The Physics Teacher*, vol. 46, no. 2, pp. 104–108.

[75] Fulton, N. L. and Huynh, U. H.-N., (2015), "Conflict management: Apollonius in airspace design," *Safety science*, vol. 72, pp. 9–22.

[76] Gowda, I. G., Kirkpatrick, D. G., DER TSAI, L., and Naamad, A., 1983, "Dynamic voronoi diagrams," *IEEE Transactions on Information Theory*, vol. 29, no. 5, pp. 724–731.

[77] Aurenhammer, F., (1991), "Voronoi diagramsa survey of a fundamental geometric data structure," *ACM Computing Surveys (CSUR)*, vol. 23, no. 3, pp. 345–405.

[78] Cheung, W. and Evans, W., (2007), "Pursuit-evasion voronoi diagrams in ell_1," in *Voronoi Diagrams in Science and Engineering, 2007. ISVD'07. 4th International Symposium on*, pp. 58–65.

[79] Gavrilova, M. L., *Generalized voronoi diagram: a geometry-based approach to computational intelligence*, vol. 158. Springer, (2008).

[80] Majdandzic, I., Trefftz, C., and Wolffe, G., (2008), "Computation of voronoi diagrams using a graphics processing unit," in *Electro/Information Technology, 2008. EIT 2008. IEEE International Conference on*, pp. 437–441.

[81] Bakolas, E. and Tsiotras, P., (2010), "Optimal pursuit of moving targets using dynamic voronoi diagrams," in *Decision and Control (CDC), 2010 49th IEEE Conference on*, pp. 7431–7436.

[82] Bakolas, E. and Tsiotras, P., (2010), "The zermelo–voronoi diagram: a dynamic partition problem," *Automatica*, vol. 46, no. 12, pp. 2059–2067.